Acta Crystallographica Section B
Structural Science
ISSN 0108-7681

Novel tools for visualizing and exploring intermolecular interactions in molecular crystals

Joshua J. McKinnon,[a] Mark A. Spackman[a]*‡ and Anthony S. Mitchell[b]

[a]Department of Chemistry, School of Biological, Biomedical and Molecular Sciences, University of New England, Australia, and [b]Centre for Magnetic Resonance, University of Queensland, Australia

‡ Present address: Department of Chemistry, School of Biomedical & Chemical Sciences, University of Western Australia, Crawley, WA 6009, Australia.

Correspondence e-mail: mas@cyllene.uwa.edu.au

Received 3 May 2004
Accepted 16 August 2004

A new way of exploring packing modes and intermolecular interactions in molecular crystals is described, using Hirshfeld surfaces to partition crystal space. These molecular Hirshfeld surfaces, so named because they derive from Hirshfeld's stockholder partitioning, divide the crystal into regions where the electron distribution of a sum of spherical atoms for the molecule (the promolecule) dominates the corresponding sum over the crystal (the procrystal). These surfaces reflect intermolecular interactions in a novel visual manner, offering a previously unseen picture of molecular shape in a crystalline environment. Surface features characteristic of different types of intermolecular interactions can be identified, and such features can be revealed by colour coding distances from the surface to the nearest atom exterior or interior to the surface, or by functions of the principal surface curvatures. These simple devices provide a striking and immediate picture of the types of interactions present, and even reflect their relative strengths from molecule to molecule. A complementary two-dimensional mapping is also presented, which summarizes quantitatively the types of intermolecular contacts experienced by molecules in the bulk and presents this information in a convenient colour plot. This paper describes the use of these tools in the compilation of a pictorial glossary of intermolecular interactions, using identifiable patterns of interaction between small molecules to rationalize the often complex mix of interactions displayed by large molecules.

1. Introduction

Desiraju (1989) described crystal engineering as 'the understanding of intermolecular interactions in the context of crystal packing and in the utilization of such understanding in the design of new solids with desirable physical and chemical properties'. That description has often been quoted and in the intervening years numerous publications have dealt with many aspects of this fascinating branch of modern chemistry, among them some key review articles (Desiraju, 1995, 1996, 1997; Aakeröy, 1997; Gavezzotti, 1998; Braga *et al.*, 2002) and books (Desiraju, 1989; Weber, 1998; Desiraju & Steiner, 1999). For a more up-to-date commentary, the reader is referred to articles by Desiraju (2001), Aakeröy & Beatty (2001), Sharma (2002) and Braga (2003). At its most basic level, crystal engineering applied to the realm of molecular crystals seeks an understanding of the nature and structural implications of intermolecular forces in crystals. Work in this direction was

pioneered by Kitaigorodsky, summarized in his books on organic molecular crystals (Kitaigorodsky, 1961, 1973), and it will become evident to the reader that our own work owes considerable debt to those seminal works. It is at this basic level that we seek to make a valuable and completely original contribution.

The observed structure of any molecular crystal represents a remarkable and delicate balance between many different intermolecular forces, some of which are weak and non-directional, while others are relatively strong and directed in quite specific ways. Thus, 'each crystal structure contains important information about the way in which intermolecular forces compete and collaborate and eventually create an energetically balanced system' (Aakeröy, 1997). It is the recognition and exploitation of this fact that underlies our approach, namely, attempting to decode in a novel fashion the information on intermolecular forces contained in the crystal structure alone. The systematic description and analysis of organic molecular crystal structures in terms of space-group statistics (Brock & Dunitz, 1994), packing motifs (Leiserowitz, 1976, 1978; Leiserowitz & Nader, 1977; Berkovitch-Yellin & Leiserowitz, 1980, 1982), hydrogen-bond networks (Etter, 1990; Bernstein *et al.*, 1995; Etter *et al.*, 1990) and supramolecular synthons (Desiraju, 1995, 1997; Nangia & Desiraju, 1998) represent increasingly important elements of crystal engineering. The continual improvements in methods of analysis and increasing ease with which they can be performed mean that access to the Cambridge Structural Database (CSD; Allen, 2002) is imperative for serious crystallographic studies of molecular crystals, and the CSD's importance to research in crystal engineering has been recently highlighted by Nangia (2002). As Aakeröy suggests, it is now appropriate 'to expect that every structural paper is accompanied by a comparative study of related structures (if available), in order to place the characteristics of a new crystal structure in the proper context. In this way, unusual intra- or intermolecular features can be detected readily and the 'unexpected' can often stimulate new ideas or interpretations of 'well known' behaviour' (Aakeröy, 1997). This statement of course begs the question of precisely how the investigator might best perform such a comparative study, especially if the goal is the detection of the unusual or the uncommon.

Chemists almost invariably employ models to discuss and interpret molecular and crystal structures. Simple models involving lines to represent bonds and balls for atoms – 'ball and stick' models – and their geometric counterparts of bond lengths, bond and torsion angles *etc.*, are central to many studies using the CSD, but these models do not convey (or utilize) the undeniable fact that molecules fill space! Space-filling models of fused spheres, van der Waals surfaces, solvent-accessible surfaces or electron density isosurfaces represent various improvements on the simple model, but none allows for deformation of the molecular space in the crystalline environment. The Hirshfeld surface, on the other hand, contains such information implicitly; this surface represents a measure of the space occupied by a molecule in a crystal and as such summarizes information on all intermolecular interactions and contacts simultaneously. Decoding this information, both qualitatively and quantitatively, is the focus of the present work, which presents one aspect of a more comprehensive exploration of Hirshfeld surfaces: their use in visualizing molecular crystals, their size, global attributes of their shape and local descriptors of shape using curvature. Future work will focus on the possible relationships to molecular and bulk properties such as lattice energies, and the use of Hirshfeld surfaces in extracting molecular properties by integration of crystalline electron distributions, both theoretical and experimental.

Our approach is not intended as an alternative to existing methods of analysing molecular crystals but should be seen as a new and complementary method, and we expect that it will be capable of widespread utilization and will considerably enhance our understanding of intermolecular interactions in solids. It will become evident in what follows that the primary focus of the present use of Hirshfeld surfaces is visualization, especially taking advantage of the human mind's extraordinary capacity for visual pattern recognition using colour. In this fashion we expect the tools we have developed to find widespread application where there is a 'compelling need to be able to visualize a crystal structure in its entirety, not just look at selected intermolecular interactions which have been deemed to be important' (Desiraju, 1997). Such a need is clearly evident in many recent publications that involve comparisons between related crystal structures; excellent examples of such studies are provided by research by Thalladi, Boese and co-workers on the fluorobenzenes (Thalladi *et al.*, 1998), *n*-alkanes (Thalladi & Boese, 2000; Boese *et al.*, 1999), α,ω-akanedithiols (Thalladi, Boese & Weiss, 2000*b*), α,ω-alkanedicarboxylic acids (Thalladi, Nusse & Boese, 2000), and α,ω-alkanediols and α,ω-alkanediamines (Thalladi, Boese & Weiss, 2000*a*). Nangia & Desiraju (1998) have recently argued that a full understanding of crystal structure and design requires a treatment of the entire molecule and all interactions, and in the section of that work entitled *Comparison of Crystal Structures* those authors write 'Given such realities, an immediate need in crystal engineering is to be able to compare crystal structures. Many will appreciate that the structure of, say, naphthalene resembles that of anthracene more than it resembles benzene. Is it possible to quantify such comparisons? If so, such quantification would amount to pattern matching and becomes important because crystals that are structurally similar are also likely to have similar properties. Ideally, one would like to arrive at an index of similarity between two crystal structures. In order that two or more structures are deemed to be similar or dissimilar, two steps are involved: (1) identification of the core structural features and (2) evaluation of the extent of their likeness'.

Hirshfeld surfaces were introduced quite recently in the context of partitioning molecular crystals into molecular regions for the purposes of electron density integration (Spackman & Byrom, 1997). Since then, we have presented greyscale three-dimensional isosurfaces for a variety of molecular crystals (McKinnon *et al.*, 1998*a*) and demonstrated their relationship with fused vdW sphere (CPK) and electron

density isosurface representations of molecules in crystals of naphthalene and terephthalic acid (McKinnon *et al.*, 1998*b*).[1] The surfaces were named in honour of F. L. Hirshfeld, whose 'stockholder partitioning' scheme (Hirshfeld, 1977) suggested the possibility to us. We find a certain amount of pleasure in the fact that Hirshfeld was a PhD student of G. M. J. Schmidt at the Weizmann Institute of Science, and Schmidt's article on solid-state photodimerization (Schmidt, 1971) is widely regarded as the first to introduce the term 'crystal engineering' with precisely the meaning it conveys at present. More recently we have introduced two-dimensional fingerprint plots, providing numerous examples of their application to molecular crystals (Spackman & McKinnon, 2002). The present work will overlap slightly with the content of that article, and for good reason; we wish to demonstrate convincingly that the simultaneous use of all our present visualization tools – surfaces mapped with several functions, as well as fingerprint plots – conveys more information than either does alone.

2. Computational procedure

2.1. Constructing the Hirshfeld surface

Molecular Hirshfeld surfaces are constructed by partitioning space in the crystal into regions where the electron distribution of a sum of spherical atoms for the molecule (the promolecule) dominates the corresponding sum over the crystal (the procrystal). Following Hirshfeld (1977), a weighting function $w(\mathbf{r})$ for a particular molecule can be defined as

$$\begin{aligned} w(\mathbf{r}) &= \sum_{a\in\text{molecule}} \rho_a(\mathbf{r}) / \sum_{a\in\text{crystal}} \rho_a(\mathbf{r}) \\ &= \rho_{\text{promolecule}}(\mathbf{r}) / \rho_{\text{procrystal}}(\mathbf{r}) \\ &\simeq \rho_{\text{molecule}}(\mathbf{r}) / \rho_{\text{crystal}}(\mathbf{r}), \end{aligned}$$

from which it follows that the volume within which the promolecule dominates the procrystal electron density is that region where $w(\mathbf{r}) \geq 0.5$; we define the Hirshfeld surface by $w(\mathbf{r}) = 0.5$. Here, $\rho_a(\mathbf{r})$ is a spherically averaged Hartree–Fock atomic electron density function (Clementi & Roetti, 1974) centred on nucleus a, and the ratio between promolecule and procrystal electron densities can be regarded as an approximation to the ratio between true molecule and crystal electron densities (although that is not an essential interpretation). For computational purposes the sum over the crystal is truncated to a cluster of molecules within approximately 10 Å of the molecule of interest. For a given crystal structure and set of atomic electron densities, the isosurface defined by $w(\mathbf{r}) = 0.5$ is unique, although changes in the atomic electron densities lead to small changes in the resulting surface. We have shown elsewhere that a promolecule electron density surface [0.002 atomic units (a.u.)] constructed with Hartree–Fock atoms and a contracted H atom ($\zeta = 1.24$ a.u., rather than 1.0 a.u.) provides remarkably reliable and consistent estimates of *ab initio* surface areas (within 0.5%) and volumes (within 4%) of molecules (Mitchell & Spackman, 2000). For this reason we employ a contracted H atom for construction of Hirshfeld surfaces in all of our work on molecular crystals.

We have used the marching-cubes algorithm (Lorensen & Cline, 1987; Heiden *et al.*, 1993) to locate and triangulate the surfaces for visual display, at the same time enabling rapid computation of molecular volume (V_H), surface area (S_H), and packing ratio ($P_H = \sum_{\text{cell}} V_H / V_{\text{cell}}$). For integration over the Hirshfeld surfaces, optimum balance between accuracy and time was achieved with a resolution of 0.2 a.u. for the marching-cubes grid, which corresponds to a typical distance between surface points of ~0.16 a.u. At this resolution all derived quantities are within 1% or better of the converged result (McKinnon *et al.*, 1998*a*; McKinnon, 2003).

Since we are concerned with comparisons between Hirshfeld surfaces for related structures, and H atoms are almost always terminal atoms, their location is of critical importance. It has become standard practice in recent quantitative studies using structural data from the CSD to normalize the lengths of X—H bonds [see, for example, pp. 6–7 of Desiraju & Steiner (1999)], and we follow this procedure throughout the present work, using standard X—H distances from the compilation of Allen *et al.* (1995).

Before presenting and discussing detailed applications of Hirshfeld surfaces, and exploring what physical insight they might reveal, it is worthwhile mentioning how they differ from other representations. Unlike other molecular volumes and surfaces (*e.g.* fused-sphere van der Waals volumes, solvent-accessible surfaces, solvent-excluded surfaces; Mezey, 1990, 1993), Hirshfeld surfaces are not simply a function of the molecular geometry; they are only defined within the crystal,[2] and hence necessarily reflect the interplay between different atomic sizes and intermolecular contacts in the crystal: intermolecular interactions. Whether Hirshfeld surfaces do this in a quantitative or qualitative manner remains to be seen. We have demonstrated elsewhere (McKinnon *et al.*, 1998*a*) that Hirshfeld surfaces and volumes are much larger than conventional ones, generally filling at least 95% of the crystal volume, compared with more conventional packing coefficients of between 0.65 and 0.80 (Kitaigorodsky, 1973). Finally, Hirshfeld surfaces obviously pack very tightly in the crystal, at most touching and never overlapping. However, quite unlike any other partitioning or packing scheme, they leave small intermolecular voids, which can be regarded as regions where the crystalline electron density is very low and is not dominated by any single molecule.

[1] From a historical viewpoint, we note that the packing of objects remarkably similar to Hirshfeld surfaces was depicted by Kitaigorodsky, probably as early as 1955 [see Fig. 62, p. 93 of Kitaigorodsky (1961), part of which appears to have been reproduced without attribution as Fig. 2.68, p. 180 of Vainshtein *et al.* (1982)].

[2] This is not a necessary restriction. We can readily envisage a generalization to any condensed phase; for example, snapshots from a liquid simulation would yield Hirshfeld surfaces, but different ones for each molecule. Likewise, the partitioning scheme can be readily applied to extended covalent networks such as diamond and graphite, or even ionic solids; in these cases atomic (or ionic) surfaces are obtained.

2.2. Properties encoded on the surface – colour graphics

In our first foray into the greyscale representation of Hirshfeld surfaces it was evident that they reflected, sometimes in a very subtle fashion, the effects of all close intermolecular contacts (see Fig. 1 for uracil). It was not so obvious how to extract this information and present it in a visually appealing and striking manner. To date we have explored the use of five different functions mapped in colour on the Hirshfeld surfaces; we describe these functions below, with reference to Fig. 1, where examples of each are given for a molecule of uracil.

Distance external to the surface, d_e, measures the distance from the surface to the nearest nucleus in another molecule. It is straightforward to map on the Hirshfeld surface and provides an excellent and immediate picture of close intermolecular contacts. From Fig. 1 it is evident that hydrogen-bond acceptor regions show up as nearly flat bright-red regions perpendicular to the N—H$\cdots$O vector; hydrogen-bond donor regions are also flat but largely green (see bottom right of the d_e surface in Fig. 1), while regions above the plane of the molecule are variously green or blue depending on their proximity to atoms in the molecule stacked above. Careful inspection of the blue features on the upper surface in this figure reveals a small blue hexagon near the lower part of the figure, with six light-blue 'spokes' radiating outwards; these patterns arise from the overlap and proximity of the two 6-rings of adjacent stacked molecules, and the location of the features on this part of the Hirshfeld surface tells us immediately that the molecules in uracil stack in layers in an offset fashion. In an analogous fashion we can define the distance internal to the surface, d_i (*i.e.* distance from the surface to the nearest atom in the molecule itself). We have found this to be much less useful than d_e for the present study, although d_i is vital for our two-dimensional fingerprint plots and is likely to be important in studies of atomic and ionic size.

Although d_e reveals details of close contacts between molecules, especially in the vicinity of hydrogen bonds (Fig. 1), it is not *a property of the surface*. Curvature has been shown to play an important, if under-appreciated, role in condensed matter physics, chemistry and biology (Hyde *et al.*, 1997), and local surface curvature is a natural property to pursue with Hirshfeld surfaces. The Hirshfeld surface is based on a smooth continuous three-dimensional function, is defined implicitly and, in practice, is given by a triangulated mesh. At any point on the surface the outward normal is given by the gradient, $\mathbf{n} = \nabla w$, and there exist two principal directions $\mathbf{u}$ and $\mathbf{v}$, which diagonalize the Hessian of w restricted to vectors perpendicular to $\mathbf{n}$ (Fig. 2). The eigenvalues of this diagonalization process are related to the principal curvatures of the surface, κ_1 and κ_2 (Do Carmo, 1976)

$$\kappa_1 = -\frac{1}{|\mathbf{n}|}\frac{\partial^2 w}{\partial u^2} \quad \text{and} \quad \kappa_2 = -\frac{1}{|\mathbf{n}|}\frac{\partial^2 w}{\partial v^2}.$$

We have used numerical first and second derivatives to obtain $\mathbf{n}$, and hence $\mathbf{u}$ and $\mathbf{v}$, and κ_1 and κ_2 (in what follows we observe the convention that $\kappa_1 \geq \kappa_2$). As described elsewhere (Hyde *et al.*, 1997; Koenderink, 1990), κ_1 and κ_2 can be combined to give two conventional measures of curvature of the surface: *Gaussian curvature*, $K = \kappa_1\kappa_2$, which has the dimensions of inverse area, and *mean curvature*, $H = (\kappa_1 + \kappa_2)/2$, which has the dimensions of inverse length. Maps of H and K encoded on the Hirshfeld surface for uracil are provided in Fig. 1. From the map of mean curvature it is clear that none of the colour highlights corresponds to obvious intermolecular interactions (although it is of interest to note that Hirshfeld surfaces are generally not minimal surfaces, for which $H = 0$ (yellow in Fig. 1) everywhere. Even less informative is the map of Gaussian curvature, K, in Fig. 1. Clearly, most of the Hirshfeld surface has a small Gaussian curvature (green), with the exception of only very small regions of

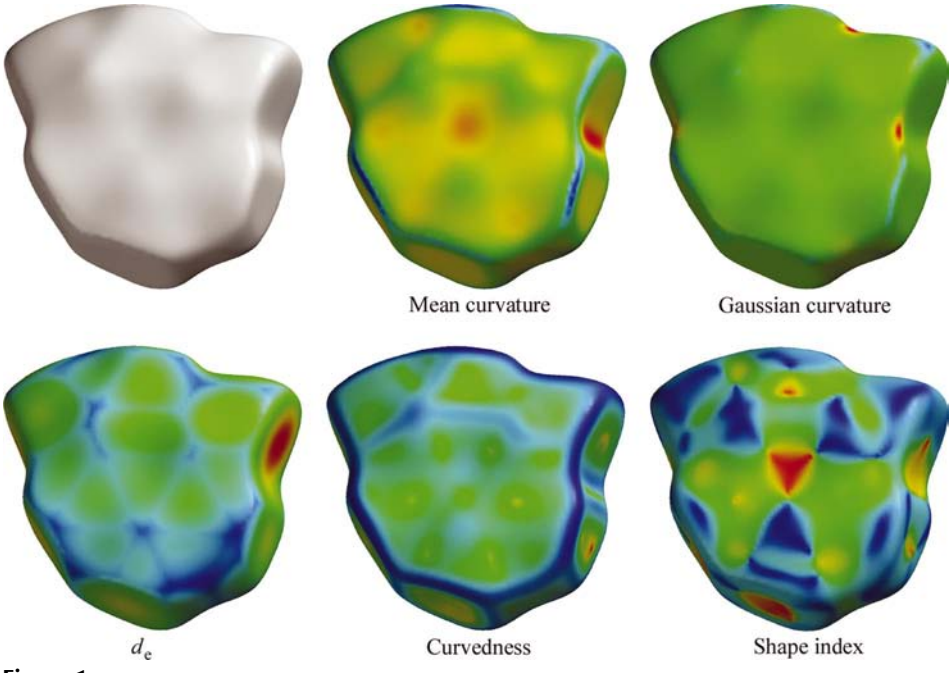

Figure 1
The Hirshfeld surface of uracil, undecorated (top left) and with a variety of properties mapped onto the surface. Top centre: mean curvature, H, mapped on its natural range (*i.e.* from minimum to maximum) of −0.46 (red) to +1.17 a.u.$^{-1}$ (blue); top right: Gaussian curvature, K, also mapped on its natural range of −0.72 (red) to +0.87 a.u.$^{-2}$ (blue); bottom left: distance external to the surface, d_e, mapped over the range 0.55 (red) $\Rightarrow$ 1.50 (green) $\Rightarrow$ 2.40 Å (blue); bottom centre: curvedness, C, mapped from −4.0 (flat; red) $\Rightarrow$ 0.0 (unit sphere; cyan–green) $\Rightarrow$ +0.4 (edge; blue); bottom right: shape index, S, mapped from −1.0 (concave umbilic; red) $\Rightarrow$ 0.0 (minimal saddle; green) $\Rightarrow$ +1.0 (convex umbilic; blue). Unless specifically noted, all maps of d_e, S and C will be mapped over the same ranges as in this figure.

pronounced saddle (red) and convex (blue) shape. It has previously been noted that 'neither the Gaussian nor the mean curvature, by themselves, capture the intuitive notion of 'local shape' very well' (Koenderink & van Doorn, 1992), and these maps of H and K demonstrate this point dramatically. To remedy this situation, Koenderink introduced two additional measures of surface curvature: shape index and curvedness.

Shape index is defined by the function

$$S = (2/\pi)\arctan\left[(\kappa_1 + \kappa_2)/(\kappa_1 - \kappa_2)\right]$$

and is a dimensionless measure of 'which' shape. The formal range of S is $[-1, +1]$, and this is also the best range for visual display (Fig. 1). S has a number of intriguing attributes, which have been described in some detail by Koenderink & van Doorn (1992). For our purposes one of the most important is the fact that two shapes for which the shape index differs only by a sign represent complementary 'stamp' and 'mould' pairs. Therefore, maps of shape index on the Hirshfeld surface can be used to identify complementary hollows (red in Fig. 1) and bumps (blue in Fig. 1) where two molecular Hirshfeld surfaces touch one another. Shape index is also claimed by Koenderink & van Doorn to be better suited than H and K when the aim is visual identification of meaningful local shape features, and that fact is certainly borne out in our own use of this measure. From the map of shape index for uracil (Fig. 1), it is immediately evident that there is a great deal of information contained in such a picture. Most obvious are the red and blue triangles on the surface, and careful inspection confirms that this 'bow tie' pattern of touching red and blue triangles is characteristic of a particular stacking arrangement of 6-rings. Also worthy of note are the hydrogen-bond donor and acceptor regions on the right-hand side of the surface.

Curvedness is defined by

$$C = (2/\pi)\ln\left[\left(\kappa_1^2 + \kappa_2^2\right)/2\right]^{1/2}$$

and is a measure of 'how much' shape. C is clearly a function of the r.m.s. curvature of the surface, and although the formal range of C is $(-\infty, +\infty)$, in practice a mapping from -4.0 to $+0.4$ (with κ_1 and κ_2 in a.u.$^{-1}$) has been found to be most useful with molecular Hirshfeld surfaces (Fig. 1). This definition of curvedness is one of two alternatives given by Koenderink and, as he has commented, there are several definitions that would suffice to convey the magnitude of the surface curvature. Unlike shape index, curvedness is not independent of the length scale chosen, as the argument of the logarithm has the dimension of reciprocal length. From Fig. 1 we see that maps of curvedness are typically characterized by relatively large regions of green (r.m.s. curvature near unity), separated by dark blue 'edges' (large r.m.s. curvature). Occasional highlights of yellow and red indicate unusually flat regions on the surface, which often (but not always) correspond to hydrogen bonds. Maps of C in fact delineate the areas on the surface that represent close contact between two molecular Hirshfeld surfaces, and hence enable us to extract information about the number of nearest neighbours or the coordination sphere of each molecule. It is surprising to us that the work of Koenderink has been almost entirely neglected by researchers outside the areas of computer graphics and image processing, with the exception only of papers by Duncan & Olson (1993*a*,*b*), who used shape index and r.m.s. curvature to characterize several types of protein molecular surfaces, and Goldman & Wipke (2000*a*,*b*), who employed shape index in their recent work on aspects of shape-based molecular similarity.

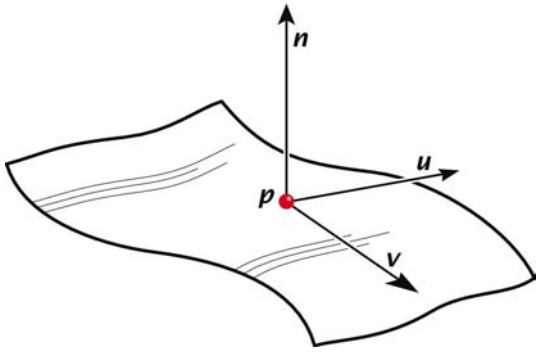

Figure 2
Schematic diagram of a surface normal, **n**, and the two principal directions **u** and **v**.

2.3. Quantitative measures

We have already mentioned Hirshfeld surface volume and surface area, and the resulting packing ratio for the crystal. Two other descriptors of global shape (Arteca, 1990) have also been explored in our previous work. *Globularity* (Meyer, 1986) is a measure of the degree to which the surface area differs from that of a sphere of the same volume

$$G = \left(36\pi V_H^2\right)^{1/3}/S_H,$$

and will be 1.0 for a sphere and progressively less than one as the molecular surface becomes more structured. *Asphericity* (Rudnick & Gaspari, 1986; Baumgärtner, 1993) is a measure of anisotropy and, when applied to the positions of nuclei in molecules, is defined by

$$\Omega = (1/2)\left[\sum_{i\neq j}(\lambda_i - \lambda_j)^2\right]\left(\sum_i \lambda_i\right)^{-2},$$

where λ_i are the three principal moments of inertia of the molecule. We have applied this descriptor to the Hirshfeld surfaces by allocating each surface point unit mass and summing over all points on the surface. Ω determined in this way assumes a value of zero for an isotropic object (*e.g.* a sphere, tetrahedron or octahedron where all principal values are identical), 1.0 for a prolate object and 0.25 for an oblate object. We have found $\Omega^{1/2}$ to be a more useful measure, as it transforms the range to 0.0 (isotropic) $\Rightarrow$ 0.5 (oblate) $\Rightarrow$ 1.0 (prolate). The combination of G and $\Omega^{1/2}$ can divulge shape information that each alone would not and, although both are crude global descriptors, along with surface area and volume they can sometimes provide significant information about the shapes of molecules in crystals.

2.4. Two-dimensional fingerprint plots

Crystal structures of even quite simple molecules can contain many different intermolecular contacts, and there have been few attempts to condense this information into a single picture. Recently, a new scheme, NIPMAT (non-bonded interaction pattern matrix; Rowland, 1995; Desiraju, 1997; Desiraju & Steiner, 1999), has been used in an attempt to provide 'a visual representation of *all* the intermolecular interactions *simultaneously*' (Desiraju, 1997). The NIPMAT scheme uses greyscale squares of varying darkness to describe intermolecular contacts, with the darkness of each square related to the difference between the internuclear distance and the sum of the van der Waals radii of the contacting atoms; darker squares show closer intermolecular contacts. The NIPMAT picture is necessarily mirrored along the diagonal, as there are two identically shaded squares for each two-atom contact.

To our knowledge, the only published applications of the NIPMAT scheme involve a study of the π-acceptor nature of three-membered rings (Allen *et al.*, 1996), comparisons between naphthalene and terephthalic acid (Desiraju, 1997), 2-, 3- and 4-aminophenol (Nangia & Desiraju, 1998), 1,4-benzoquinone and fluoranil (Desiraju, 1996; Desiraju & Steiner, 1999), two isomers of anisylpinacolone (Kuduva *et al.*, 2000), and comparisons within a family of aminophenols (Vangala *et al.*, 2003). By way of example, and for later comparison, the NIPMAT diagrams comparing naphthalene with terephthalic acid are reproduced in Fig. 3. While useful as an aid to summarizing intermolecular interactions in a single picture, the NIPMAT scheme is limited by several factors, including the fact that a NIPMAT diagram for any molecular crystal is not unique, but rather the picture depends on the atom ordering chosen for the plot. In addition, the number of elements in the NIPMAT matrix increases as the square of the number of atoms in the structure, rendering the NIPMAT method unsuitable for larger molecules (Fabian *et al.*, 1999).

We have recently introduced a different method for summarizing the complex information contained in a molecular crystal structure into a single unique colour plot, which provides a vivid 'fingerprint' of the intermolecular interactions in the crystal (Spackman & McKinnon, 2002). Derived from the Hirshfeld surface, these two-dimensional fingerprint plots provide a summary of the frequency of each combination of d_e and d_i across the surface of a molecule and so indicate not only which interactions are present, but also the relative area of the surface corresponding to each such interaction.

A molecular Hirshfeld surface typically contains tens of thousands of individual points. Each of these surface points

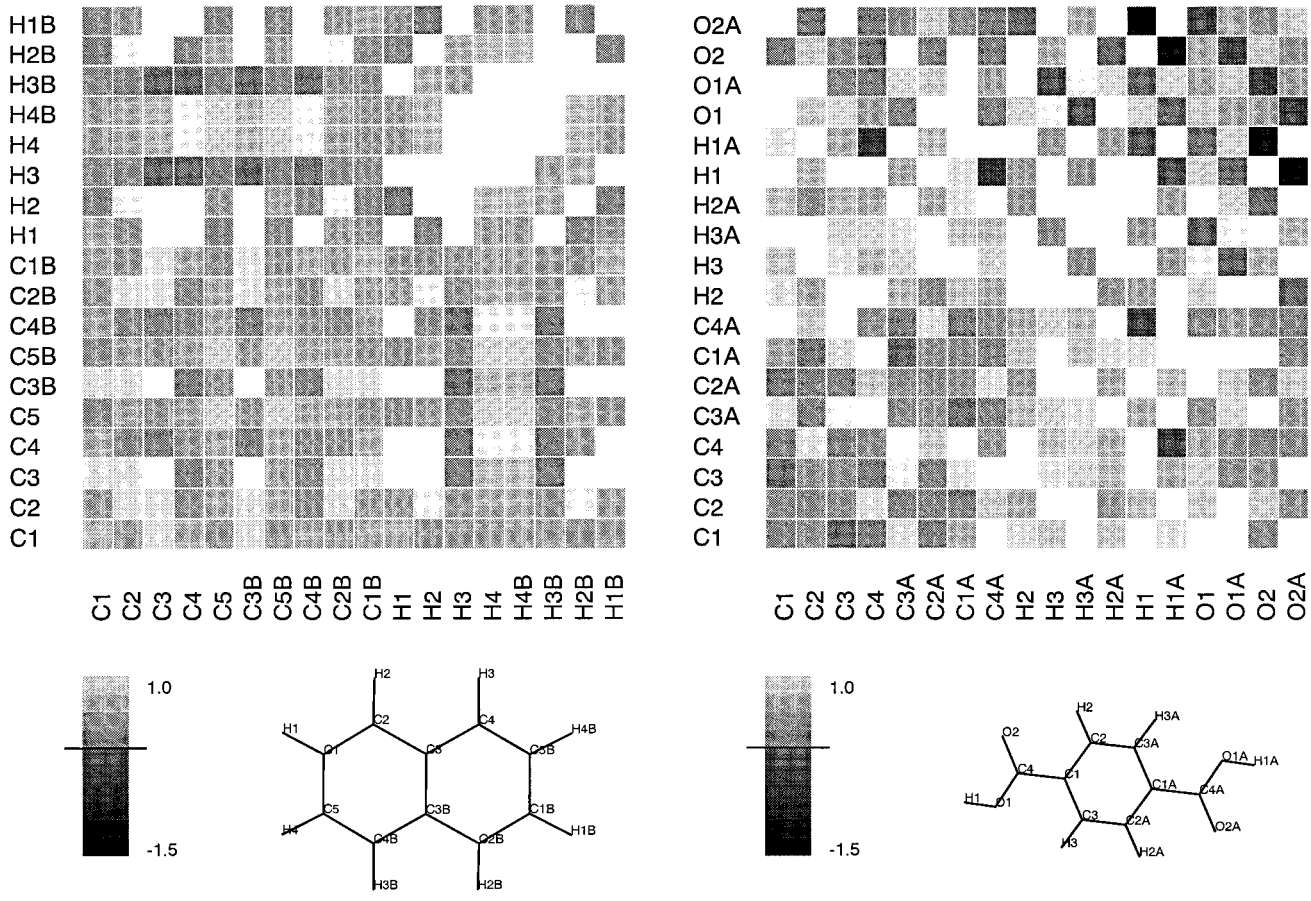

Figure 3
NIPMAT diagram for (left) naphthalene and (right) terephthalic acid. Reproduced from Desiraju (1997), *Chem. Commun.* pp. 1477–1482, with permission from the Royal Society of Chemistry.

contains information about the immediate physical environment of the molecule at that point; specifically, each point on the surface has a well defined (d_i, d_e) pair. For the purpose of constructing a two-dimensional fingerprint plot, the value of each of d_e and d_i is calculated at the centroid of each surface triangle by taking the average of the property values at the vertices of the triangle. A data bin is constructed for each (d_i, d_e) pair in the range $0.0 < d < 3.0$ Å, and the area of each triangle on the surface is added to the bin to which that triangle belongs. The two-dimensional fingerprint plot is constructed by colouring points on a two-dimensional grid according to the fraction of the total surface area contained by that bin. Empty bins are left uncoloured, bins with the smallest non-zero contribution are coloured blue, and the colour of the bins changes around the circumference of the RGB colour wheel through to red for a contribution of 0.1% or greater to the total surface area. The limit of 0.1% surface area is chosen to give the greatest colour contrast for surfaces calculated using a marching-cubes resolution of 5 a.u.$^{-1}$ and with a bin width of 0.01 Å.

Two-dimensional fingerprint plots for naphthalene and terephthalic acid (Fig. 4) illustrate the dramatic difference between the intermolecular interaction patterns for these two compounds. While the crystal structure of naphthalene is dominated by C—H$\cdots\pi$ (seen as 'wings' in the figure) and H$\cdots$H interactions (these appear where $d_e \simeq d_i$ at around the H-atom van der Waals radius of 1.20 Å), the plot for terephthalic acid features a pair of long sharp spikes characteristic of a strong hydrogen bond, and the red area near 1.7–1.8 Å shows the significant contribution made by the π–π stacking interaction. Detailed descriptions of the features of the two-dimensional fingerprint plots will be provided as each molecule or series of molecules is discussed in the relevant sections that follow, and the intimate relationship between the two-dimensional fingerprint plot and the original Hirshfeld surface for each molecule will also be considered and discussed in detail.

The two-dimensional fingerprint plots (Fig. 4) contrast with the NIPMAT diagrams for the same crystal structures (Fig. 3).

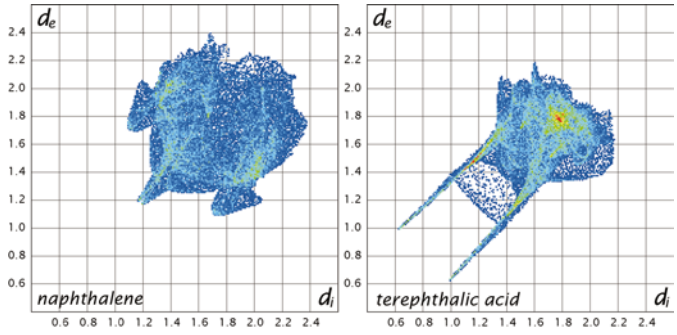

Figure 4
Two-dimensional fingerprint plots for naphthalene and terephthalic acid. Blue corresponds to the low frequency of occurrence of a (d_i, d_e) pair, while red points indicate the high frequency of the surface points with that (d_i, d_e) combination. For consistency and clarity, all two-dimensional fingerprint plots are generated showing only the region between 0.4 and 2.6 Å.

A feature shared between the NIPMAT scheme and the Hirshfeld fingerprint plots is the apparent reflection of the plots across the diagonal. While a NIPMAT diagram is necessarily exactly mirrored, this is not a required feature of a Hirshfeld surface fingerprint plot. However, because the Hirshfeld surface fills so much space, and voids are comparatively small, in many cases a point on one surface is also very close to the surface of an adjoining molecule, resulting in the apparent mirroring of the fingerprint plot. In structures having only one unique molecule in the crystal, regions on the fingerprint plot that are not mirrored across the diagonal occur *only* because of the voids between the Hirshfeld surfaces, and for this reason such features may be significant in themselves. Finally, we note that the two-dimensional fingerprint plots derived from the Hirshfeld surfaces do not scale with molecular size – the size of the plot is constant irrespective of the number of atoms in the molecule, making this method suitable for comparing crystal structures of molecules that are different in size.

3. Applications

3.1. Introduction

The Hirshfeld surface, the scalar properties that can be mapped onto the surface and the two-dimensional fingerprint plots described in the previous section represent a radically new way of looking at intermolecular interactions in molecular crystals, and one that is fundamentally different from conventional methods of crystal structure analysis. This section provides an introduction to the analysis of molecular crystal structures using the Hirshfeld surface *via* a systematic and detailed exploration of the structures of a wide range of simple molecular crystals. Examples have been chosen to cover the most common types of intermolecular interactions in molecular crystals, in order to establish the manner in which the Hirshfeld surfaces and two-dimensional fingerprint plots convey information on intermolecular interactions in the crystal.

In order to present a systematic study of intermolecular interactions such as that attempted here it is necessary to adopt some classification scheme to divide structures according to the types of intermolecular interactions present. We follow the example of Desiraju (1989), dividing structures into those featuring mainly van der Waals interactions (aliphatic hydrocarbons in §3.2 and polycyclic aromatic hydrocarbons in §3.3), structures dominated by hydrogen bonding (§3.4), and structures featuring intermolecular contacts to halogens (§3.5) and to sulfur (§3.6).

As we have already mentioned, the scale of the properties mapped onto the Hirshfeld surface, and in particular d_e, varies according to the atom types and intermolecular interactions present in the structure. In the following discussion, curvedness is always mapped on the Hirshfeld surfaces between −4.0 (red) and +0.4 (blue), and shape index is always mapped between −1.0 (red) and +1.0 (blue). In order to maximize the information conveyed by d_e, this property is mapped on the

Hirshfeld surfaces on a scale most appropriate for the molecules featured in each section. To enable direct comparison between structures, d_e is mapped on the same scale within each section, and the range of d_e on the Hirshfeld surfaces is explicitly specified in the first figure of each section. For consistency and clarity, all two-dimensional fingerprint plots display only the region between 0.4 and 2.6 Å.

Although our discussion of molecular crystals will refer to molecules most often by their common name, we identify all crystal structures used to create the various maps and plots by their CSD refcode, which uniquely identifies the particular structural study for the compound; references to the original literature accompany the refcodes in the figure captions. Analysis of individual intermolecular contacts in the crystal was undertaken at times with the recently released *MERCURY* package (Bruno *et al.*, 2002), now part of the CSD software, although detailed analysis with this software was hampered by its present inability to standardize covalent X—H bond lengths to average neutron diffraction values. Our present software package for the generation and analysis of Hirshfeld surfaces is exclusively command-line driven for rapid development, and produces output compatible with the three-dimensional data visualization program *Geomview* (Geomview, 1992–1996) for the display of surfaces and tube-style molecular diagrams. Two-dimensional fingerprint plots are currently generated in PostScript.

3.2. Aliphatic hydrocarbons

Crystal structures of aliphatic hydrocarbons are of interest because they are bound almost entirely by weak dispersion forces, and analysis of these structures allows the identification and detailed examination of patterns of C—H···H—C contacts, as well as C···H contacts, in relative isolation.

3.2.1. The normal alkanes. Although structural studies of the normal paraffins were pioneered by Müller (1930, 1932), who investigated these compounds as well as other long-chain molecules, Kitaigorodsky's (1961, 1973) classic books conveniently summarized previous work and provided new insight into the packing of these hydrocarbons. The quality of the crystallographic data used by Kitaigorodsky was reasonable at best and the analysis was limited to parameters such as the distance between layers of molecules. The data were good enough, however, to enable an analysis of crystal packing in terms of the cross section of the molecule, with interlayer distance shown to increase monotonically with increasing chain length.

Our present study takes advantage of structural studies conducted more recently and aimed at investigating the curious melting-point trends among the normal alkanes. Boese and co-workers (Boese *et al.*, 1999; Thalladi & Boese, 2000) have investigated the trend that sees the alkanes with an even number of C atoms having a relatively higher melting point than the odd members of the series. The structures of the *n*-alkanes featured here are those determined by Boese *et al.* (1999) at 90 K, with the exception of propane (which was determined at 30 K) and ethane (previously determined at 90 K by van Nes & Vos, 1978).

Hirshfeld surfaces for the *n*-alkanes are shown in Fig. 5. With the exception of propane, heptane and nonane, all structures have $Z' = 0.5$, so the reverse view of the surface is identical to that shown in Fig. 5. For structures with $Z' = 1.0$, the differences in the reverse view are very subtle and are barely observable at the size displayed. In addition to noting the general appearance of the Hirshfeld surfaces of these simple hydrocarbons, where intermolecular contacts are exclusively of the type H···H or C···H, much more subtle differences between the environments of the molecules can be identified from the surfaces. A characteristic pattern of C···H contacts is evident on the surface of pentane, with contacting regions of complementary blue (convex) and red (concave) shape index, labelled 1 and 2, respectively, in Fig. 5. This pattern continues in the higher *n*-alkanes, although subtle differences in the pattern are apparent between the even and odd members of the series.

A pattern of H···H contacts is evident along the right-hand side of the molecules, starting from hexane. This pattern appears as a series of bright-orange spots with small d_e, marked 3 in Fig. 5, in conjunction with a feature on the shape index map that characterizes a direct like-atom–like-atom approach; where two C—H groups in adjacent molecules approach each other in a head-to-head arrangement, the shape index mapped onto the surface shows a distinctive blue cross. The close approach of two identical atoms results in a marked flattening of the Hirshfeld surface and when the surface is very flat, the shape index is very sensitive to minor changes in surface shape. In this situation the second-nearest atoms to the surface impart a greater influence on the appearance of the shape index. This feature often appears in conjunction with a yellow or red spot on the curvedness picture (depicting an especially flat region) and is more prominent where the contacting atoms are larger (such as chlorine and sulfur); this feature will be discussed in more detail in §3.6.

The crystal structure of *n*-butane is anomalous in this series and is of particular interest because the CSD contains five reported structures. Although Refson & Pawley (1986) previously reported four structures at temperatures ranging from 5 to 120 K, we have used the 90 K structure from Boese *et al.* (1999), who reported disorder in that structure and an R factor of 0.019. All five structures in the CSD result in distinctly different two-dimensional fingerprint plots, but the more recent structure (DUCKOB04) is considered the most acceptable, as the others exhibit what appear to be non-physical values for $d_e^{\min}$, between 1.07 and 0.98 Å. Such short contacts may be a result of the orientational disorder or they may reflect an average orientation of the H atoms. For DUCKOB04, $d_e^{\min}$ is a more reasonable 1.18 Å, much more in line with accepted values of the van der Waals radius (1.20 Å; Bondi, 1964). The practice of using the Hirshfeld surfaces and fingerprint plots to determine the most reliable of the published structures of *n*-butane highlights a potentially valuable application as a crystallographic tool.

Each fingerprint plot of the *n*-alkanes (Fig. 6) summarizes the interactions experienced by the entire molecule and condenses this information into a single two-dimensional plot. While these plots again mainly highlight the similarities between these structures, and the two-dimensional fingerprint plots are broadly similar across each class of compound presented in this paper, close inspection of the two-dimensional fingerprint plots highlights very subtle differences between these crystal structures. The fingerprint plot for propane is clearly anomalous in this series. The diffuse blue region (labelled 1) results from a small part of the surface with large distances to the nearest atoms and suggests a less than ideal packing arrangement for the molecule in the crystal. While the closest distances are similar to those for the other small alkanes, the longest distances are significantly larger than those for other molecules smaller than heptane and this apparently poor packing efficiency of propane suggests a possible explanation for its low melting point. The two-dimensional fingerprint plots for both propane and pentane show a lesser contribution from the red streak of H···H contacts that features prominently in the plots of the other *n*-alkanes, indicating that head-to-head H···H contacts are less prevalent in these two structures. This difference can also be seen on the d_e surfaces (Fig. 5), where the surface feature resulting from head-to-head H···H contacts (labelled 3 and noted earlier) appears to be absent from the surfaces of propane and pentane.

The fingerprint plot for butane shows one distinct difference from those for the other *n*-alkanes: a sharp point (2 in Fig. 6) due to short H···H contacts giving a distinctly different fingerprint from those contacts in the other structures in Fig. 6. As noted above, the minimum d_e of 1.18 Å is not unrealistically short, but it is unusual and the shortest for all the *n*-alkanes in the figure (the actual range of $d_e^{\min}$ for this series is 1.18–1.23 Å). This anomaly may be an artefact of the disorder in the structure and related to the *R* factor of almost 0.20 reported for this structure. The d_e surface for *n*-butane shows a bright-orange spot on the surface at the central methylene group (4 in Fig. 5) and a red spot appears in the same region on the curvedness surface, reflecting a very flat region. These features result from two symmetry-equivalent H···H contacts, giving four contacts to hydrogen at 2.37 Å and involving all four methylene H atoms.

From hexane onwards the crystal structures of the *n*-alkanes display a regular pattern (Boese *et al.*, 1999). They all crystallize in $P\bar{1}$ and the even members have one centrosymmetric molecule in the unit cell, while the odd members have $Z' = 1.0$ and two molecules in the unit cell. All of the *n*-alkane structures exhibit a narrow range of d_e over the surface (the difference between the longest and the shortest d_e across the whole series is around 1.0 Å, lower than for any other family of molecules studied in this section), confirming that these crystal structures form in a way that optimizes close-packing efficiency rather than any particular atom–

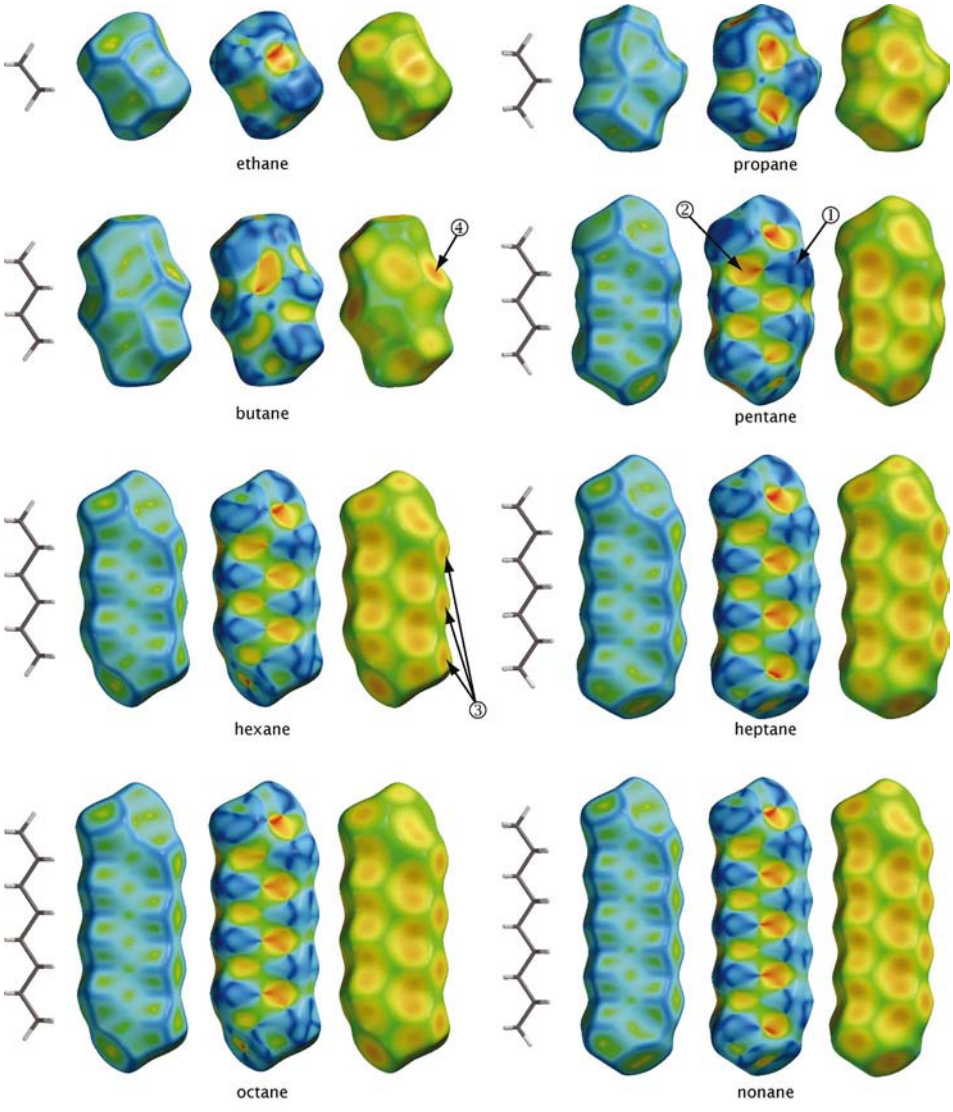

Figure 5
Hirshfeld surfaces for the *n*-alkane series: ethane (ETHANE01; van Nes & Vos, 1978) and propane through nonane (JAYDUI, DUCKOB04, PENTAN01, HEXANE01, HEPTAN02, OCTANE01 and QQQFAY01; Boese *et al.*, 1999). Each molecule is shown with the Hirshfeld surface mapped with curvedness (left), shape index (centre) and d_e [right; for this series mapped between 1.0 (red) and 2.5 Å (blue)].

atom intermolecular contact. Fig. 7 plots the melting-point alternation for the *n*-alkanes alongside the range of d_e for each molecule in the series. Here, a trend emerges relating the d_e range and melting point for hexane and beyond; the higher-melting even members have a relatively lower d_e range (reflecting a more efficient close-packing mode) than the lower-melting-point odd members. Fingerprint plots for heptane and nonane both feature a region of diffuse long-distance contacts, similar to that previously noted in propane (3 in Fig. 6), and these arise from the poor packing efficiency at one end of the molecule, as previously reported by Boese *et al.* (1999). After nonane, the smallest *n*-alkanes for which crystal structures have been accurately determined are *n*-octadecane ($C_{18}H_{38}$), *n*-eicosane ($C_{20}H_{42}$) and *n*-tetracosane ($C_{24}H_{50}$), and the Hirshfeld surfaces and fingerprint plots for these molecules (not shown) quite clearly reveal that the molecular packing for these longer-chain even *n*-alkanes remains very similar to that for the smaller even *n*-alkanes.

3.2.2. Ethane, ethylene and acetylene. This section focuses on three molecules of similar size, but with the main non-bonded contact changing from H···H for ethane through to C···H for acetylene. Hirshfeld surfaces for these molecules (Fig. 8) reflect the change in intermolecular contact patterns with increasing saturation, but this is most strikingly seen in the two-dimensional fingerprint plots (Fig. 9). The fingerprint plot for ethane is dominated by H···H contacts, giving rise to the red streak where $d_e \simeq d_i$, as discussed in the previous section, although the spread of points across the diagonal is slightly greater than for the longer *n*-alkanes. This difference is at least in part due to a significant C···H contact to the back of each methyl group, one of which is visible as a broad red spot on the d_e surface (1 in Fig. 8).

The C═C double bond in ethylene provides both the geometric and the electronic conditions to enable close C—H···π contacts in the crystal. This contact is manifested as a bright-orange spot on the d_e surface (2 in Fig. 8), directly above the centre of the C═C bond, and generates a distinct pattern of a pair of 'wings' in the two-dimensional fingerprint plot (1 in Fig. 9); it will become evident that this is a characteristic feature of any C—H···π or similar contact. The fingerprint plot for ethylene retains the central red streak evident for ethane and due to H···H contacts in the crystal, although this feature is clearly less dominant in the crystal structure of ethylene.

The two-dimensional fingerprint plot for acetylene shows immediately that this crystal structure is fundamentally different from those of ethane and ethylene. This plot is completely devoid of close H···H contacts and is instead dominated by C—H···π 'weak hydrogen bonds' (Desiraju & Steiner, 1999), which appear again as wings in the fingerprint

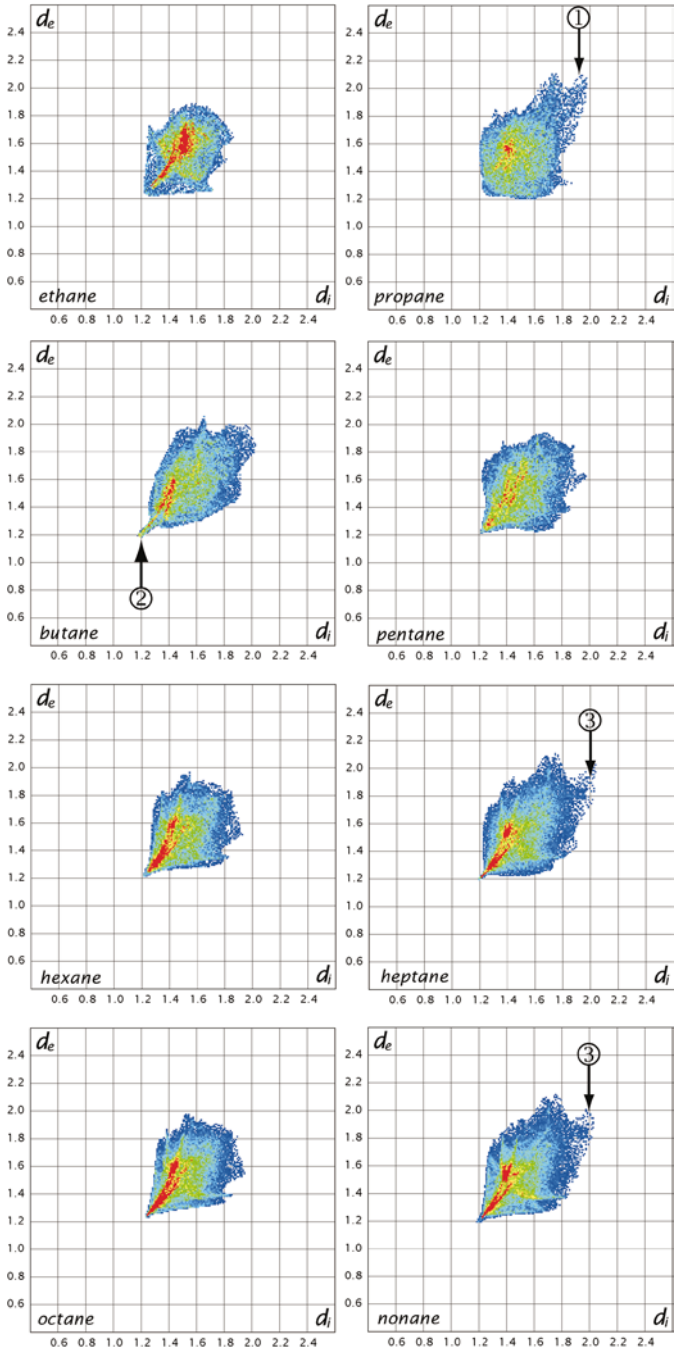

Figure 6
Two-dimensional fingerprint plots for the *n*-alkanes; see Fig. 5 for Hirshfeld surfaces and refcodes.

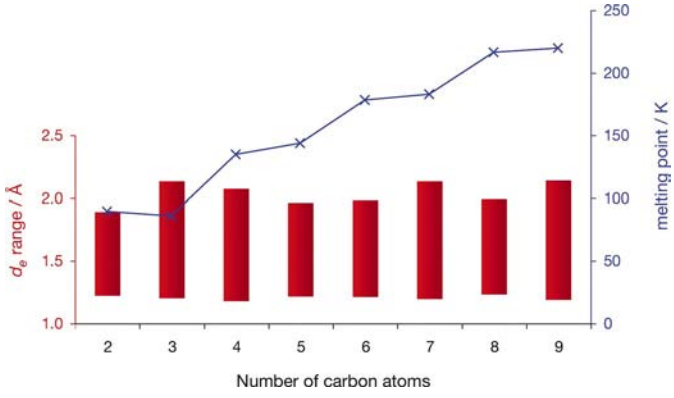

Figure 7
Trends in the range of d_e (red), and the melting points (blue) for the *n*-alkanes.

plot (2 in Fig. 9). Each triple C≡C bond accepts six of these very weak hydrogen bonds in the crystal and they appear on the d_e surface as orange spots. Acetylene is also characterized by a considerably less efficient close packing in the crystal with contact distances in the fingerprint plot extending much farther than those for ethane and ethylene. This difference is manifested on the d_e surface by the dark-blue regions representing large contact distances, which are absent on the Hirshfeld surfaces of ethane and ethylene, and also on the fingerprint plot, where d_e extends well beyond 2.4 Å.

3.3. Polycyclic aromatic hydrocarbons

The crystal structures of polycyclic aromatic hydrocarbons are largely dominated by weak van der Waals interactions, and interactions between π systems are ubiquitous in nature, playing an important role in determining the structures and properties of many molecular aggregates (Hunter *et al.*, 2001; Hunter & Sanders, 1990). The lack of strong directional forces in the crystal structures of polycyclic aromatic hydrocarbons has motivated attempts to rationalize their crystal structures using purely geometrical considerations (Desiraju & Gavezzotti, 1989) and, in a similar fashion to the *n*-alkanes, attempts have been made to correlate the physical properties of polycyclic aromatic hydrocarbons with molecular shape and size (Dunitz & Gavezzotti, 1999). The crystal structures of the polycyclic aromatic hydrocarbons were originally given two classifications depending on their molecular shape. Robertson (1951) suggested that if the molecule is disk-like, with a surface area that is large compared with its thickness, there is a tendency for the molecule to pack in offset columns, with the molecular plane inclined at an angle of about 45° to the translation axis. The second category includes molecules with smaller surface areas, which pack with greater inclination to the symmetry plane, in a herringbone motif. Desiraju & Gavezzotti (1989) refined and extended the classification of these crystal structures and arrived at four distinct structure classes: 'herringbone structures' correspond to Robertson's second class and optimize C—H···π contacts in the crystal; 'γ structures' correspond to Roberston's offset column stacking and feature π–π stacking as the dominant intermolecular contact, but still with some C—H···π contacts; 'sandwich herringbone' structures are a hybrid of herringbone and γ structures (two parallel molecules arranged in a sandwich motif, with each 'sandwich' arranged in turn in a herringbone motif); 'β structures' are completely devoid of C—H···π contacts, the molecules being arranged in flat sheets where the only significant intermolecular contacts are π–π interactions between sheets and H···H contacts within sheets. This section features an exploration of the Hirshfeld surfaces and fingerprint plots of several structures belonging to each of the classes described by Desiraju & Gavezzotti, focusing on the molecules mentioned in that study for which accurate crystal structures, including H-atom positions, have been published.

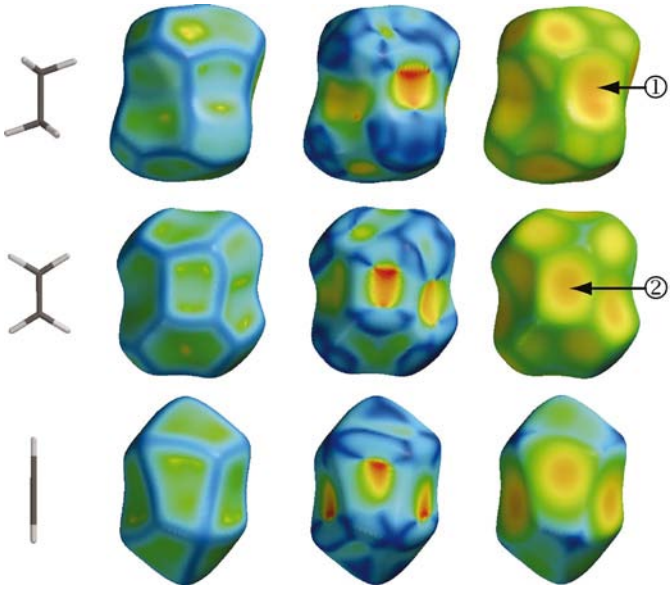

Figure 8
Hirshfeld surfaces for ethane (top; ETHANE01; van Nes & Vos, 1978), ethylene (centre; ETHLEN10; van Nes & Vos, 1979) and acetylene (bottom; ACETYL02; McMullan *et al.*, 1992).

3.3.1. Herringbone structures. For molecules packing in a herringbone arrangement, the dominant intermolecular interaction is the C—H···π (or C—H···C) contact. Structures in this category include benzene and the linear fused

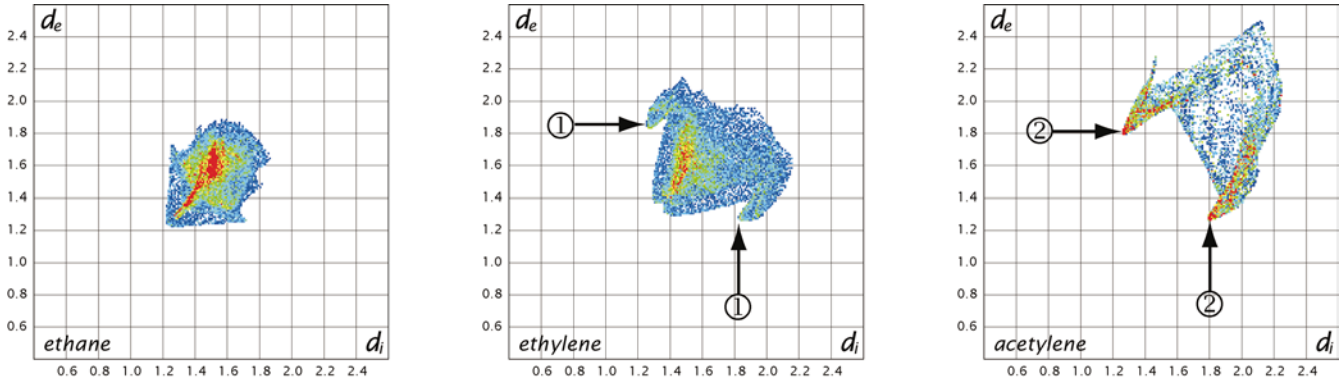

Figure 9
Two-dimensional fingerprint plots for ethane, ethylene and acetylene; see Fig. 8 for Hirshfeld surfaces and refcodes.

aromatics naphthalene, anthracene, tetracene and pentacene. Tetracene and pentacene both crystallize with two molecules in the asymmetric unit, and so each structure contains two distinct Hirshfeld surfaces; for the sake of clarity these are not discussed in this section. For crystal structures where the molecule does not lie on a centre of inversion, leading to patterns of intermolecular interactions that are different on each side of the molecule, the Hirshfeld surface is shown in two views, arbitrarily labelled 'front' and 'back'. In all other cases, a single view of the Hirshfeld surface is shown.

The C—H$\cdots\pi$ interaction manifests itself on the Hirshfeld surfaces of benzene, naphthalene and anthracene in several interesting ways. We have previously noted that the shape of the surface clearly reflects this contact (McKinnon *et al.*, 1998*b*), with a broad depression in the surface above the ring for benzene, and extended along the rings of naphthalene and anthracene. The map of shape index clearly shows these depressions as large red regions of concave curvature, while C—H donor regions have exactly the opposite curvature and thus have shape indexes of equal magnitude and opposite sign, and are blue. Such clear regions of complementary colour on the shape index surface are characteristic of any regions of the surface that come into contact with each other, and subtle differences in each of these complementary regions allow the unique identification of each individual interaction. For example, careful inspection of the shape index surface for anthracene (Fig. 10) shows that the two regions labelled 1 make contact with one another and the two regions labelled 2 make contact with one another. Such detailed inspection is greatly aided by the ability to rotate the surface using three-dimensional graphics software, an aspect of the use of Hirshfeld surfaces that cannot be easily conveyed in this paper.

Two-dimensional fingerprint plots for benzene, naphthalene and anthracene (Fig. 11) provide a concise summary of the intermolecular interactions occurring in these crystals. It is immediately apparent from these plots that the structure of benzene is anomalous in this series of herringbone aromatics, as noted previously by Desiraju & Gavezzotti (1989); its fingerprint plot is clearly different from those of the other two members of this family. For benzene, the C—H$\cdots\pi$ contact is directed very close to the centroid of the benzene ring, producing a distinctive feature in the fingerprint plot, labelled 1, which is very different to the appearance of the C—H$\cdots\pi$ contact in the fingerprint plots of naphthalene and anthracene, also labelled 1 on their respective plots. This difference is also noticeable in Fig. 10, where the d_e surface shows the close contact as a large red depression directly above the centre of the ring, while in naphthalene and anthracene this contact is offset slightly to the left of the molecule. It is clear from the positions of the 'wings' in the fingerprint plots that the C—H$\cdots\pi$ contact is shorter in naphthalene ($d_{C\cdots H} = 2.81$ Å) than in benzene ($d_{C\cdots H} = 2.93$ Å) and shorter still in anthracene ($d_{C\cdots H} = 2.70$ Å). The Hirshfeld surface of anthracene (Fig. 10) displays two distinct depressions above the molecular rings, resulting from two different C—H$\cdots\pi$ contacts, one clearly closer than the other. The shorter contact is that labelled 1 on the two-dimensional fingerprint plot, while the longer contact produces a more subtle fingerprint, labelled 5.

The Hirshfeld surface and its fingerprint plots are able to provide information not only about areas of close contacts, and hence strong interaction, but also about more distant contacts and areas where interactions are weakest. Benzene exhibits three distinct voids in the crystal, areas where d_e is large. The largest value of d_e for benzene is 2.53 Å and the corresponding void in the structure appears as a characteristic feature in the fingerprint plot, labelled 2 in Fig. 11. The region of the Hirshfeld surface that gives rise to this fingerprint is also labelled 2 in Fig. 10 and the other voids in the crystal structure of benzene, with fingerprints labelled 3 and 4, are similarly labelled on the d_e surface.

Phenanthrene crystallizes in at least two polymorphic forms (Petrícek *et al.*, 1990). The room-temperature ordered phase (Kay *et al.*, 1971) adopts a non-centrosymmetric 'herringbone' structure and its Hirshfeld surface is shown along with the two-dimensional fingerprint plot in Fig. 12. An unusually short intermolecular H$\cdots$H contact in the crystal shows up as a characteristic spike in the fingerprint plot, where $d_e = d_i \simeq 1.15$ Å (1 in Fig. 12), and two bright-red spots on the d_e surface (labelled 1 and 2). Two longer H$\cdots$H contacts are also observed, at 2.53 and 2.56 Å, causing the H$\cdots$H fingerprint to broaden substantially at $d_e = d_i \simeq 1.25$ Å. The dominating motif of the structure of phenanthrene, and hence of the Hirshfeld surface and fingerprint plot, is produced by C—H$\cdots\pi$ contacts. The evidence of these contacts on the d_e

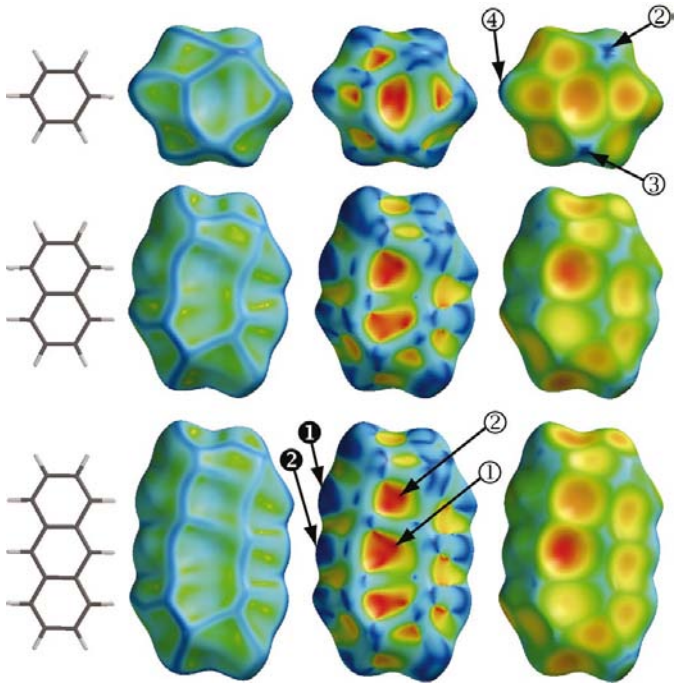

Figure 10
Hirshfeld surfaces for benzene (top; BENZEN07; Jeffrey *et al.*, 1987), naphthalene (middle; NAPHTA10; Brock & Dunitz, 1982) and anthracene (bottom; ANTCEN10; Brock & Dunitz, 1990). For this series d_e is mapped between 1.0 (red) and 2.5 Å (blue).

surface is clear and the shape index provides an even clearer indication *via* its complementary colour scheme, with the ribs of red colour marking depressions above the π-electron system and the corresponding blue regions adjacent to the H atoms. Each of these contacts can be individually identified from the colour patterns on the shape index surface, an example being the C—H marked 3 contacting with the π-electron cloud in the region marked 4.

The crystal structure of triphenylene is the first in this section to feature any significant contribution from π–π interactions in the crystal, although it is still classified by Desiraju & Gavezzotti (1989) as a 'herringbone structure'. The presence of π–π stacking is evident on the Hirshfeld surface (Fig. 13), as a large flat region towards the bottom of both sides of the molecule in the figure, and is most clearly visible on the curvedness surface. On the d_e surface this feature appears as a relatively flat green region, where the contact distances are all very similar ($d_e \simeq 1.8$ Å). The corresponding fingerprint plot in Fig. 13 shows this interaction as a region of pale blue/green colour on the diagonal at around $d_e \simeq d_i \simeq 1.8$ Å (1 in Fig. 13). The pattern of red and blue triangles on the same region of the shape index surface is characteristic of π–π stacking, and can actually be used to determine the way in which the molecules overlap and make contact with each other. The pattern of red and blue triangles on this region of both sides of the molecule shows how adjacent molecules in the crystal are related by translation; the region on top of the molecule (labelled 2 in the front view) packs against the region on the bottom of the surface (labelled 2 in the back view). This conclusion is further evident from the shape of the blue outline on the curvedness surface, which unambiguously delineates contacting patches of the molecules.

In addition to the π–π stacking motif mentioned above, the crystal structure of triphenylene features a significant contribution from C—H$\cdots\pi$ interactions, including a distinctive row of contacts across the top of the back view in Fig. 13, and by examining the shape index map the three red depressions in this region can be readily matched to the corresponding region adjacent to the C—H groups at the top of that surface. A crystal-packing diagram (Fig. 14) illustrates how this combination of intermolecular π–π stacking and C—H$\cdots\pi$ motifs produces the patterns seen on the Hirshfeld surface.

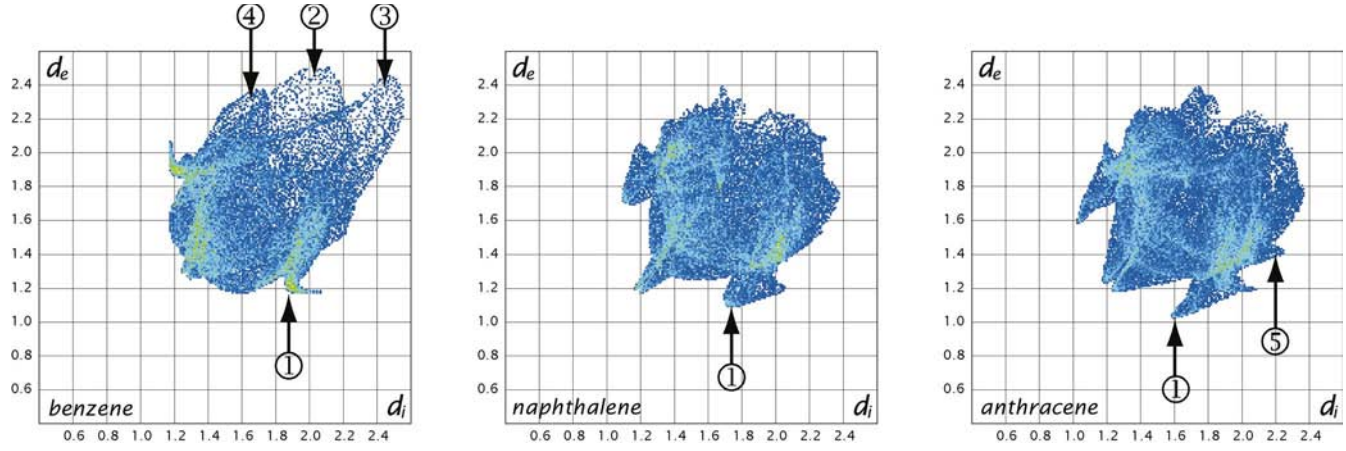

Figure 11
Two-dimensional fingerprint plots for benzene, naphthalene and anthracene; see Fig. 10 for Hirshfeld surfaces and refcodes.

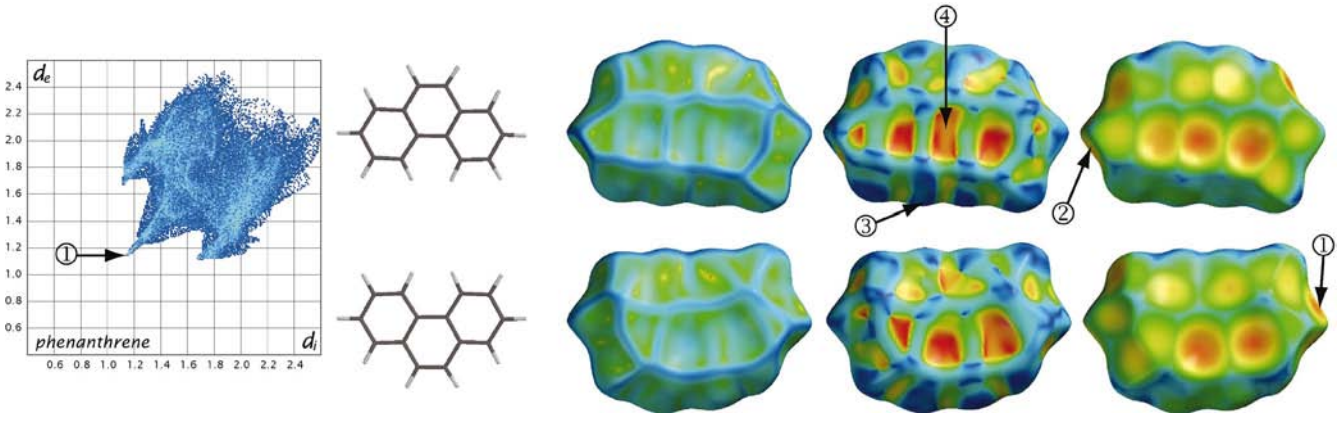

Figure 12
Two-dimensional fingerprint plot and Hirshfeld surfaces (front and back views) for phenanthrene (PHENAN13; Kay *et al.*, 1971).

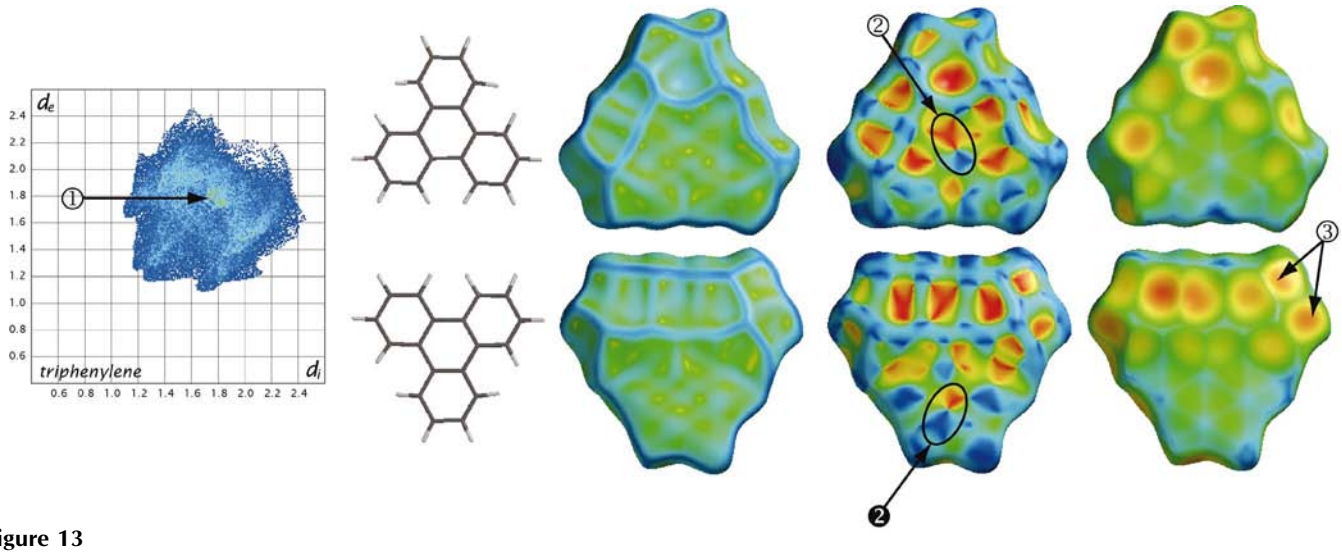

Figure 13
Two-dimensional fingerprint plot and Hirshfeld surfaces (front and back views) for triphenylene (TRIPHE11; Ferraris *et al.*, 1973).

A somewhat more subtle feature is evident in the fingerprint plot for triphenylene and it was also visible, though less so, in the corresponding plots of benzene, naphthalene and anthracene. In each of these cases there is a distinct splitting of the short H···H fingerprint at $d_e \simeq d_i \simeq 1.2$ Å. This splitting occurs when the shortest contact is between three atoms, rather than a direct two-atom contact. Fig. 15 shows a schematic diagram of such a three-centre contact; for point A on the surface (shaded) d_i is a minimum and d_e is larger, while at B, d_e is a minimum and d_i is larger. At C, $d_e \simeq d_i$, but both are larger than the minima in either case. For triphenylene, this feature arises from two close C—H approaches from above the plane of the molecule, which appear as two orange spots on the d_e surface, labelled 3 in Fig. 13.

3.3.2. Sandwich herringbone structures. These structures feature two crystallographically related molecules paired *via* a π–π stacking arrangement, the pair packing in turn in a herringbone arrangement, so that one side of each molecule is dominated by π–π stacking interactions, while the other side is dominated by C—H···π contacts. This arrangement is evident in the crystal-packing diagram for pyrene (Fig. 16) and the corresponding Hirshfeld surface of the molecule (Fig. 17) clearly reflects this packing arrangement; the top view of the molecule shows the same pattern of C—H···π contacts previously noted in the herringbone structures and the closest C—H···π contact is quite short ($d_e^{\min} = 1.05$ Å in this region). The view from the other side of the molecule shows a very flat surface characteristic of π–π contacts, where two molecules pack in offset, parallel, graphite-like sheets. The π–π stacking motif is manifested in the two-dimensional fingerprint plot (Fig. 18) as a green region with $d_e \simeq d_i$, starting at ~ 1.75 Å (labelled 1) and corresponding to an interlayer distance of 3.5 Å.

The alternating blue and red triangles on the back view of the shape index surface result from the offset stacking of the dimer. As described earlier, the colour of the shape index is exactly complementary where two molecular surfaces touch each other, and this feature can be used to establish the precise relationship between molecules in the crystal without viewing a packing diagram. This feature is discussed in more detail in the following section, but for now we note that the alternating red and blue triangles on the shape index surface in Fig. 17 are characteristic of graphite-like layered packing.

The crystal structure of pyrene also features an unusually short H···H contact, with $d_e^{\min} = d_i^{\min} = 1.02$ Å. Using coordinates corrected for rigid-body motion, this H···H contact distance was reported in the original room-temperature neutron diffraction study as 2.07 (1) Å (Hazell *et al.*, 1972), but curiously this unusually short contact elicited no discussion in the text of that paper. Earlier structural work by Camerman & Trotter (1965) also completely neglected this close contact in a table of shortest intermolecular contacts, though it is clearly present in their structure. The crystal structure of pyrene has now been the subject of several reinvestigations and there seems no doubt about the existence of this unusually short

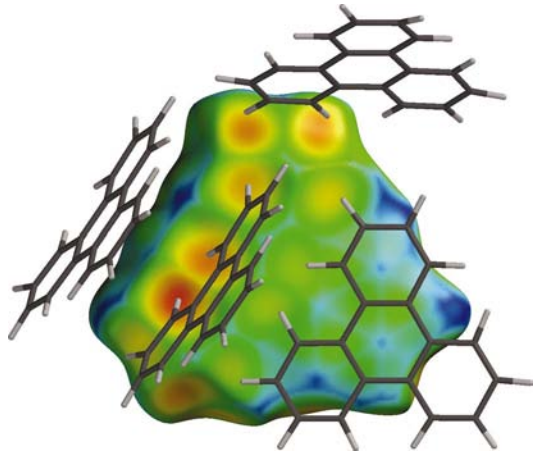

Figure 14
Crystal-packing diagram for triphenylene, with the Hirshfeld surface of the central molecule mapped with d_e.

contact (Dunitz & Gavezzotti, 1999). The low-temperature form of pyrene (PYRENE07) features a similarly π–π stacked dimer, although the closest contacts are significantly longer than those in the high-temperature form.

Fingerprint plots for two more 'sandwich herringbone' structures, perylene and quaterrylene, are shown along with that for pyrene in Fig. 18. These two-dimensional fingerprint plots show that a short H$\cdots$H contact of just over 2.0 Å occurs in all three crystal structures, although it is slightly longer in quaterrylene. It is also clear from these plots that as the size of the molecule increases, the two major interactions in the crystal, C—H$\cdots\pi$ and π–π stacking, become more visually dominant in the plots. The colour of the π–π stacking fingerprint, near $d_e = d_i \simeq 1.8$ Å, changes from pale green in pyrene (1 in Fig. 18) to yellow in quaterrylene as the relative contribution from π–π stacking over the entire surface increases.

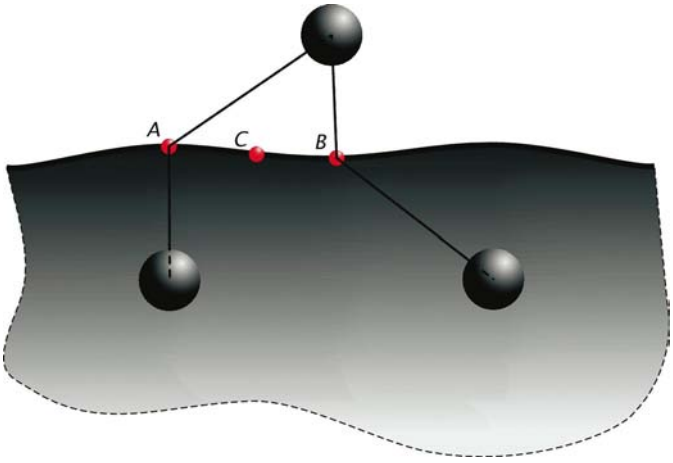

Figure 15
Schematic diagram of a three-atom close contact; the relevant Hirshfeld surface is the shaded region.

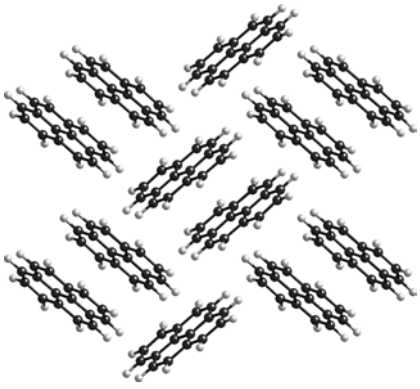

Figure 16
Crystal-packing diagram of pyrene (PYRENE02; Hazell *et al.*, 1972).

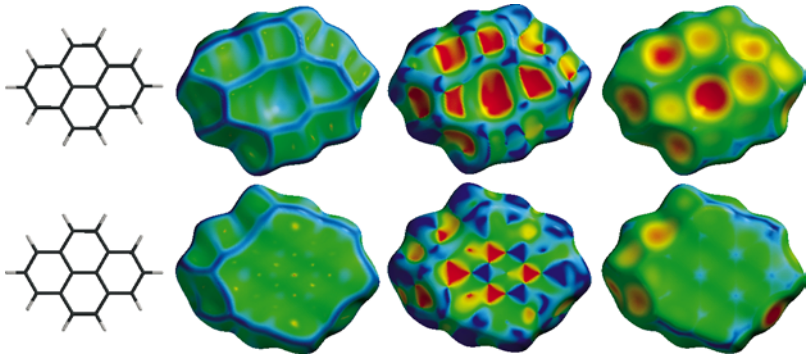

Figure 17
Front and back views of the Hirshfeld surface of pyrene.

The corresponding Hirshfeld surfaces for perylene and quaterrylene (Fig. 19) highlight the very similar nature of the packing for these two molecules in particular, and for the sandwich herringbone structures in general. The front of each surface shows that the C—H donors now approach the π acceptors parallel to the long molecular axis and a side view of quaterrylene (Fig. 20) emphasizes the complementary nature of the shape index, where the blue region on the surface adjacent to each C—H group can be visually matched to each individual red depression above the rings in Fig. 19.

3.3.3. The γ structures. As the size of the molecule increases for these fused polycyclic aromatic hydrocarbons the C—H$\cdots\pi$ interaction becomes less dominant and π–π stacking becomes increasingly important to the crystal packing. Fig. 21 displays Hirshfeld surfaces for three examples characterized as γ structures: coronene, hexabenzocoronene and benzodicoronene. The large flat faces of these molecular surfaces ensure that for any close-packing arrangement, π–π stacking is the dominant feature in these crystal structures, as exemplified by the crystal-packing diagram of coronene (Fig. 22). The Hirshfeld surfaces in Fig. 21 illustrate the manner in which the mapping of various functions on these surfaces can strongly reflect the crystal packing in both dramatic and subtle ways. As already noted, the very flat nature of the surface above the plane of the molecule, with alternating red (concave) and blue (convex) regions of the shape index, is characteristic of π–π stacking of aromatic molecules. The d_e surface clearly conveys the position of neighbouring aromatic rings above the plane of these molecules, where the centre of each ring corresponds to a local peak in d_e and appears as a blue spot on the surface. However, the offset of stacked molecules with respect to each other is even more dramatic on the shape index surface. Fig. 23 illustrates this for benzodicoronene, with the Hirshfeld surface mapped with the shape index displayed in a semi-transparent mode; the nearest neighbour in the crystal is also shown. Where there are atoms directly outside the surface, but none directly inside, the surface is concave, the shape index approaches −1.0 and the surface is red. Where there are atoms directly inside the surface, but none directly outside, the surface is convex, the shape index approaches +1.0 and the surface is blue. Green, essentially flat, regions of the surface result from an atom outside the surface lying directly above an atom inside the surface. In this manner the difference between packing modes of benzodicoronene and hexabenzocoronene is easily elucidated from the surfaces in Fig. 21, with the graphite-like offset in benzodicoronene produ-

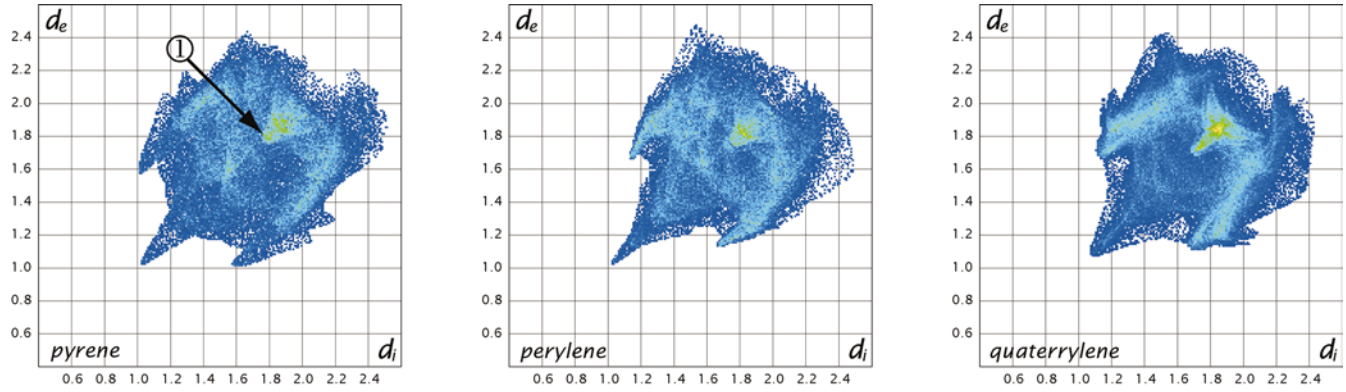

Figure 18
Two-dimensional fingerprint plots for pyrene (PYRENE02; Hazell *et al.*, 1972), perylene (PERLEN04; Näther *et al.*, 1998) and quaterrylene (QUATER10; Kerr, 1987).

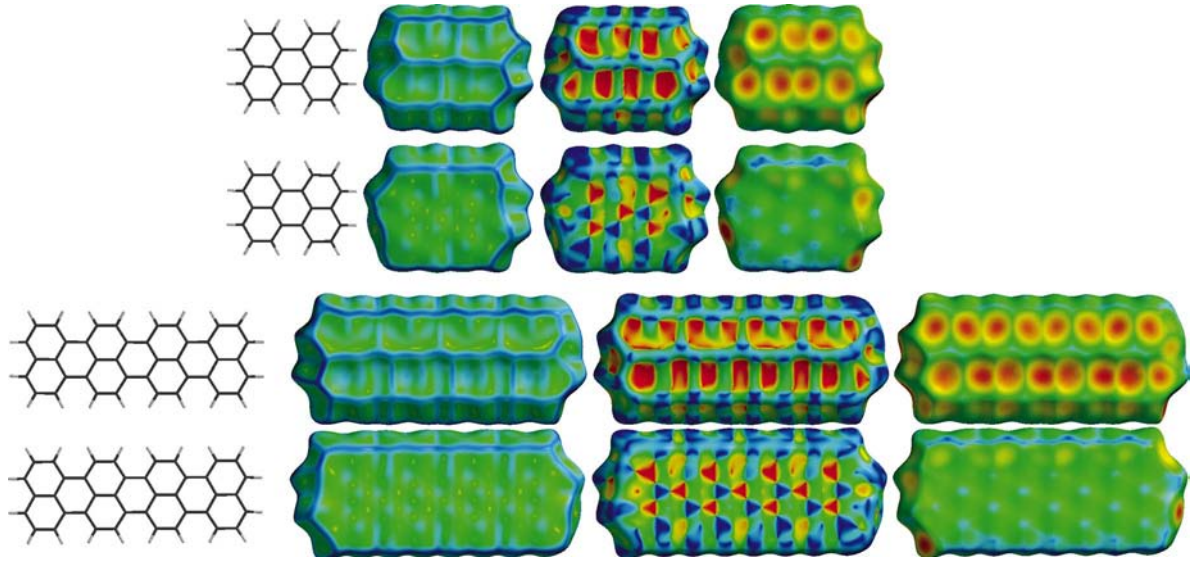

Figure 19
Hirshfeld surfaces (front and back views) of perylene (PERLEN04; Näther *et al.*, 1998) and quaterrylene (QUATER10; Kerr, 1987).

cing a pattern in the shape index of equilateral red and blue triangles with local threefold symmetry, while the offset in hexabenzocoronene produces an alternating rhomboidal pattern of blue and red regions of the shape index.

The fingerprint plots of these γ structures (Fig. 24) show strikingly how the three main types of intermolecular contacts prevalent in these crystal structures vary in their relative contribution to each of the structures. The H$\cdots$H contacts labelled 1 on the plot for coronene, and clearly visible on all three fingerprint plots, are shortest in coronene, where $d_e^{\min} = 1.09$ Å, slightly longer in benzodicoronene ($d_e^{\min} = 1.11$ Å) and considerably longer in the structure of hexabenzocoronene ($d_e^{\min} = 1.20$ Å). The C—H$\cdots\pi$ fingerprint, labelled 2 in the figure, is most prominent in the crystal structure of hexabenzocoronene and is also clearly present in coronene. However, the fingerprint plot for benzodicoronene is set apart from all previous fused aromatic hydrocarbons in this section in that it shows almost no contribution from the C—H$\cdots\pi$ fingerprint, by virtue of the fact that the stacking direction is now very close to perpendicular to the molecular plane (Fig. 25). The number of C—H$\cdots\pi$ contacts in the crystal is also related to the offset between two adjacent

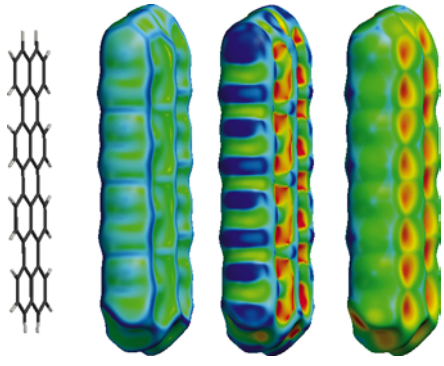

Figure 20
Side view of the Hirshfeld surface of quaterrylene (QUATER10; Kerr, 1987), showing the C—H$\cdots\pi$ donors as a series of blue (convex) regions on the shape index surface.

molecules when viewed perpendicular to the molecular plane (as in Fig. 23); the much larger offset between the two adjacent hexabenzocoronene molecules reflects a greater contribution from C—H$\cdots\pi$ contacts in the crystal than in benzodicoronene. The C$\cdots$C contact (from π–π stacking) appears on the diagonal of the fingerprint plots (*i.e.* where $d_e \simeq d_i$), beginning near the C-atom van der Waals radius (1.7 Å; Bondi, 1964) and extending towards the upper right of the plots. Labelled 3 on the benzodicoronene fingerprint plot, this feature increases in size and relative contribution as the size of the molecule increases and is most prominent in the structure of benzodicoronene, where it is no longer yellow but red.

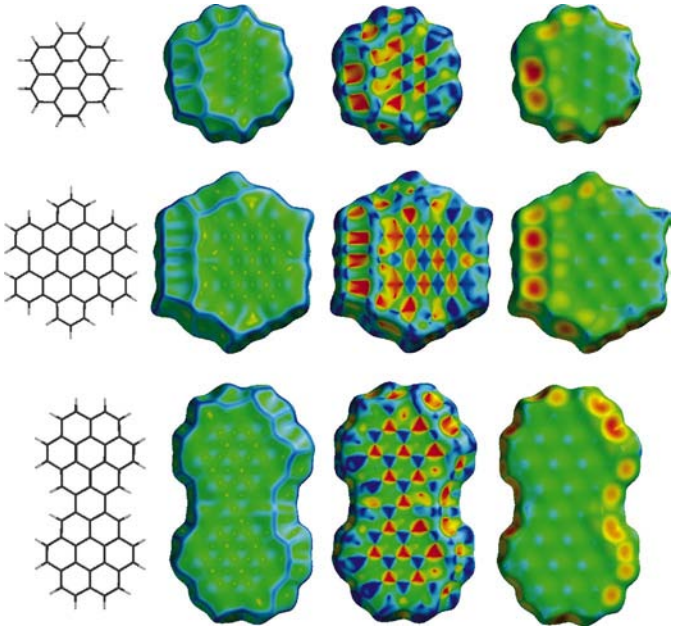

Figure 21
Hirshfeld surfaces for coronene (top; CORONE; Fawcett & Trotter, 1965), hexabenzocoronene (middle; HBZCOR01; Goddard *et al.*, 1995) and benzodicoronene (bottom; YOFCUR; Goddard *et al.*, 1995).

Figure 22
Crystal-packing diagram for coronene, viewed down the *c* axis, highlighting the π–π stacking motif. The interplanar angle between molecules in adjacent stacks is 85°.

3.3.4. The β structures. The β structures have been described as characterized by 'strong C$\cdots$C interactions without much contribution from C$\cdots$H contacts' (Desiraju & Gavezzotti, 1989). One additional feature that distinguishes these structures is the fact that they are all non-planar to varying degrees, and this may be the most significant factor dictating their particular packing arrangement in the crystal. The Hirshfeld surface of diperinaphthyleneanthracene (NAPANT01; Fig. 26) reflects the significant twist in the molecular structure caused by repulsion between H atoms bonded to 1,4-C atoms, across the 'bay regions' of these hydrocarbons. Contrary to its classification as a β structure, the Hirshfeld surface of NAPANT01 (particularly the front view in Fig. 26) shows that there is a significant contribution from C—H$\cdots\pi$ contacts in the crystal; these are certainly a direct consequence of the twist in the structure and the requirement for close packing in the crystal, as clearly illustrated by the crystal packing diagram, Fig. 27.

The two-dimensional fingerprint plot for NAPANT01 (Fig. 26) shows that the C—H$\cdots\pi$ contact in this structure is not as distinct as the same feature in structures examined above, a fact that may be related to the slight angle between the approaching C—H and the C-atom sheet; the packing diagram (Fig. 27) suggests that this contact resembles something between π–π stacking and a conventional C—H$\cdots\pi$ contact. The fingerprint plot for NAPANT01 also shows an exceptionally short H$\cdots$H contact, with $d_e = d_i \simeq 1.0$ Å (*i.e.* an H$\cdots$H separation of 2.0 Å), evident on the d_e surface at the point labelled 1. It does not, however, show a dominance of C$\cdots$C contacts of the type that are expected to define the β structure type. The shape index surface suggests that there is very little contribution from this type of interaction, with the exception of a small area of the surface, where complementary red and blue triangles are labelled 2 in Fig. 26.

The Hirshfeld surface and fingerprint plots for anthrabenzonaphthopentacene (BOXGAW01) are shown in Fig. 28. As for NAPANT01, this molecule is not centrosymmetric, so two views of the surfaces are shown. The molecular structure of BOXGAW01 in the crystal is less twisted than that of NAPANT01, and the preferred packing mode, dominated by π–π stacking, is not substantially disrupted in this case, as

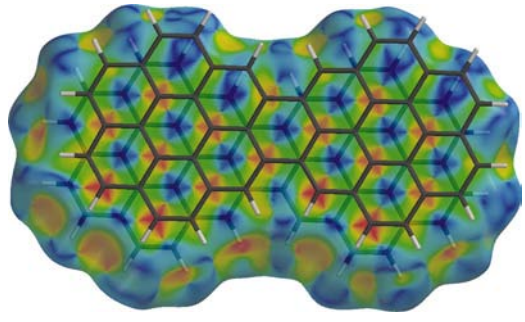

Figure 23
Semi-transparent Hirshfeld surface of benzodicoronene, mapped with shape index and with an adjacent molecule above the plane.

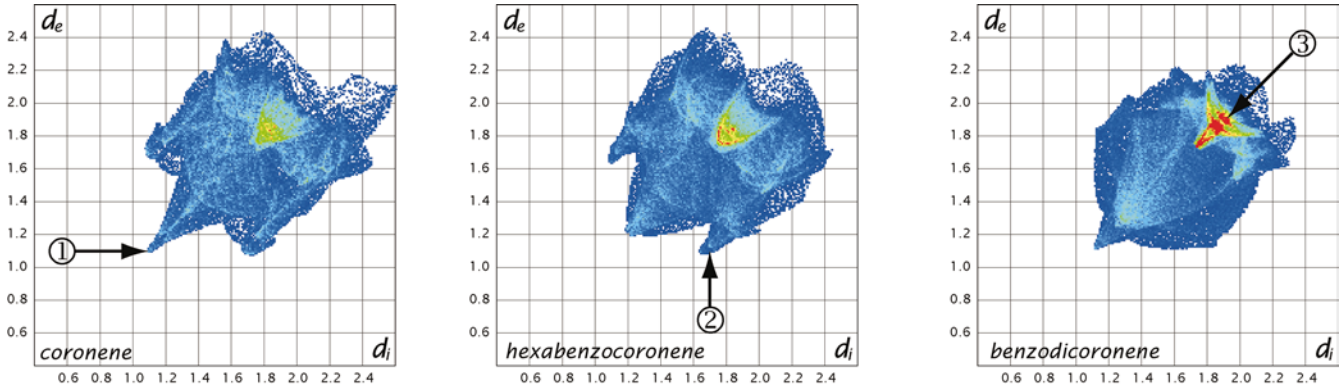

Figure 24
Two-dimensional fingerprint plots for coronene, hexabenzocoronene and benzodicoronene; see Fig. 21 for Hirshfeld surfaces and refcodes.

shown by the pattern of alternating blue (convex) and red (concave) regions on both sides of the shape index surface of the molecule. The two-dimensional fingerprint plot confirms that the structure is indeed largely dominated by π–π contacts, as shown by the red, yellow and green region on the plot resulting from a large number of surface points corresponding to a van der Waals separation typical of C atoms. The only other significant feature on the plot reveals the presence of a large number of H$\cdots$H contacts.

Figure 25
Crystal-packing diagram for benzodicoronene, viewed down the *c* axis, highlighting the π–π stacking motif. The interplanar angle between molecules in adjacent stacks is 130° (*cf.* Fig. 22).

3.4. Hydrogen-bonded compounds

There is no disagreement that hydrogen bonding is the most important weapon in the crystal engineer's armoury. Conventional hydrogen bonds are strongly binding, highly directional and typically formed between acidic O—H and N—H donors, with electropositive H atoms and electronegative acceptors such as O and N. However, there is still vigorous debate about whether weaker interactions involving H atoms are similar in character and hence should be classified as weak hydrogen bonds. The reader is referred to the excellent book on weak hydrogen bonds by Desiraju & Steiner (1999), which contains a comprehensive bibliography of work in this area up to 1998. A more recent overview of hydrogen bonding in solids has been provided by Steiner (2002) and investigations into various aspects of weak or non-conventional hydrogen bonds, often based on a combined CSD and theoretical study, continue unabated [see, for example, recent studies focused on C—H$\cdots X$ (Aakeröy *et al.*, 1999; van den Berg & Seddon, 2003) and C—H$\cdots\pi$ (Takahashi *et al.*, 2001) interactions, and halogens as hydrogen-bond acceptors (Brammer *et al.*, 2001)]. Perhaps much of the controversy surrounding the classification of these weaker interactions as hydrogen bonds would have been avoided had the term 'hydrogen bridge' (Huggins, 1936) remained in common

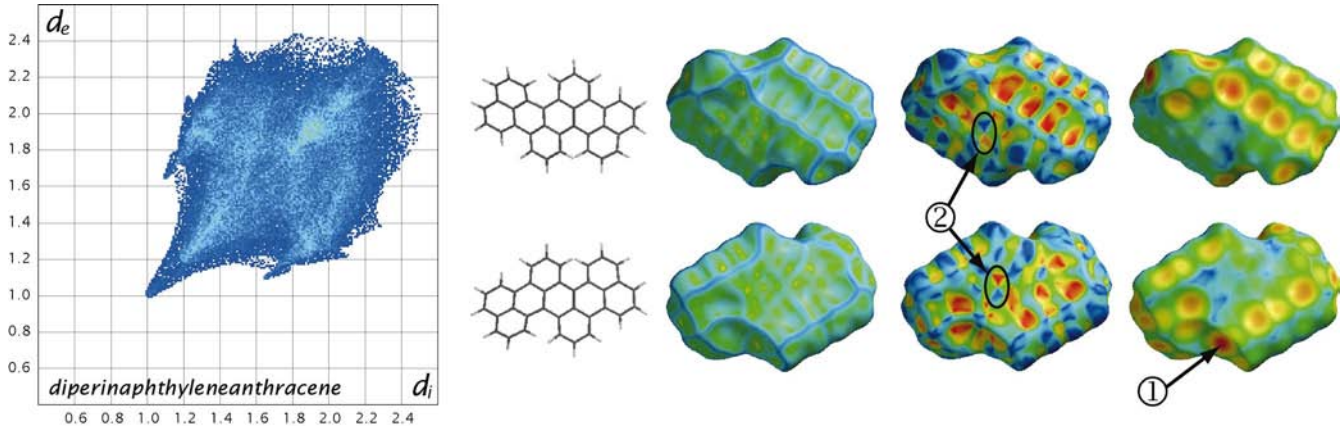

Figure 26
Two-dimensional fingerprint plot and Hirshfeld surface (front and back views) for diperinaphthyleneanthracene (NAPANT01; Izuoka *et al.*, 1992).

usage, and an argument for its reintroduction has recently been provided by Desiraju (2002). It is not among our aims to contribute to the debate over the existence or classification of certain types of hydrogen bonds, conventional or non-conventional. While the reader may disagree with the implicit classification of some *interactions* discussed in this section as hydrogen bonds, in particular weak hydrogen bonds, there should be no doubt that such close *contacts* exist and they may be important as supramolecular synthons or building blocks for molecular crystals, regardless of the label applied to such contacts. Most importantly, however, the present tools based on Hirshfeld surfaces know nothing about hydrogen bonding, only about crystal structure and spherical atomic electron distributions, and it is important to ascertain what differences (and similarities) these tools might reveal between conventional strong hydrogen bonds and their much weaker relations.

3.4.1. Carboxylic acids. Carboxylic acids, RCO_2H, typically form one of two packing arrangements in the crystal (Leiserowitz, 1976). Most carboxylic acids form a centrosymmetric dimer of hydrogen-bonded molecules, classified as a zero-dimensional motif (or a one-dimensional motif if the molecule is a diacid). Less common is the catemer motif, featuring an infinite chain of symmetry-related molecules forming a one-dimensional motif or chain of hydrogen-bonded molecules. While the catemer motif is thought to be energetically favourable, packing limitations of the *R* substituent tend to prevent this packing arrangement in all but the smallest carboxylic acids.

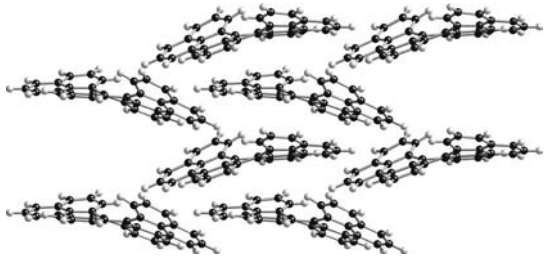

Figure 27
Crystal-packing diagram for diperinaphthyleneanthracene, viewed down the *c* axis.

In order to make accurate and meaningful comparisons between related structures, it is essential to use structural data that were collected under conditions that are as close as possible to identical. Thalladi *et al.* (2000) have recently determined accurate crystal structures at 130 K for the series of 1,*n*-alkanedicarboxylic acids (diacids) containing two to ten C atoms, in an attempt to rationalize the observed melting-point alternation in this series. Although similar to that observed for the *n*-alkanes and discussed in §3.2.1, the melting-point alternation in the diacids is significantly more pronounced than that for the *n*-alkanes.

Hirshfeld surfaces for the nine diacids studied by Thalladi *et al.* are shown in Fig. 29. For all hydrogen-bonded compounds in this section, the d_e surface is mapped over the range 0.6–2.6 Å; curvedness and shape index are mapped over the same range as before. Fig. 29 highlights a significant difficulty in presenting a three-dimensional object in a two-dimensional medium, namely choosing a single orientation of the object that conveys the most information in two dimensions. Each molecule in Fig. 29 is viewed with the upper carboxylate group approximately in the plane of the page and in the same orientation, and this arrangement highlights the twist in the alkane backbone for the odd members, as discussed further below. All surfaces have also been tilted slightly forward at the top to expose the hydrogen bond.

Polymorphism is known to be common in the odd members of this series, as well as the smaller even members (oxalic and succinic). Where this is the case, we have used the structure of the stable form studied by Thalladi and co-workers at 130 K, all of which pack in the crystal *via* a cyclic hydrogen-bonded dimer arrangement [$R_2^2(8)$ in graph-set notation (Etter, 1990; Etter *et al.*, 1990)] at each end of the molecule. A second polymorph of oxalic acid is characterized by the hydrogen-bonded catemer motif and a comparison between these two crystal structures, along with other examples of polymorphism, will be presented in a subsequent paper. For all the other diacids considered here, the structures of the other known polymorphs are also based on a similar carboxylic acid dimer.

The structures of oxalic and malonic acids are somewhat anomalous in this series; oxalic acid is the only planar molecule and malonic acid differs because it is the only structure in

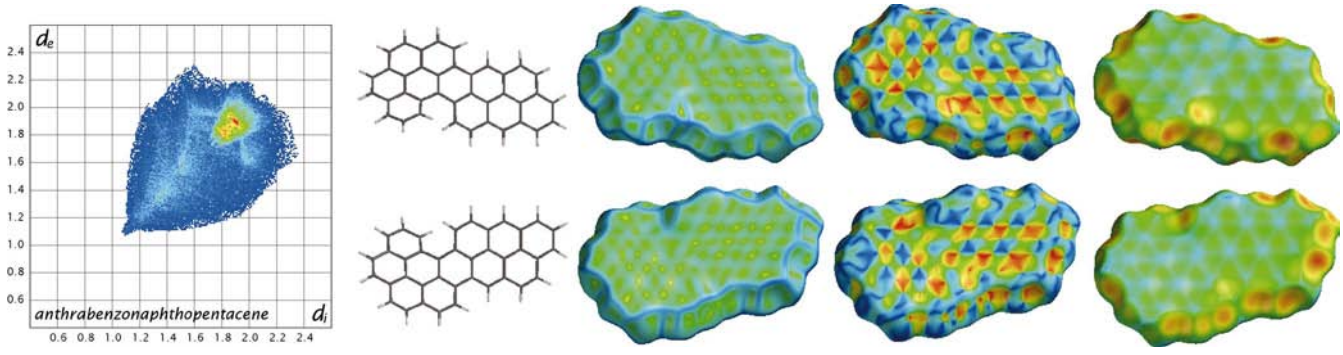

Figure 28
Two-dimensional fingerprint plot and Hirshfeld surface (front and back views) for anthrabenzonaphthopentacene (BOXGAW01; Marsh & Herbstein, 1988).

this series with $Z' = 1.0$ (all other structures have $Z' = 0.5$), resulting in two slightly different cyclic dimer motifs at the two ends of this molecule. For diacids beyond malonic acid, the even members pack in space group $P2_1/c$, and the β forms of the odd members pack in $C2/c$, reflecting the fact that two distinct packing patterns exist for the even and odd members of the series.

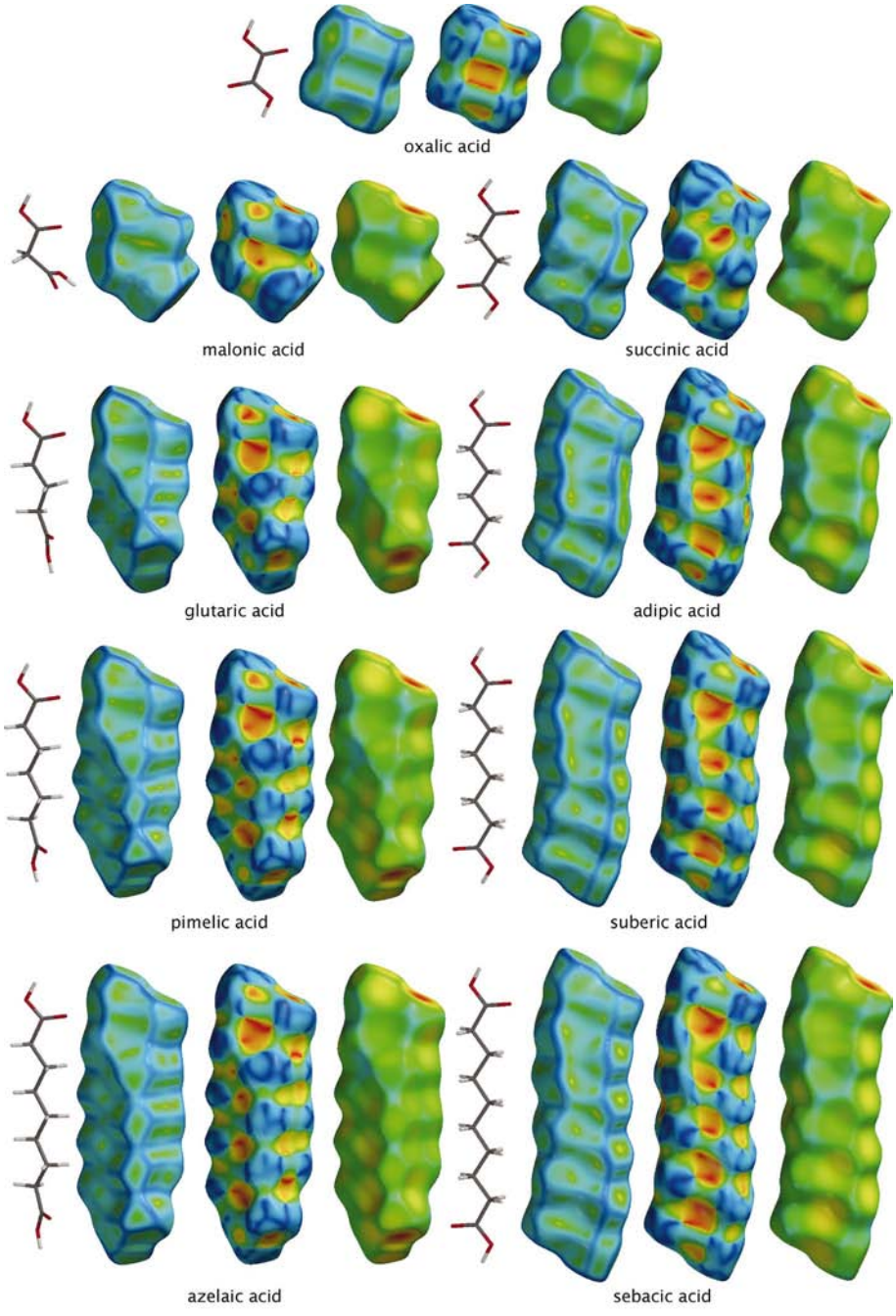

Figure 29
Hirshfeld surfaces for the 1,*n*-alkanedicarboxylic acids: β-oxalic (OXALAC04; Derissen & Smit, 1974), and malonic through sebacic (MALNAC05, SUCACB09, CLURAC03, ADIPAC07, PIMELA04, SUBRAC04, AZELAC04 and SEBAAC04; Thalladi, Nusse & Boese, 2000). For all Hirshfeld surfaces in this section d_e is mapped between (red) 0.6 and (blue) 2.6 Å; curvedness and shape index are mapped over the same range as before (see Fig. 1).

The most obvious feature on the Hirshfeld surfaces of these molecules (Fig. 29) is the pair of red dots on the d_e surface at the ends of the molecules, arising from the hydrogen bonds. In any hydrogen bond, a large red region appears adjacent to the hydrogen-bond acceptor, while a smaller orange–red dot appears adjacent to the hydrogen-bond donor. With all the surfaces mapped over the same range of d_e, the size and colour of these regions is directly related to the closeness of the atom–atom contacts, which is often taken as synonymous with the strength of the individual hydrogen bond. While the pair of bright donor–acceptor dots on the d_e surface characterizes all hydrogen bonds, it is particularly distinctive in the case of these cyclic hydrogen-bonded dimers where the two spots are immediately adjacent.

The two-dimensional outlines of the Hirshfeld surfaces for these structures are similar to the parallelograms and trapezoids used by Thalladi and co-workers to describe the structures of the even and odd members of the series, respectively. The twist in the molecular backbone observed for the odd members, and particularly prominent for pimelic and azelaic acids, causes a significant deviation from this basic shape and is difficult to visualize even with the use of molecular stick diagrams.

Two-dimensional fingerprint plots for the diacids (Fig. 30) provide quantitative information to reinforce impressions gained from the surfaces themselves. The hydrogen bond dominates the appearance of all these plots, appearing as a pair of sharp spikes pointing towards the bottom left of each plot. In each case the upper spike (where $d_e > d_i$) corresponds to the hydrogen-bond donor and the lower spike (where $d_e < d_i$) corresponds to the hydrogen-bond acceptor. The closest atom–atom contact can be deduced from the plots by taking the sum of d_e and d_i at the point of the spike. The range of d_e for the diacids shows no significant correlation with the melting points of these structures, which is not surprising given that there are now two distinct types of contacts in these molecules, *viz.* H···H and hydrogen bonds, and they both display different characteristic ranges of d_e and d_i.

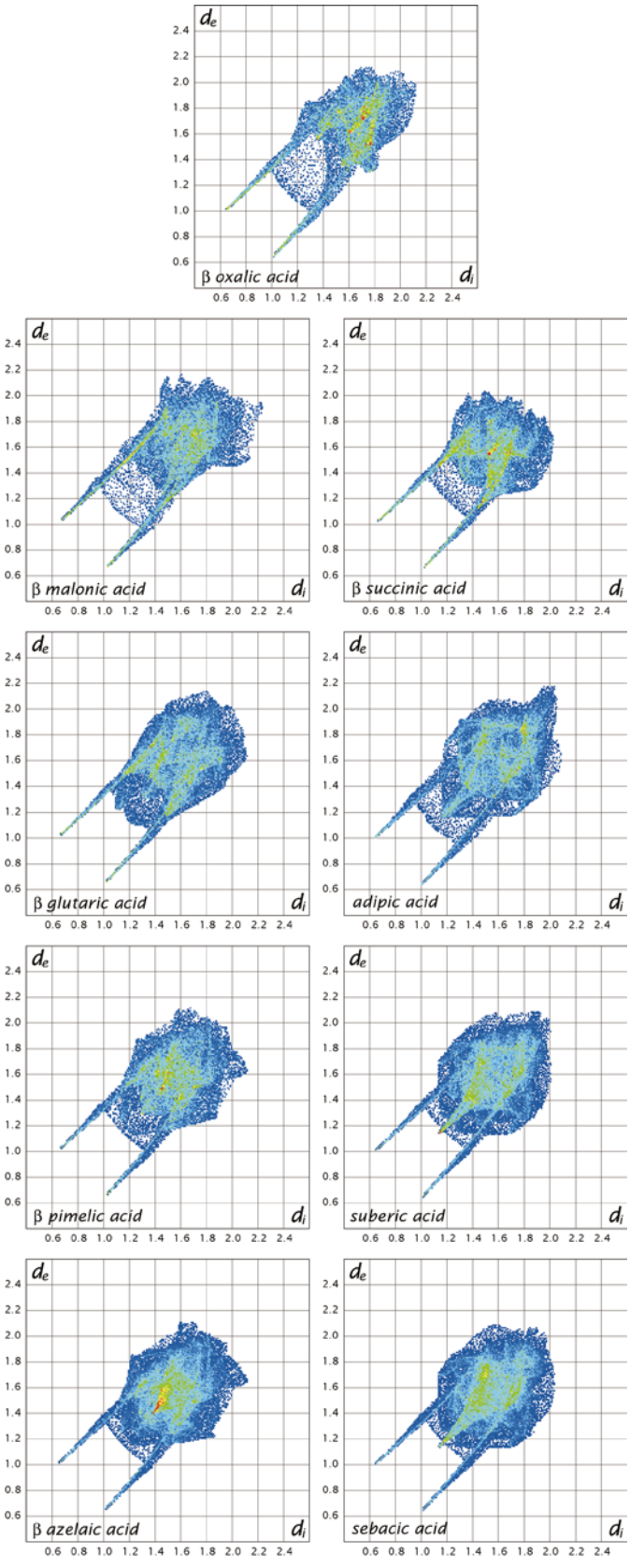

Figure 30
Two-dimensional fingerprint plots for the 1,*n*-alkanedicarboxylic acids *β*-oxalic acid through sebacic acid; see Fig. 29 for Hirshfeld surfaces and refcodes.

A detail of the two-dimensional fingerprint plot for malonic acid (Fig. 31) highlights a sparse region of blue points between the hydrogen-bond spikes, at a reasonably close contact distance. This feature is characteristic of a cyclic hydrogen-bonded dimer and a similar pattern is observed in the fingerprint plots of all such hydrogen-bonded dimers. It arises from a very small number of points on the Hirshfeld surface between the donor and acceptor regions, where the two H atoms involved in the dimer are the closest atoms internal and external to the surface [see, for example, the mean geometry of the carboxylic acid dimer in Scheme 7 of Steiner (2002), in which the H···H distance across the ring is 2.34 Å]. This diffuse set of points is particularly interesting in the fingerprint plot for malonic acid (C3) which, as mentioned above, is the only structure in this series of diacids in which the two ends of the molecule are not identical. The two hydrogen bonds in malonic acid are very similar, both having H···O distances of 1.70 Å but with O—H···O angles of 178.4 and 167.1°. Although the spikes due to these two hydrogen bonds are superimposed upon each other in the two-dimensional fingerprint plot, close inspection of the region between the spikes in the plot for malonic acid reveals patterns arising from two different contacts (as shown by the arrows labelled 1 and 2 in Fig. 31), evidence that the chemical environment of the two regions is somewhat different. Fig. 32 shows a side-on view of both cyclic hydrogen bonds for malonic acid; the dimer on the right, corresponding to the hydrogen bond with an O—H···O angle of 178.4°, displays a very different surface outline from that for the hydrogen bond on the left. The former surface is much flatter, and this in turn is the origin of the more distant sparse region of points between the spikes on the fingerprint plot, starting at $d_e \simeq d_i \simeq 1.25$ Å (2 in Fig. 31). Fig. 32 shows that the more structured surface evident in the hydrogen bond on the left of the figure arises from the translation of one molecule relative to the other, such that the H···H non-bonded distance across the dimer is shorter (2.20 Å) for the arrangement on the left of Fig. 32 than for that on the right (2.45 Å).

Thalladi and co-workers have commented that, for members of this diacid series with five or more C atoms, a pattern emerges where the packings of the odd members are similar to each other and the packings of the even members are similar to each other but different from those of the odd members. This fact is easily confirmed by inspection of the relevant fingerprint plots in Fig. 30. Starting from adipic acid, the even members feature close H···H contacts, evidenced by a reasonably sharp point at $d_e \simeq d_i < 1.2$ Å; these contacts are as short as 1.14 Å in sebacic acid (where the closest H···H contact is 2.28 Å). This feature is nowhere near as prominent in the fingerprint plots of the odd members, for which H···H contacts occur at a longer distance; this difference is particularly noticeable in the case of azelaic acid, where the closest H···H contacts between the alkane backbones are manifested as a red region on the fingerprint plot at around $d_e \simeq d_i \simeq 1.4$ Å. These longer distances may be a result of the twist of the molecular backbone preventing a closer approach of the H atoms in neighbouring molecules and are almost

certainly implicated in the lower stabilities, and hence lower melting points, of the odd members in this series.

As mentioned above, most carboxylic acids form cyclic dimers in the crystal, but the two smallest carboxylic acids, formic acid and acetic acid, both exhibit a catemer motif. Hirshfeld surfaces for these two compounds (Fig. 33) show the different nature of the hydrogen-bonding arrangement in these crystals compared with that in the structures of the diacids above. In both of these examples (Fig. 33), the hydrogen-bond donor, shown by the orange spot on the d_e surface above the H atom, approaches the carboxyl O atom from the left of the molecule (as viewed), resulting in a characteristic bright-red spot on the left-hand side of these surfaces. In each case, the carboxyl O atom also appears to accept a weaker hydrogen bond, shown by a pale-yellow spot on the d_e surface above the O atom (1 in Fig. 33). These features correspond to close C—H···O contacts in the crystals, observed at 2.58 and 2.40 Å in formic and acetic acid, respectively. The resulting similar networks of strong and weak hydrogen bonds in these crystal structures are illustrated in Fig. 34.

The two-dimensional fingerprint plots for these two small carboxylic acids (Fig. 35) are significantly different from those of the centrosymmetric dimers featured previously in Fig. 30. The sparse region of points between the two hydrogen-bonding spikes is notably absent, as the close intermolecular contacts across the dimer ring required to produce these points on the fingerprint plot do not exist in these crystals. The short C—H···O contacts in both structures are not readily apparent in the fingerprint plot, as the points arising from these contacts are superimposed on the sharp spikes of the strong O—H···O hydrogen bonds, but the C—H···O contacts can be seen in the green colouring towards the top of the spikes, representing a greater relative contribution to the surface. The methyl group in acetic acid reduces the overall packing efficiency between the catemer chains and results in more surface points at greater d_e and d_i, causing the fingerprint plot for acetic acid to extend further to the top right.

The carboxyl group is regarded by many to be an effective structure-directing functional group (Leiserowitz, 1976) and two examples of this role are provided by the crystal structures of benzoic acid (Fig. 36) and terephthalic acid (Fig. 37). Benzoic acid forms centrosymmetric hydrogen-bonded dimers in the crystal, and the optimization of this interaction, at the expense of other interactions in the crystal, significantly modifies the herringbone motif favoured by benzene. A close contact occurs between a ring H atom and the *para*-C atom, seen as a large red depression on the shape index surface in Fig. 36. This contact leaves a qualitatively different fingerprint (1 in Fig. 36) from that for the C—H···π contact in benzene (Fig. 11), where the C—H donor is directed towards the ring centre; the fingerprint changes as this contact becomes

Figure 32
The different cyclic hydrogen bonds at the two ends of a malonic acid molecule in the crystal, highlighting the different ring arrangements, and the resultant different shapes of the Hirshfeld surfaces.

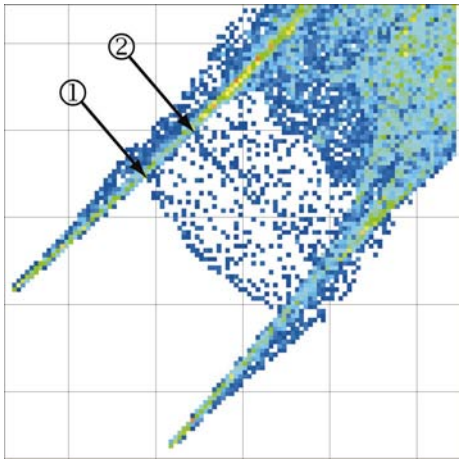

Figure 31
Detail of the two-dimensional fingerprint plot for malonic acid, highlighting features due to cyclic hydrogen-bonded dimers.

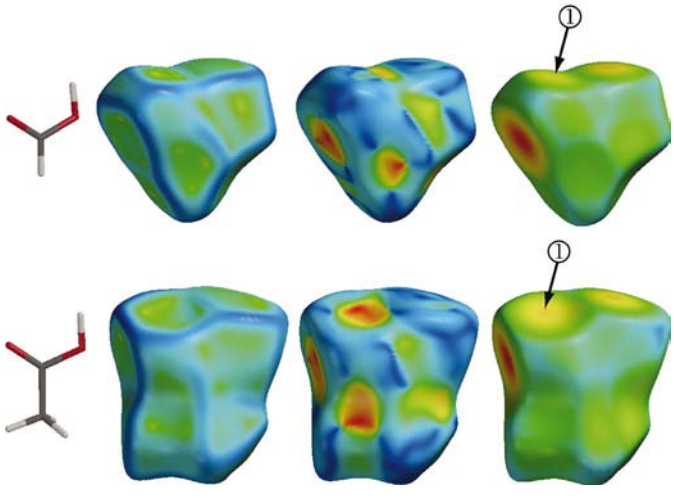

Figure 33
Hirshfeld surfaces for formic acid (top; FORMAC01; Nahringbauer, 1978) and acetic acid (bottom; ACETAC03; Jönsson, 1971).

directed more towards the edge of the ring, as in naphthalene and anthracene (also Fig. 11). In the case of benzoic acid, the C—H donor is pointing directly towards a single C atom, hence the very different fingerprint. Some π–π stacking is also evident from the green region on the fingerprint plot around $d_e \simeq d_i \simeq 1.8$ Å, and the adjacent blue and red patches on the lower shape index surface inform us that this interaction occurs on only one side of the molecule. In the fingerprint plot, a region of large d_i is observed, labelled 2 on the plot, which corresponds to the region above the centre of the ring (also labelled 2 on the d_e surface), but on the other side of the molecular plane and close to the C—H···C contact mentioned above. We conclude that the overall packing efficiency of benzoic acid is far from optimal.

The crystal structure of terephthalic acid (α form, Fig. 37) features even greater dominance of the π–π stacking motif than benzoic acid, and the 1,4-substitution of the benzene ring enables the molecule to pack in infinite hydrogen-bonded ribbons in the crystal. As discussed previously in relation to the larger polycyclic aromatic hydrocarbons, the π–π stacking motif is evident from the pair of complementary red and blue triangles on the shape index surface, showing precisely how adjacent molecules pack, as well as by a distinct red region on the fingerprint plot at $d_e = d_i \simeq 1.8$ Å. The fingerprint plot for terephthalic acid in fact shows all of the dominant intermolecular contacts in the crystal with remarkable clarity: the π–π stacking mentioned above, as well as the strong hydrogen bonds, and even the fact that the hydrogen bonding is clearly cyclic. With practice in interpreting these diagrams, such conclusions can be made with confidence and without the need for crystal-packing diagrams. However, to confirm these observations, Fig. 38 shows the Hirshfeld surface of terephthalic acid in the context of the crystal-packing arrangement. In this figure, d_e is mapped over the entire range of the property on this surface (0.63–2.20 Å) in order to provide the maximum colour contrast and this approach highlights surface features that are more subtle, such as markings due to the π–π stacking arrangement. An imprint due to the adjacent benzene ring is clearly visible on the d_e surface, reflecting the offset stacking arrangement in the crystal.

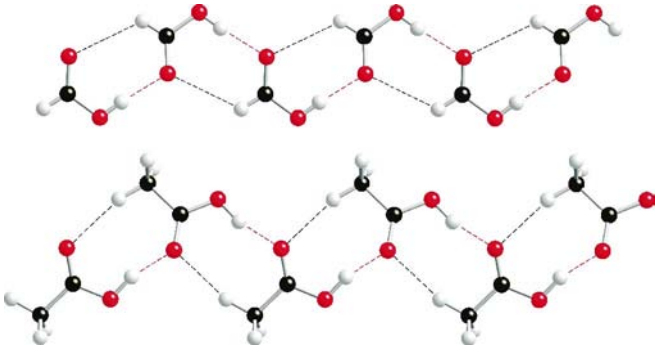

Figure 34
The hydrogen-bonded catemer motifs in formic acid (top) and acetic acid (bottom); O—H···O hydrogen bonds are shown by red dashed lines and short C—H···O contacts are shown by black dashed lines.

3.4.2. Alcohols. Alcohols are rarely considered in detail when hydrogen bonding is discussed in the context of crystal engineering, mostly because the hydroxyl O atom has a much weaker directing effect in hydrogen-bonded crystals than the carbonyl O atom (Desiraju, 1989), as well as the fact that there is obvious rotational freedom about the O—C bond, which limits the reliable structure-directing capability of the hydroxyl group. Brock & Duncan (1994) have considered in detail the spatial requirements of O—H···O contacts for monoalcohols and that work was extended by Taylor & Macrae (2001), who deduced rules for aiding in predicting crystal packing for both mono- and dialcohols. Many of the known structures that contain C—O—H groups are large polysaccharides and carbohydrates, with a great deal of conformational freedom; these structures are considered too complex to be included in any rational study of crystal structures and this restriction applies to the present study. Simpler alcohols are nevertheless of interest and several examples are presented below.

The 1,*n*-alkanediols have also been the subject of a recent study by Thalladi & Boese (2000) to investigate an alternation in their melting points, as was the case for the *n*-alkanes and the 1,*n*-alkanedicarboxylic acids. As a result, accurate crystal structures were determined at 130 K for members of this series up to $n = 10$. The patterns in the crystal packing of the *n*-alkanes and the 1,*n*-alkanedicarboxylic acids have already been discussed, and the 1,*n*-alkanediols exhibit a similar pattern of alternating crystal structures and physical properties, including melting point and density. In the case of the 1,*n*-alkanediols, the alternation in these physical properties correlates with an alternation in some key properties of the Hirshfeld surfaces.

In many of the preceding analyses of two-dimensional fingerprint plots we have seen that molecules that pack by optimizing close packing in the crystal (for instance, the *n*-alkanes) exhibit a much smaller range of d_e over the surface than molecules that pack by optimizing specific individual atom–atom interactions at the expense of the overall geometrical packing efficiency of the crystal (for example, hydrogen-bonded compounds); this fact is striking from even the briefest of glances at Figs. 6 and 30. It would therefore appear that the range of d_e might be useful for contrasting the packing effi-

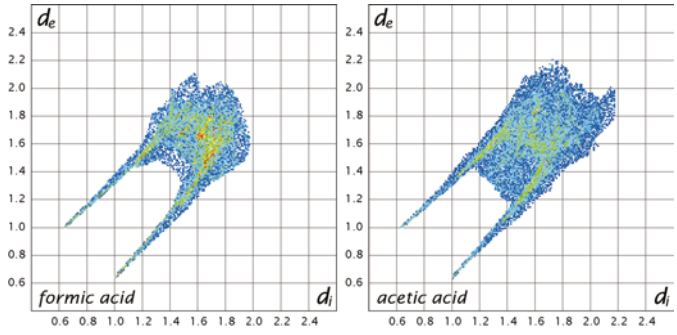

Figure 35
Two-dimensional fingerprint plots for formic acid and acetic acid; see Fig. 33 for Hirshfeld surfaces and refcodes.

ciencies of different families of molecules; for instance, $d_e^{\max} - d_e^{\min}$ is 0.76 Å for *n*-octane and 1.46 Å for suberic acid. This assumption ignores the obvious fact that only H···H contacts are involved for the *n*-alkanes, while H···H contacts and O—H···H hydrogen bonds are included for the diacids, rendering such global comparisons of little value. However, comparisons of the range of d_e *within* a family of molecules can be significant when analysing crystal-packing efficiencies, as already shown for the *n*-alkanes. Fig. 39 plots the melting points for the 1,*n*-alkanediols alongside the range of d_e over each surface. With the exception of 1,2-ethanediol, an inverse relationship is observed between the melting point and the range of d_e; the more efficient packing (and higher melting point) of the even members (Thalladi, Boese & Weiss, 2000*a*) is reflected in the systematically smaller range of d_e for these structures. Previous authors have related the alternation in density and melting point of these diols to packing efficiency, but with the use of the Hirshfeld surface, the packing differences can be easily described, and even quantified, in terms of differences in the close and distant intermolecular contacts.

The Hirshfeld surfaces of the 1,*n*-alkanediols for $n = 2$–8 (Fig. 40) show that a clear pattern in the crystal structures of these molecules emerges for $n \geq 4$ (1,4-butanediol). The even members pack in two-dimensional sheets of hydrogen-bonded molecules and, because the O—H bonds at opposite ends of the molecule are closely coplanar, the hydrogen bonds propagate roughly in the plane of the figure. The odd members exhibit a three-dimensional hydrogen-bond network, a result of the orthogonal orientation of the O—H bonds at opposite ends of the molecules. The Hirshfeld surfaces also show clearly that crystals of 1,2-ethanediol and 1,3-propanediol are not isostructural with the other members of this series. The crystal structures of these smaller molecules are fundamentally different because they lack the long hydrocarbon backbone that helps to dictate the packing of the longer members of the series.

The two-dimensional fingerprint plot for 1,2-ethanediol (Fig. 41) is dominated by the two sharp spikes due to the two very similar hydrogen bonds, as well as a short H···H contact at $d_e = d_i \simeq 1.20$ Å. A feature of the fingerprint plots for $n > 3$

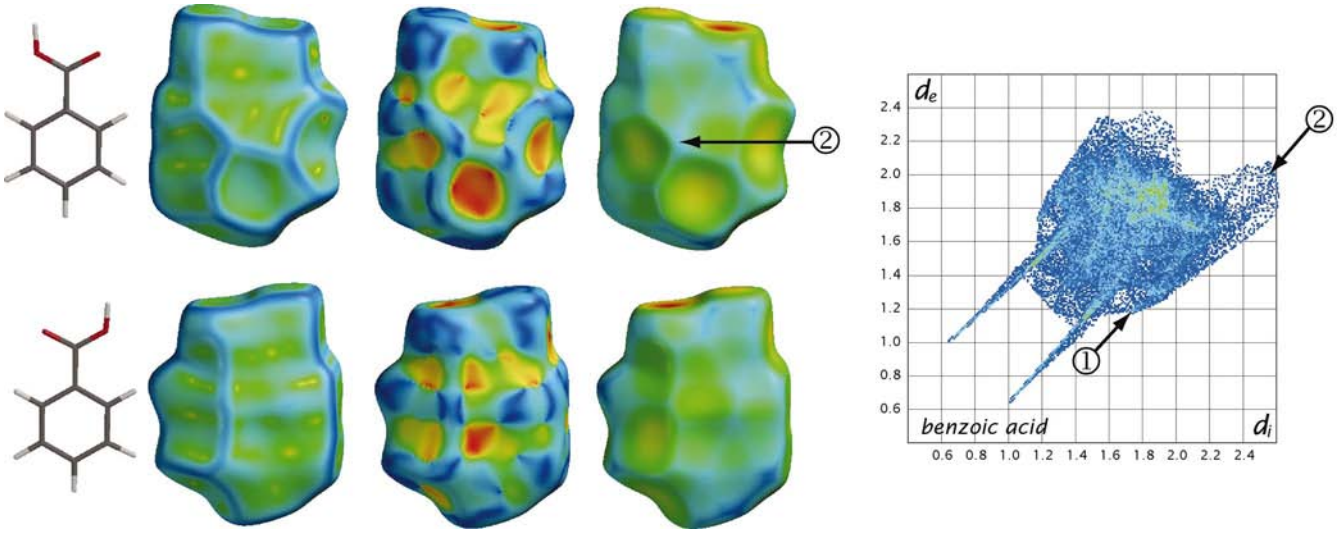

Figure 36
Hirshfeld surface (front and back views) and two-dimensional fingerprint plot for benzoic acid (BENZAC02; Feld *et al.*, 1981).

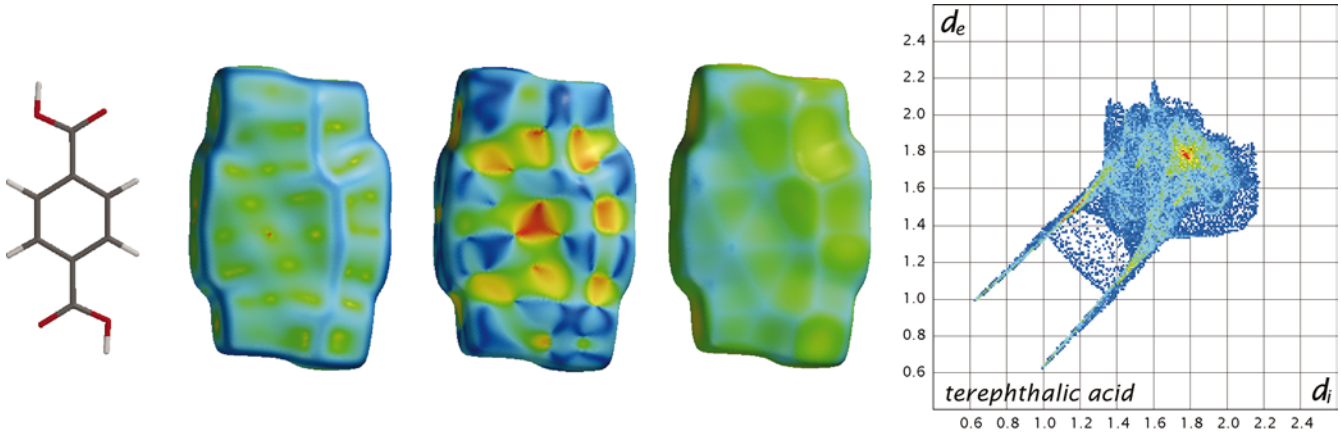

Figure 37
Hirshfeld surface and two-dimensional fingerprint plot for terephthalic acid (TEPHTH03; Fischer *et al.*, 1986).

is their increasing resemblance to the fingerprint plots of the *n*-alkanes (Fig. 6) as the length of the hydrocarbon chain increases. For the longer members of this series, the red streak in the middle of the plot shows the increasingly important contribution from H···H intermolecular contacts in these crystal structures. The two-dimensional fingerprint plots in Fig. 41 also show clearly that the hydrogen bonds are systematically shorter in the odd members (the mean $d_e^{\min}$ for the odd members is 0.68 Å, while for the even members with $n \geq 4$ this mean value is 0.73 Å). It is a testament to the quality of the reported structures that such a small systematic difference is present, and it is also remarkable that such a small difference is visible on the two-dimensional fingerprint plots derived from the Hirshfeld surfaces. The fingerprints due to the hydrogen bonds in the even diols also show a significant broadening towards the top (1 on the fingerprint plot of 1,6-hexanediol in Fig. 41), which appears to be unique to the particular geometry of interaction involved in these structures. It is worth noting that the structural patterns of the diols continue to a longer chain length. Hirshfeld surfaces and the corresponding fingerprint plots have been computed for 1,9-nonanediol, 1,10-decanediol, 1,11-undecanediol, 1,14-tetradecanediol, 1,15-pentadecanediol and 1,18-octadecanediol, and these plots continue to reinforce the trends discussed above.

3.4.3. Amines. The hydrogen-bonding capabilities of H atoms bonded to nitrogen are of interest primarily because of the biological function of compounds containing nitrogen, such as amino acids. While nitrogen is a weaker hydrogen-bond donor than oxygen, the prevalence of nitrogen in biological structures provides a focus for hydrogen-bonding investigations in these compounds. Simple examples of molecules whose structures are directed, at least in part, by N—H···N hydrogen bonds are rare; however, the systematic study of the 1,*n*-alkanediamines by Thalladi, Boese & Weiss (2000*a*) provides another opportunity to compare the Hirshfeld surfaces for a series of related structures, this time involved in N—H···N hydrogen bonding, which have been determined under the same experimental conditions. As with the previous series, Thalladi and co-workers noted a distinct alternation in solid-state physical properties of these structures; melting points and densities of the even 1,*n*-alkanediamines are systematically higher than those with an odd number of C atoms. The melting-point alternation for the diamines is plotted alongside the d_e range for each compound in Fig. 42 and in this case we see that d_e^{min} and $d_e^{\max}$ are directly correlated; the higher melting points for the even members correspond to lower values for both $d_e^{\min}$ and $d_e^{\max}$. This behaviour is distinctly different from that of the diols, where these two quantities were observed to be inversely correlated.

Hirshfeld surfaces for 1,2-ethanediamine through 1,6-hexanediamine are shown in Fig. 43, with the H atoms of the amino group at the top pointing away from the viewer in each case. One of the obvious features emerging from these surfaces is one that was not mentioned by the authors of the original study of the packing patterns in these structures, namely that the hydrogen-bond acceptor nature of the N atoms clearly differs between the odd and even members. Each N atom in the odd members accepts one relatively close and one more distant hydrogen bond, as shown by the two orange–red dots on the d_e surface adjacent to the N atom. For example, in 1,5-pentanediamine the shorter H···N distance is 2.25 Å and the corresponding N—H···N angle is 161.3°, while the longer contact is at 2.43 Å and 150.6°. Hirshfeld surfaces for the even members show that there is clearly just a single contact that could be classified as a hydrogen bond; for example, the contact in 1,6-hexanediamine occurs at a distance of 2.16 Å, with an H···N angle of 169.8°, and the next shortest H···N distance in 1,6-hexanediamine is 2.73 Å.

The two-dimensional fingerprint plots for the 1,*n*-alkanediamines (Fig. 44) highlight the systematic differences between the even and odd members of this series (apart from 1,2-ethanediamine, whose fingerprint plot is somewhat different from those of the larger even members). The odd members, with two adjacent hydrogen bonds at each end of the molecule, feature a region of blue points filling the area between the characteristic hydrogen-bond spikes. This pattern is reminiscent of the feature in the same area of the two-dimensional fingerprint plots for the cyclic carboxylic acid dimers already discussed and occurs for a similar reason: points on the surface between the two hydrogen-bonding

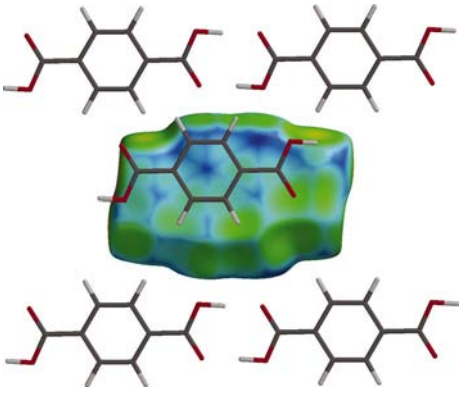

Figure 38
Hirshfeld surface of terephthalic acid in the context of the crystal packing; the property mapped on the surface is d_e.

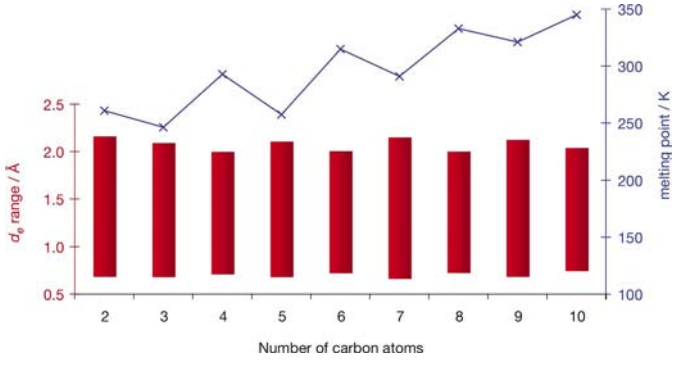

Figure 39
Trends in the range of d_e (red) and the melting points (blue) for the 1,*n*-alkanediols.

regions. A similar but smaller region appears at a greater distance in the fingerprint plots of the even members, reflecting the fact that the 'secondary' adjacent hydrogen bond in these structures is much longer than those in the odd members. These features have the effect of making the hydrogen-bond fingerprint of the even members appear to be significantly more prominent on the plot, despite the fact that the hydrogen bonds in the even members are only slightly shorter.

The pattern of H···H contacts that appears as a red streak along the diagonal of these fingerprint plots is strongly reminiscent of the *n*-alkanes (Fig. 6), reflecting the overall similarity of the crystal structures and the intermolecular interactions in this hydrophobic region of the molecule, and it is worthy of note that this H···H pattern is distinctly different for the even and odd members. It would be extremely interesting, and highly informative, to decompose these fingerprint plots into contributions from H···H contacts and from hydrogen bonding, and work in that direction is already underway.

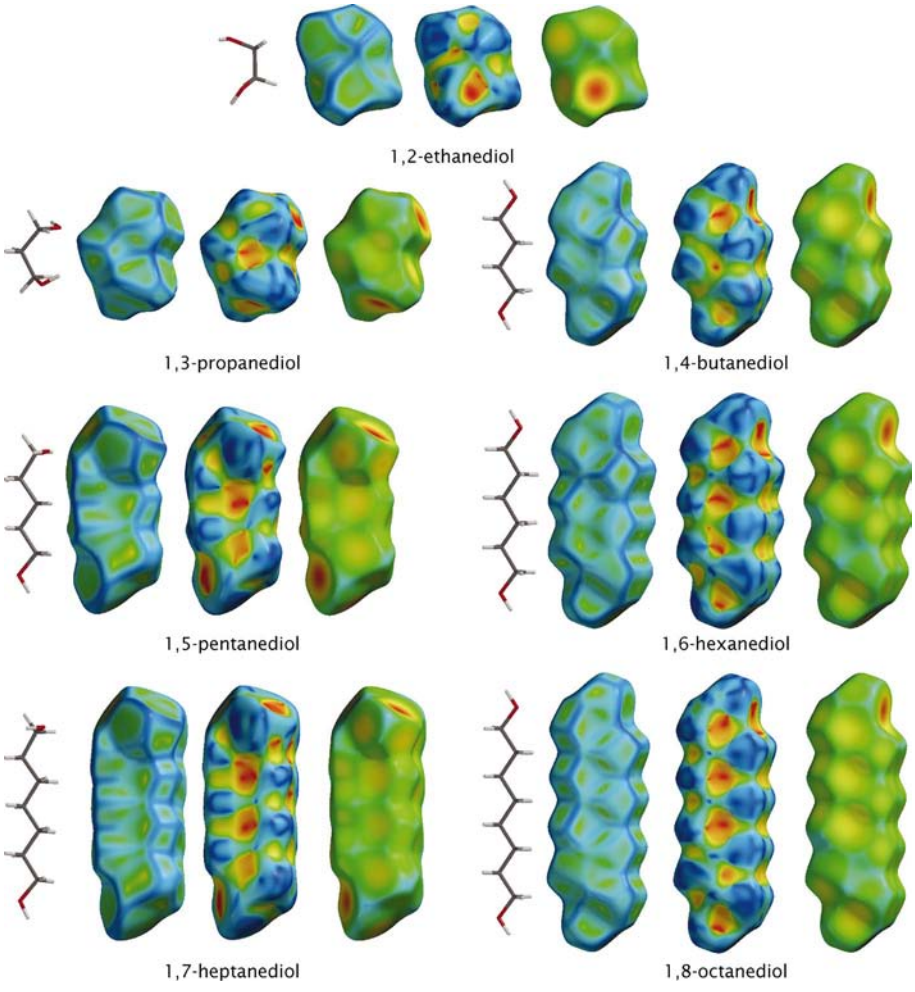

Figure 40
Hirshfeld surfaces for the series of 1,*n*-alkanediols: 1,2-ethanediol (NOZKES; Boese & Weiss, 1998) and 1,3-propanediol to 1,8-octanediol (QATTEK, QATTIO, QATTOU, FECCOF01, QATVAI and QATVEM; Thalladi, Boese & Weiss, 2000*a*).

3.4.4. Miscellaneous examples. Examples presented in the previous sections were chosen to provide a logical and stepwise introduction to the way that hydrogen bonding manifests itself on the Hirshfeld surface. The different interactions in the crystal were kept to a minimum by focusing on families of simple structures that provided a single type of hydrogen-bond donor and acceptor. Many compounds contain several possible hydrogen-bond donors and acceptors, and the structures formed are a result of a combination of competing and cooperating influences from different strong and weak intermolecular interactions, while others simply do not fit into the schemes presented in the previous sections. In this section, we present some miscellaneous hydrogen-bonding examples.

Imidazole and 2-pyridone are both planar heterocycles, each with one conventional hydrogen-bond donor and one conventional hydrogen-bond acceptor. Two-dimensional fingerprint plots for the crystal structures of imidazole and 2-pyridone (Fig. 45) suggest that crystals of these two compounds share some similar structural features. Both structures feature a strong hydrogen bond (N—H···N in imidazole and N—H···O in 2-pyridone), some degree of C—H···π interaction and short H···H contacts. While these features are common to both structures, each appears different in the fingerprint plot and these differences are investigated here.

The hydrogen-bond fingerprint of 2-pyridone reflects a marginally shorter hydrogen bond ($d_{H\cdots O}$ = 1.79 Å) than in imidazole ($d_{H\cdots N}$ = 1.86 Å), although the spike is somewhat broader in 2-pyridone, despite the fact that in both cases the spikes are due to a single short contact. The broadness of this spike may be related to differing hydrogen-bond geometries; the N—H···O angle in 2-pyridone is 160.3°, while in imidazole, the N—H···N angle is 173.3° (see packing diagram, Fig. 46). In imidazole the very narrow hydrogen-bond spike broadens at $d_e = 1.1$ Å and $d_i = 1.5$ Å, because of the presence of a second close contact to nitrogen, a C—H···N contact at 2.66 Å.

The crystal structures of both imidazole and 2-pyridone feature close H···H contacts, at 2.32 and 2.35 Å, respectively; however, the fingerprints of these interactions show that there is some difference between the two. The relevant fingerprint for imidazole is significantly sharper than that for 2-pyridone and, as discussed earlier, the shape of the fingerprint is

related to the angle of contact. For a C—H···H—C contact, there are two C—H···H angles that describe the angular arrangement of the contact. In imidazole, the two angles are 146.9 and 146.1°, while the corresponding angles for the H···H contact in 2-pyridone are 144.3 and 126.4°. Thus, the H···H contact in imidazole is a more direct head-to-head contact than that in 2-pyridone, producing a sharper spike in the centre of the fingerprint plot.

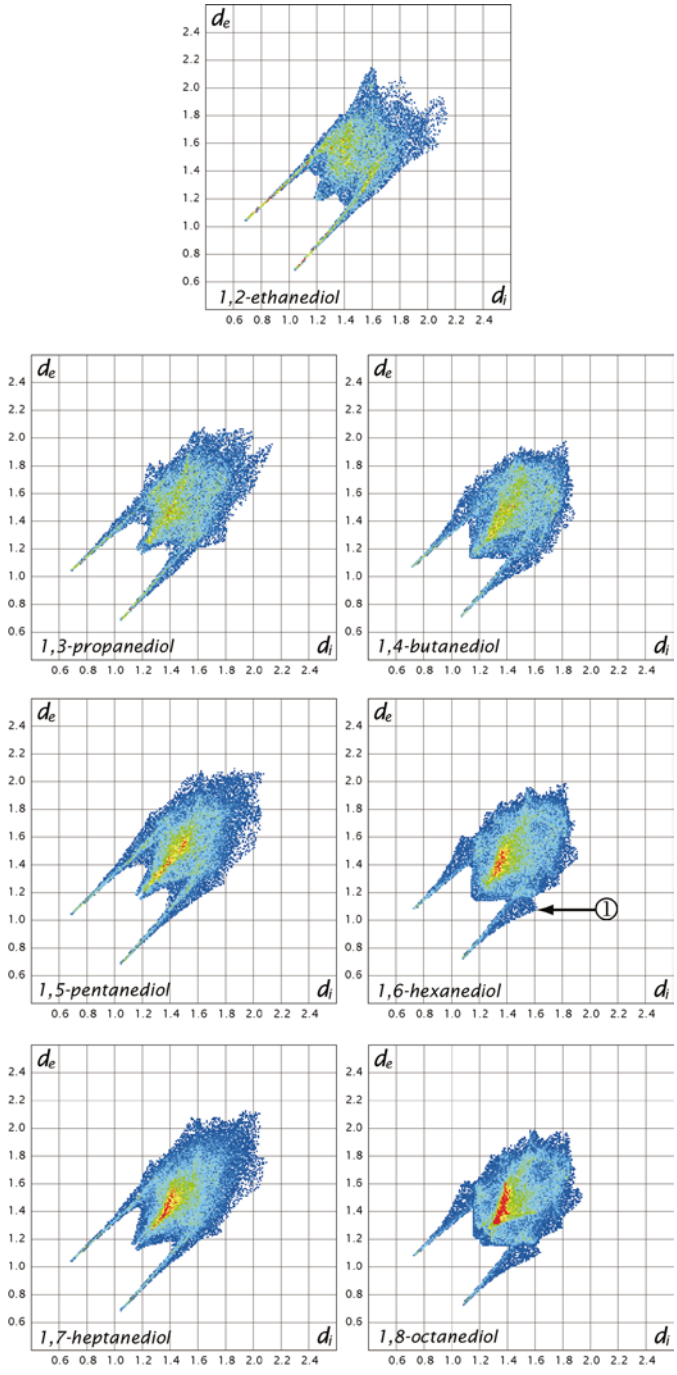

Figure 41
Two-dimensional fingerprint plots for the series of 1,*n*-alkanediols; see Fig. 40 for Hirshfeld surfaces and refcodes.

The third intermolecular interaction of interest in these two structures is the C—H···π contact. Inspection of the fingerprint plots shows that this contact is significantly different in the two structures and is shorter in 2-pyridone than in imidazole, and this difference is also obvious from the Hirshfeld surface diagrams in Fig. 47. The C—H···π interaction appears much more compact on the fingerprint plot of imidazole and resembles that of a direct atom–atom contact, and while the C—H group is directed more towards the centre of the ring in 2-pyridone, the contact in imidazole points almost directly towards the vinyl C atom adjacent to the imide N atom (labelled 1 in Fig. 47). Note that the C—H···π contact in these structures does not appear as a red spot on the d_e surface, as it did on the Hirshfeld surface of benzene (Fig. 10), because the property here is mapped over a different range and a red colour on the d_e surface corresponds to a much closer (hydrogen bond) contact in the present case.

Uracil is another planar heterocyclic molecule that forms hydrogen bonds in the crystal. Uracil contains two carbonyl groups, each capable of accepting two hydrogen bonds, two conventional hydrogen-bond donors (N—H groups) and two weak hydrogen-bond donors (sp^2-hybridized C—H groups), and packs in layers of planar hydrogen-bonded sheets, with all hydrogen-bond donors and acceptors fully utilized. Fig. 48 features the Hirshfeld surface of uracil viewed from both sides of the molecule, and from this figure it is readily seen that the structure is dominated by the hydrogen-bonding interactions in the plane of the molecule, with all atoms at the extremity of the molecule involved in hydrogen bonding; the Hirshfeld surface strongly resembles a tile with flat sides. The surface around the carbonyl O atoms is sharply 'pinched' by the close approach of the hydrogen-bond donors; Fig. 49 shows more clearly how the close intermolecular interactions in a plane of the crystal influence the shape of the Hirshfeld surface of uracil. In Fig. 48 d_e is mapped over the actual range of values on the surface and this figure highlights an imprint with sixfold symmetry, due to π–π stacking, on the surface, with a blue spot marking the centre of the neighbouring molecule, where d_e is a maximum (*cf.* terephthalic acid, Fig. 38). A pair of comple-

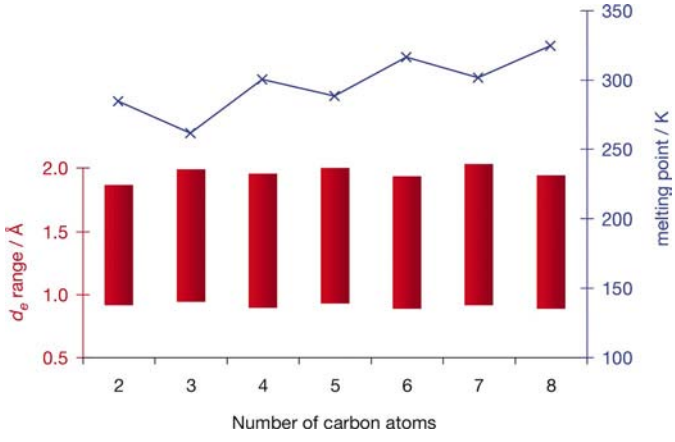

Figure 42
Trends in the range of d_e (red) and the melting points (blue) for the 1,*n*-alkanediamines.

mentary red and blue triangles is evident on the shape index surface on *both* sides of the molecule (labelled 1 in Fig. 48) and the way that these two pairs of complementary regions on the surface match one another (the blue triangle on the top surface matches the red triangle on the bottom surface, *etc.*) emphasizes the mode of translational stacking of molecules in the crystal. As with many aspects of interrogating the Hirshfeld surface, this relationship is much easier to visualize in the laboratory, with the aid of real-time rotation of the surfaces. Finally, we note that the two-dimensional fingerprint plot for uracil (Fig. 48) clearly shows patterns due to several cyclic hydrogen bonds, as well as the important π–π stacking

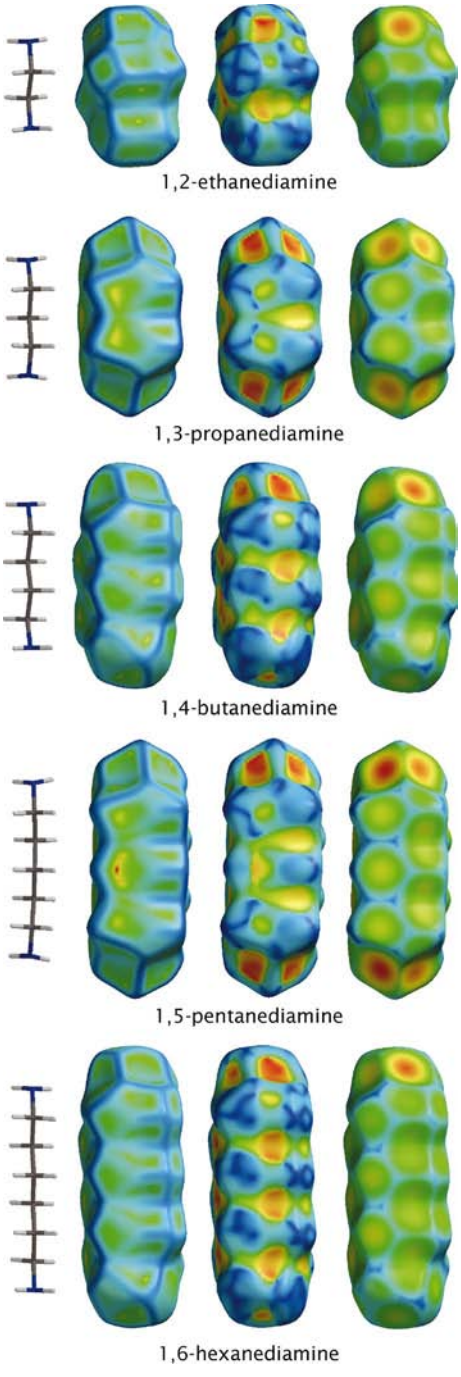

Figure 43
Hirshfeld surfaces for the 1,*n*-alkanediamines (ETDIAM01, QATVUC, QATWAJ, QATWEN and HEXMDA01; Thalladi, Boese & Weiss, 2000*a*). For this series d_e surfaces (right) are mapped between 0.8 and 2.0 Å.

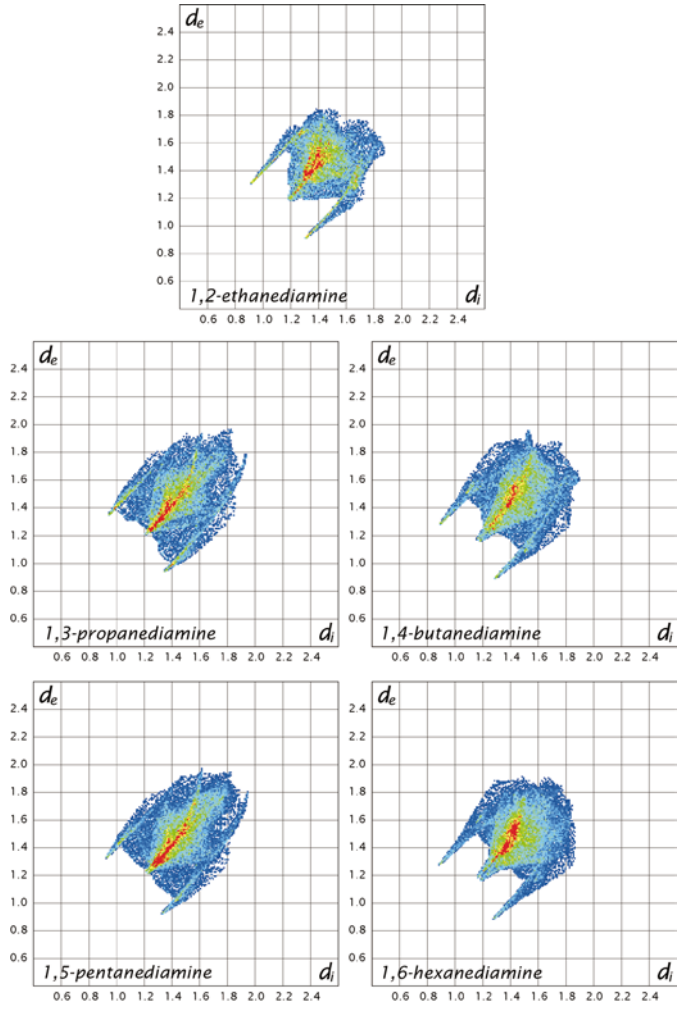

Figure 44
Two-dimensional fingerprint plots for the 1,*n*-alkanediamines; see Fig. 43 for Hirshfeld surfaces and refcodes.

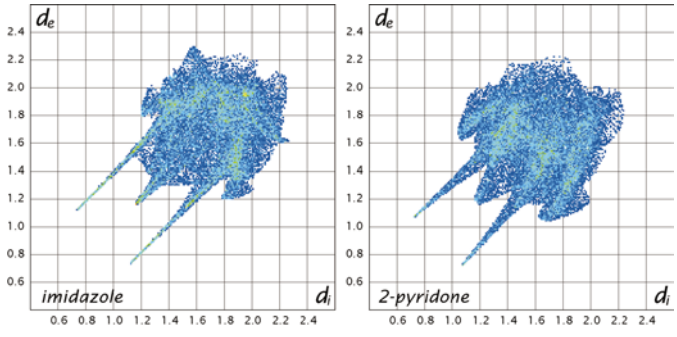

Figure 45
Two-dimensional fingerprint plots for imidazole (IMAZOL13; Craven *et al.*, 1977) and 2-pyridone (PYRIDO04; Ohms *et al.*, 1984).

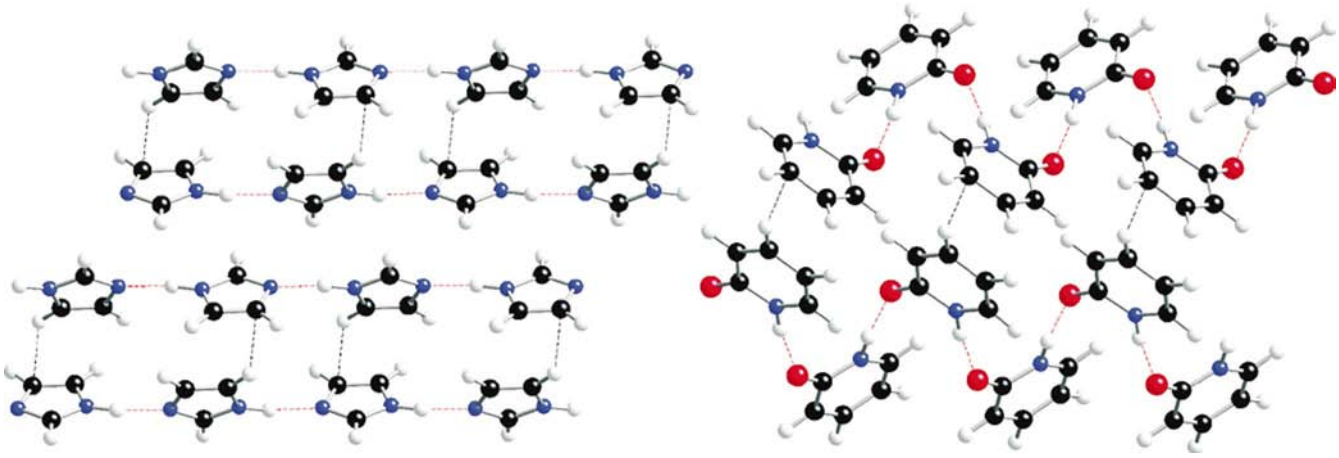

Figure 46
Crystal-packing diagrams for imidazole (left) and 2-pyridone (right). Red dashes depict strong hydrogen bonds; black dashes depict the shortest C—H···C contact in each structure.

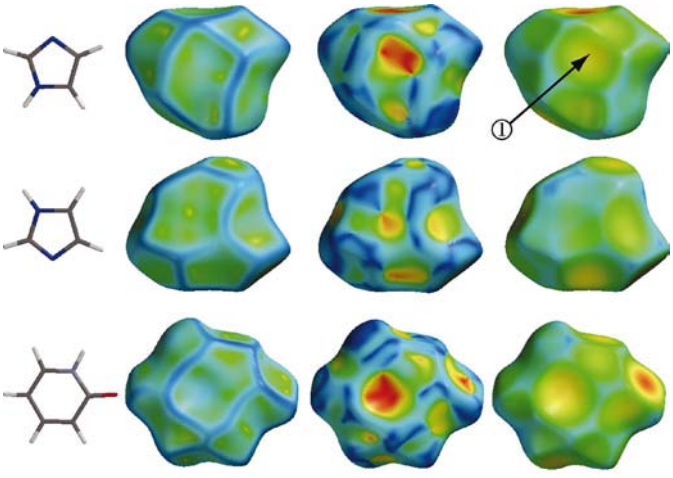

Figure 47
Hirshfeld surfaces for imidazole (top two rows; front and back views) and 2-pyridone (bottom row); see Fig. 45 for fingerprint plots and refcodes. For these diagrams d_e is mapped over the range 0.6–2.6 Å.

contacts; no evidence is found for a large contribution from H···H contacts.

The crystal structure of urea is unique; it may be the only instance where a carbonyl O atom accepts four hydrogen bonds (Swaminathan *et al.*, 1984). The Hirshfeld surface of urea mapped with d_e (Fig. 50) clearly shows the close approach of the four hydrogen-bond donors to the O atom; Fig. 51 shows the hydrogen-bonding environment of the O atom, highlighting the pair of identical in-plane hydrogen-bond contacts at 2.01 Å and the pair of identical out-of-plane contacts at 2.07 Å. The two-dimensional fingerprint plot for urea (Fig. 50) is quite unlike any previously observed for hydrogen-bonded structures. The hydrogen-bonding fingerprint dominates the plot and is itself quite different from those observed for other molecular crystals; it features much broader spikes than typical hydrogen-bond fingerprints, at least in part owing to the fact that several hydrogen bonds are located so close to each other on the surface, and points on the

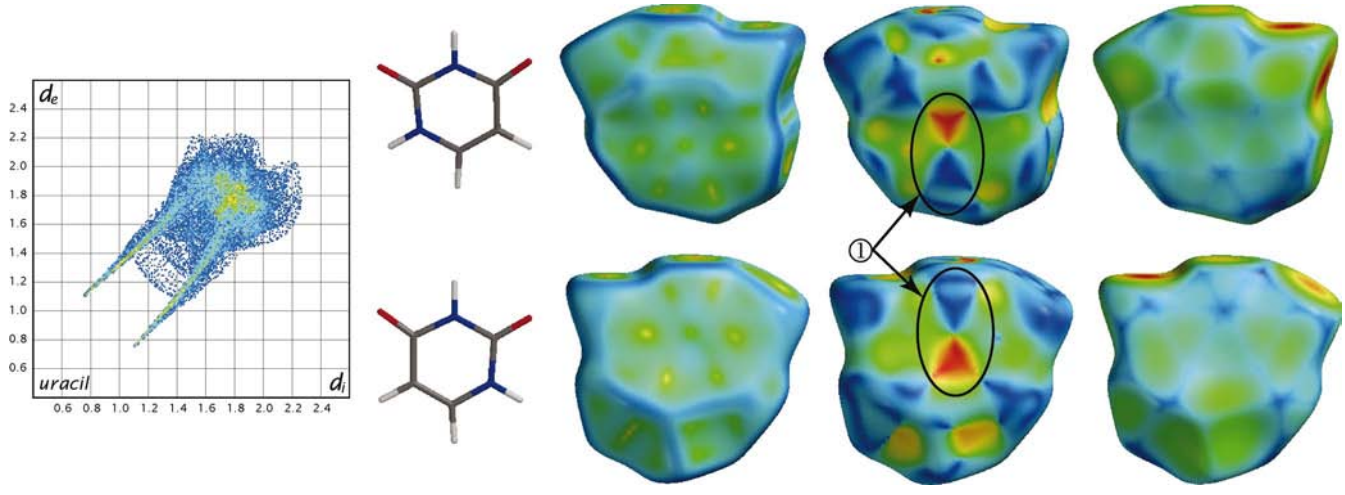

Figure 48
Two-dimensional fingerprint plot and Hirshfeld surface (front and back views) for uracil (URACIL; Stewart & Jensen, 1967). In these diagrams d_e is mapped over the actual range on the surface (0.76–2.25 Å).

surface that lie between the adjacent hydrogen bonds contribute to the broadening of the fingerprint. While the N—H···O angle for the out-of-plane hydrogen-bond is relatively normal at 166.8°, the in-plane hydrogen bond is geometrically constrained, with an N—H···O angle of 147.6°, and this constraint also contributes to the particularly broad fingerprint for these interactions.

1,4-Benzoquinone (Fig. 52) has four weak C—H hydrogen-bond donors and two carbonyl acceptor groups and, from the Hirshfeld surface mapped with d_e, it is clear that in these centrosymmetric molecules hydrogen bonding is fully utilized in the crystal structure. Each carbonyl O atom accepts two hydrogen bonds, with H···O distances of 2.29 and 2.37 Å. The two-dimensional fingerprint plot (Fig. 52) shows that this weak hydrogen-bond interaction is identical in nature to the strong hydrogen bonds explored earlier in this section, although at a longer distance (*i.e.* the characteristic spikes are shorter). Molecules in the crystal of 1,4-benzoquinone pack in hydrogen-bonded sheets, and the interlayer packing is easily elucidated from the Hirshfeld surfaces. The three-centre hydrogen-bond motif lies almost directly above the ring of its neighbour in the crystal, leaving an obvious imprint on the curvedness surface, where three surface patches meet. In addition, the position of the O atom above the surface causes a slight depression that appears as a red spot on the shape index surface. Fig. 53 illustrates the interlayer packing in 1,4-benzoquinone as described above, with a crystal-packing diagram of curvedness surfaces, showing how the location of adjacent molecules influences the shape of the Hirshfeld surface above the plane of the molecule. The blue lines of high curvedness delineate the surface patches that contact the central molecule.

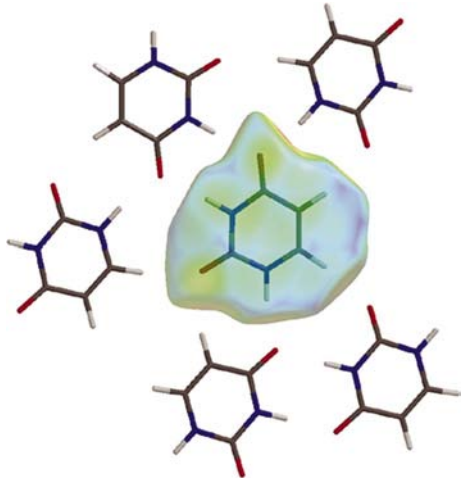

Figure 49
Semi-transparent d_e surface of uracil, showing how the close approach of neighbouring H atoms in the plane of the molecule influences the surface shape.

3.5. Molecules containing chlorine

The role of halogen atoms in directing the architecture of molecular crystal structures has been the subject of some discussion, and there has been disagreement about the manner in which functional groups containing halogens influence the final structure and even whether the influence that has been attributed to these groups is real. The propensity for chlorinated aromatics and related compounds to form crystal structures with a short axis (~4 Å) has been comprehensively reviewed by Desiraju and co-workers (Sarma & Desiraju, 1986; Desiraju, 1987; Desiraju & Parthasarathy, 1989). Such structures feature Cl···Cl contacts shorter than the van der Waals separation, either within a sheet or between adjacent sheets. Desiraju & Parthasarathy (1989) have also argued that the frequency of short halogen–halogen contacts in crystal structures of chlorinated hydrocarbons provides evidence of a specific attractive force in operation. In a more recent study, Price *et al.* (1994) analysed only the chlorinated hydrocarbons using a version of the CSD database containing many more structures than that used in the earlier study by Desiraju & Parthasarathy (1989) and found that most of the close Cl···Cl contacts occurred in heavily or fully chlorinated hydrocarbons, where 'any reasonably dense crystal packing must involve van

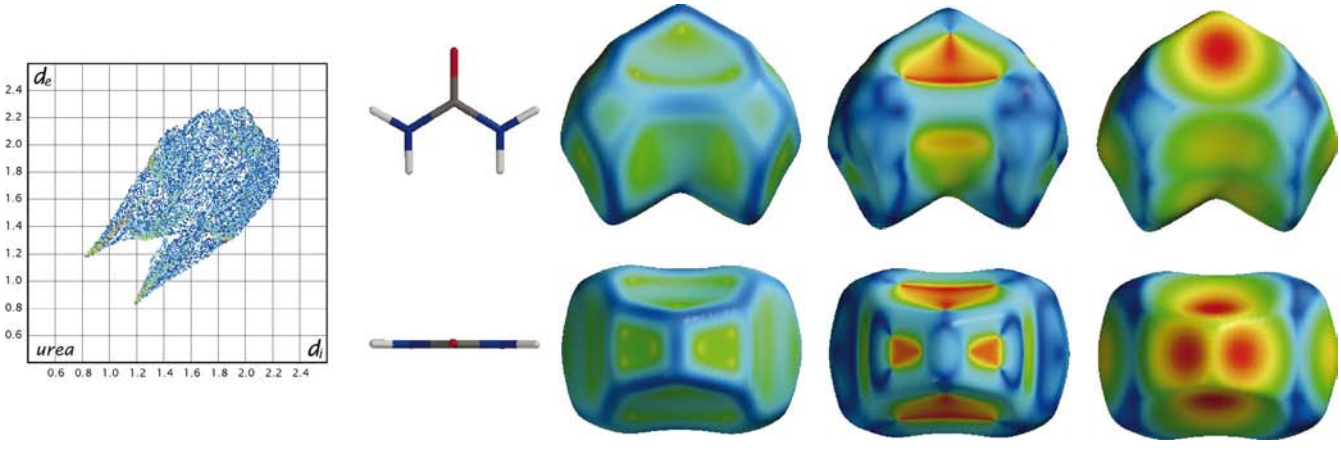

Figure 50
Two-dimensional fingerprint plot and Hirshfeld surface for urea in two orientations (UREAXX14; Swaminathan *et al.*, 1984). In these diagrams d_e is mapped over the actual range on the surface (0.83–2.30 Å).

der Waals contacts between the Cl atoms'. Several authors have noted a perceived preference of Cl···Cl contacts towards the linear and bent configurations shown in Fig. 54, with the double and triple contacts shown in that figure occurring in the more heavily chlorinated compounds. This angular preference of Cl···Cl contacts was established in an analysis of the 1984 version of the CSD by Ramasubbu *et al.* (1986), but repetition of this analysis using a subsequent version of the CSD suggests that there is little evidence for preferred orientations (Price *et al.*, 1994), and our own recent re-analysis confirms this conclusion (McKinnon, 2003).

The hydrogen-bonding nature of the C—H···Cl interaction was unequivocally confirmed by Aakeröy *et al.* (1999) through a substantial CSD study that showed a distinct preference towards a linear interaction, even at distances greater than the sum of the van der Waals radii. On this basis these authors suggested that a van der Waals cut-off for classification of hydrogen-bonding interactions is inappropriate, a sensible conclusion given that the van der Waals radius is an arbitrary quantity for any atom, and any distinction between shorter and longer than van der Waals contacts is similarly arbitrary. In this work we make no attempt to debate the nature of any kind of intermolecular interaction, although it will become clear from the Hirshfeld surfaces of the halogen-containing molecules presented in this section that the interactions involving halogens are different from the interactions discussed in previous sections.

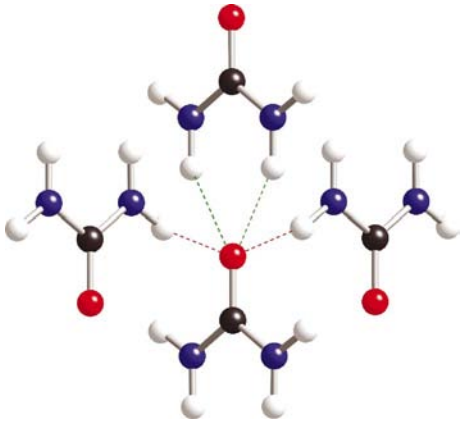

Figure 51
The four hydrogen bonds accepted by the carbonyl O atom in the crystal structure of urea. Out-of-plane contacts at 2.01 Å are in red, and in-plane contacts at 2.07 Å are in green.

Molecular chlorine provides a very simple example to introduce the nature of the Hirshfeld surface produced by the C···Cl interaction. The first notable aspect of the surface (Fig. 55) is the fact that it is made up of a series of almost flat faces, with each face bordered by a blue region on the curvedness surface and corresponding to a close contact to a single neighbouring molecule. The curvedness in the regions of close Cl···Cl contact is very low, with relatively large distinctive red spots at the top and bottom right of the surface, in the same area on the surface that has the minimum d_e, also shown by two red regions on that surface. The shape index mapped on the surface of Cl_2 is quite striking, with each flat patch marked with a distinctive blue cross linking the 'corners' of each face; these crosses are a direct result of the very flat surface in these regions. Where the principal curvatures are low, the shape index is sensitive to very small changes in the relative values of the principal curvatures of the surface and hence to contributions to the weight function from second-nearest neighbours. This surface pattern has already been noted for H···H contacts in the alkanes (see Fig. 5); it appears to be a particular feature of direct like-atom–like-atom contacts in the crystal and is more prominent for heavier atoms. The origin of this feature of the shape index surface is examined further in the following section.

As expected, the range of contact distances in the Cl_2 molecular crystal is small (1.64–2.42 Å) and in this case the actual range is used in Fig. 55 to map the property, in order to maximize the visibility of surface features. The two-dimensional fingerprint plot for Cl_2 (Fig. 55) reflects this narrow range of surface contacts and also shows that the closest contact, the location of which is clear from the two bright-red spots on the d_e surface, is significantly shorter than the van der Waals radius of 1.75 Å (Bondi, 1964). The sharp nature of the spike between 1.64 and 1.85 Å is due to a single bent (type *B*) Cl···Cl contact. With symmetry, this results in four red spots on the d_e surface, two of which are hidden in the view

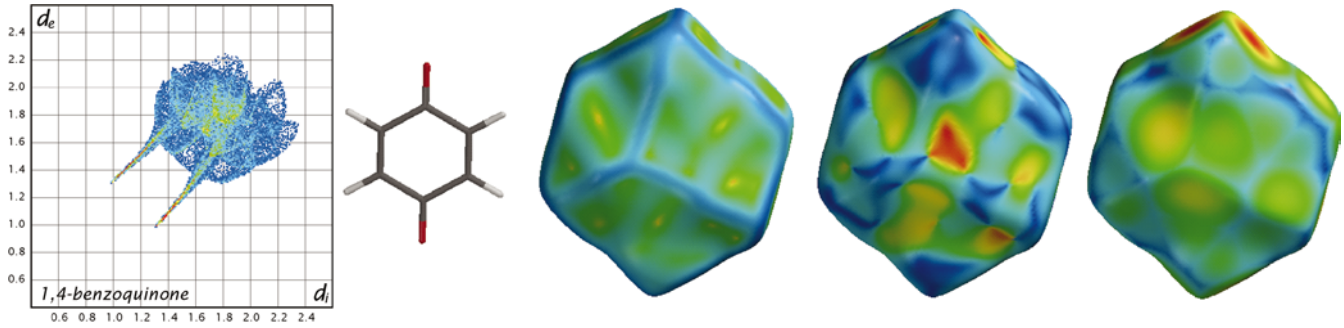

Figure 52
Two-dimensional fingerprint plot and Hirshfeld surface for 1,4-benzoquinone (BNZQUI02; van Bolhuis & Kiers, 1978). In this diagram d_e is mapped over the actual range on the surface (0.99–2.24 Å).

presented in Fig. 55, and the point where this fingerprint begins to broaden corresponds to all the other Cl···Cl contacts. We have noted previously (Spackman & McKinnon, 2002) that it is probably not a coincidence that the generally accepted van der Waals radius for Cl is near 1.75 Å. At longer distances than this, the fingerprint plot suggests an isotropic van der Waals contact, but the extreme narrowness of the distribution of points for d_e and d_i of less than 1.75 Å closely resembles the hydrogen-bond spikes and hints at some intermolecular contacts in molecular chlorine being different from, and not just shorter than, others.

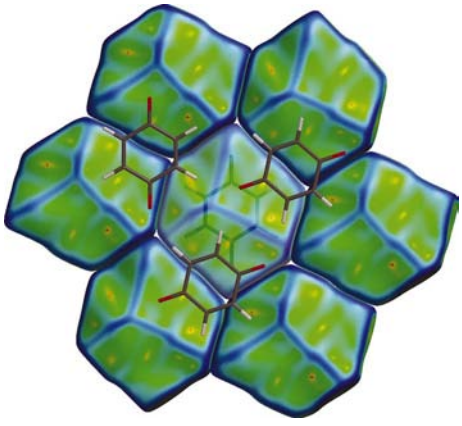

Figure 53
Hirshfeld surface-packing diagram of 1,4-benzoquinone molecules mapped with curvedness. The Hirshfeld surface in the centre is shown in semi-transparent mode.

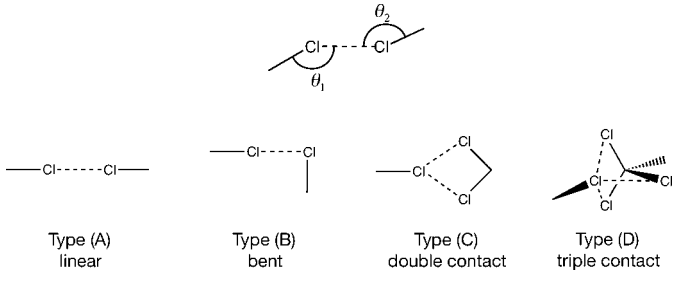

Figure 54
Top: angles θ_1 and θ_2 used to describe an arbitrary Cl···Cl contact. Bottom: common motifs for Cl···Cl contacts in organic molecular crystals.

The series of chlorinated methanes, chloromethane (CH_3Cl), dichloromethane (CH_2Cl_2), chloroform ($CHCl_3$) and carbon tetrachloride (CCl_4), exhibit different combinations of H···H, Cl···H and Cl···Cl intermolecular interactions depending on the chlorine content of the molecule. The Hirshfeld surfaces of the chlorinated methanes are given in Fig. 56, with d_e for these crystals mapped between 1.10 and 2.80 Å, along with the corresponding two-dimensional fingerprint plots. Together, these figures dramatically highlight the changing combination of interaction type across the series.

The Hirshfeld surfaces for the chlorinated methanes are much more faceted than any previously discussed and particularly more so than the rounded surfaces of the hydrocarbons in §§3.2 and 3.3. The faceted nature of the surfaces is especially noticeable on the curvedness surfaces, which show the surfaces as a collection of almost flat faces with reasonably sharp edges highlighted in blue; red spots, where the curvedness is close to or less than −4.0, are quite common. The shape index shows that these surfaces are largely convex (blue in colour) and extensively feature the blue crosses and lines indicative of like-atom–like-atom contacts described above.

The two-dimensional fingerprint plots in Fig. 56 provide an especially clear picture of the intermolecular interactions in these crystals and from these plots several general observations can be made. From the absence of certain characteristic patterns it is clear that there are no Cl···Cl contacts in chloromethane and no H···H contacts in chloroform, but C—H···Cl contacts occur in all cases except CCl_4, where such contacts are not possible, although the exact nature of these contacts is different in each crystal. Each structure is discussed in detail below in relation to its two-dimensional fingerprint plot.

As mentioned, the crystal structure of chloromethane does not contain any Cl···Cl close contacts. This fact is clear on the fingerprint plot from the absence of a red streak of points on the diagonal between 1.7 and 2.0 Å, which is present in each of the other three plots in Fig. 56 (and also for Cl_2 in Fig. 55). The very sharp C—H···Cl fingerprint is due to three relatively close hydrogen contacts to the Cl atom. Two of these are

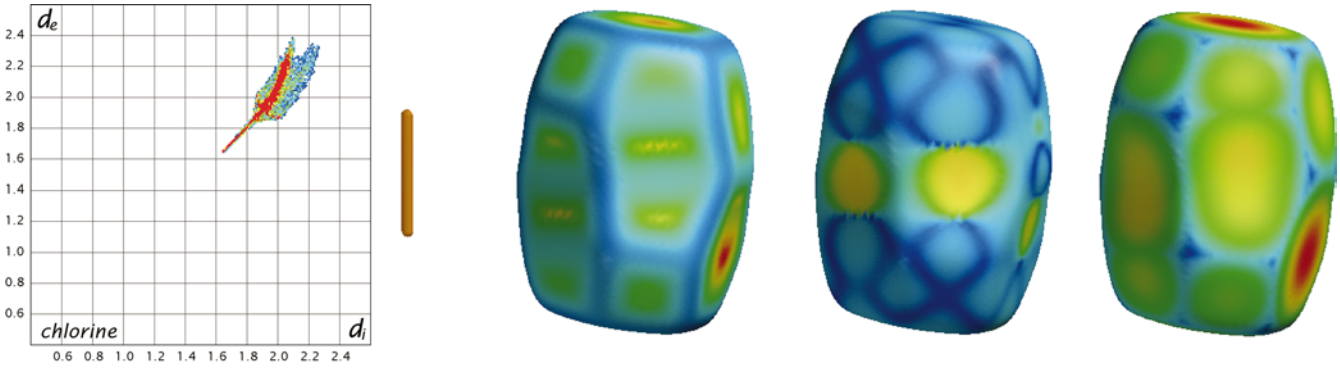

Figure 55
Two-dimensional fingerprint plot and Hirshfeld surface of molecular chlorine, Cl_2 (Stevens, 1979); the d_e surface is mapped over the range 1.64–2.42 Å.

symmetry-equivalent contacts at 3.00 Å and the third is almost identical, at 3.01 Å. The fingerprint for these contacts looks very much like a hydrogen bond and these contacts are almost linear; the C—H···Cl angles are 172.2 and 171.8°, respectively. The small region of concave curvature visible on the shape index surface (1 in Fig. 56) is also indicative of a hydrogen-bond acceptor (see, for example urea, Fig. 50). H···H contacts occur in the crystal, although they are at a longer distance than observed so far (the shortest d_e here is almost 1.4 Å), and in

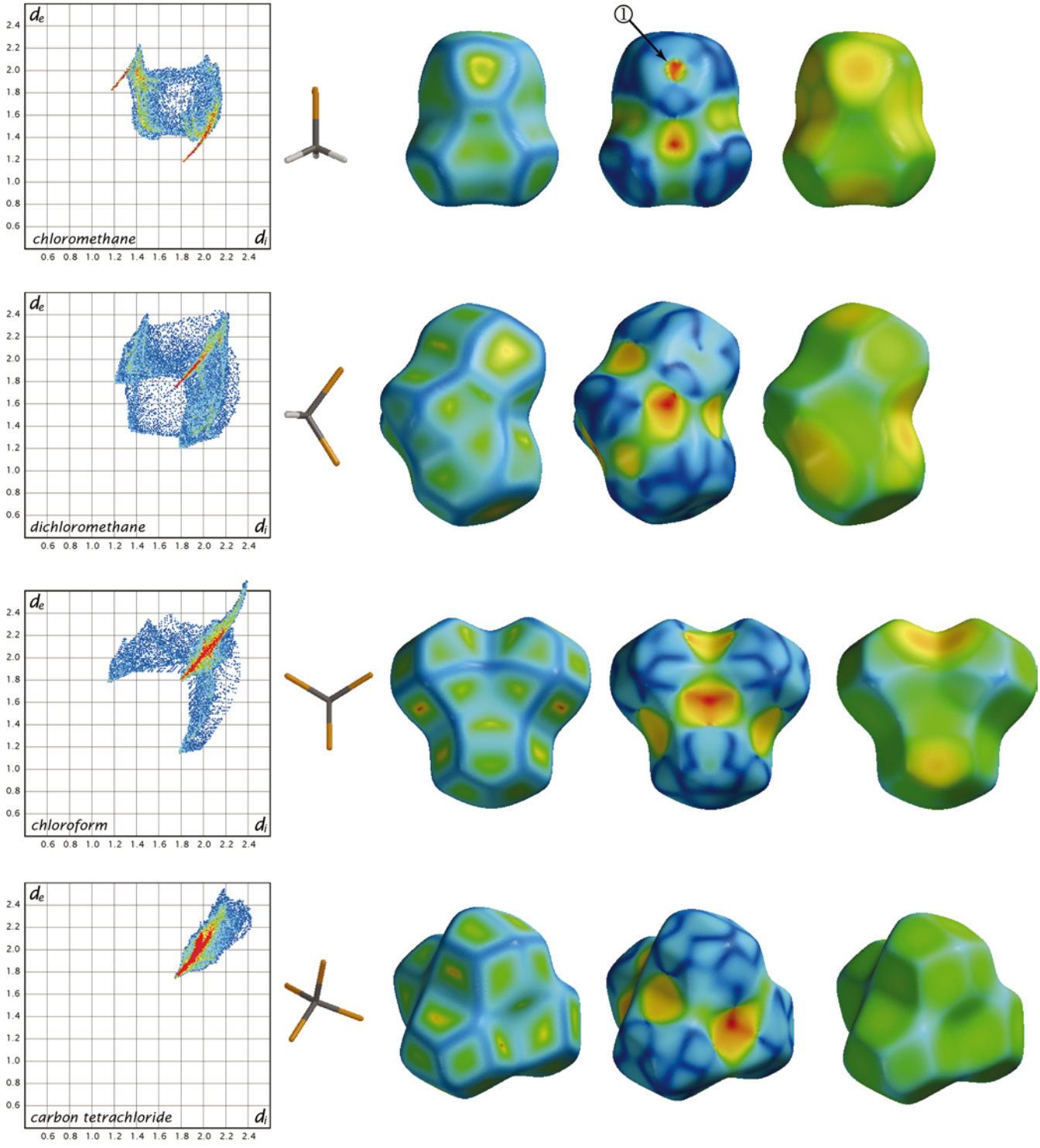

Figure 56
Two-dimensional fingerprint plots and Hirshfeld surfaces of the chlorinated methanes: chloromethane (CLMETH; Burbank, 1953), dichloromethane (DCLMET10; Kawaguchi *et al.*, 1973), chloroform (CLFORM; Fourme & Renaud, 1966) and carbon tetrachloride (CARBTC; Piermarini & Braun, 1973). For these and remaining surfaces in this section, d_e is mapped over the range 1.10–2.80 Å.

this case the shortest is a three-centre contact (type *C* in Fig. 54), producing the broad fingerprint in the figure.

The two-dimensional fingerprint plot for dichloromethane features a distinctive sharp fingerprint on the diagonal of the plot, starting from $d_e = d_i \simeq 175$ Å, due to Cl···Cl contacts. Each Cl atom in dichloromethane is involved in two symmetry-equivalent bent contacts at 3.49 Å, with $\theta_1 = 168.5°$ and $\theta_2 = 116.1°$. If, for descriptive purposes, this interaction is considered a donor–acceptor interaction, where the C—Cl···Cl angle at the donor is closest to 180°, then each Cl atom in this crystal can be said to donate one bent contact and to accept one bent contact. The H···Cl contact fingerprint is now

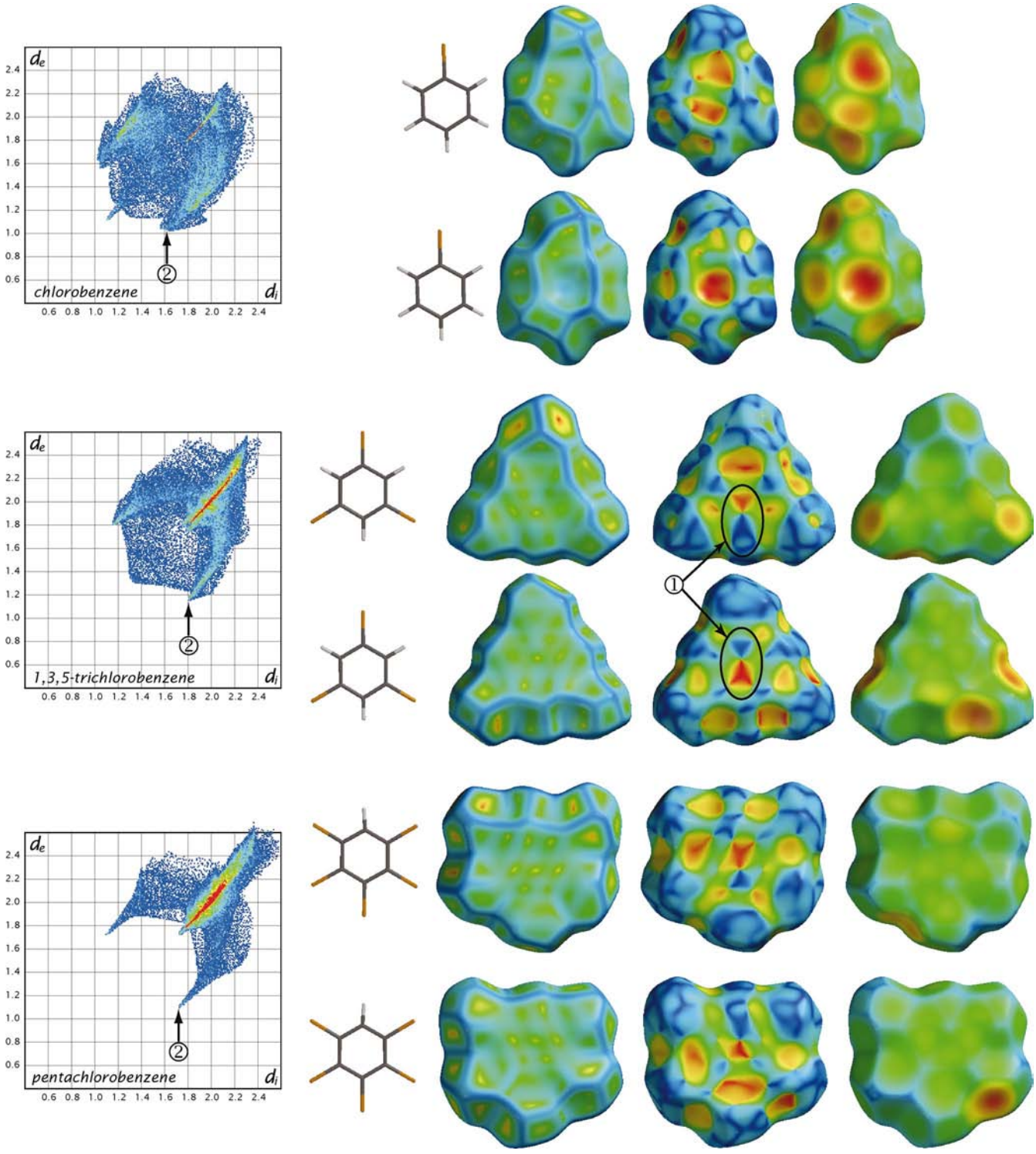

Figure 57
Two-dimensional fingerprint plots and Hirshfeld surfaces (front and back views) for chlorobenzene (top; MCBENZ; André *et al.*, 1971), 1,3,5-trichlorobenzene (middle; TCHLBZ; Milledge & Pant, 1960) and pentachlorobenzene (bottom; PNCLBZ; Marsh & Williams, 1981).

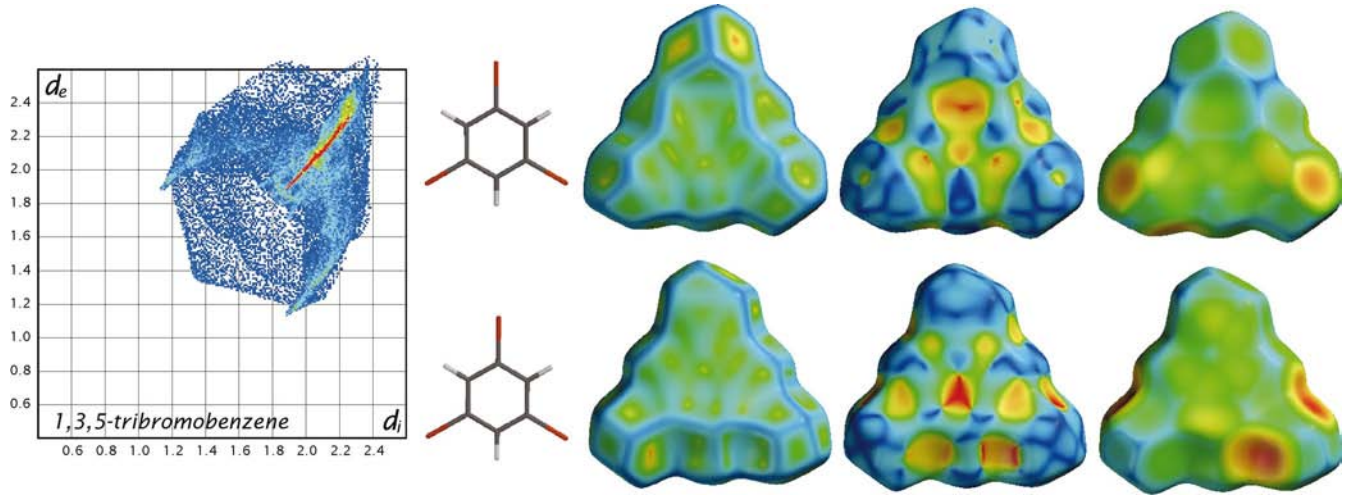

Figure 58
Two-dimensional fingerprint plot and Hirshfeld surface (front and back views) for 1,3,5-tribromobenzene (TBRMBZ; Milledge & Pant, 1960).

very broad, despite the fact that the H···Cl distance (3.00 Å) is the same as that in chloromethane; this broadening results from a low-angle contact ($\theta_1 = 114°$ and $\theta_2 = 99°$, similar in some respects to urea, §3.4.4)

The structure of chloroform is dominated by three-centre (type *C*) Cl···Cl contacts (which are actually two Cl···Cl contacts), causing a fairly broad fingerprint that extends to the upper right of the plot ($d_e^{\max} > 2.7$ Å). The broad C—H···Cl fingerprint in this plot results from a C—H contact to two Cl atoms related by a mirror plane.

The fingerprint plot for carbon tetrachloride is best compared with that for molecular chlorine (Fig. 55), although carbon tetrachloride displays a greater range of d_e and d_i, suggesting a less efficient packing mode that probably results from the change in molecular geometry from linear to the more difficult to pack tetrahedral geometry. The minimum value of d_e is 1.74 Å, almost exactly the accepted van der Waals radius and considerably longer than the minimum d_e of 1.64 Å in Cl_2, again suggesting that there might be an attractive interaction in Cl_2 that is not present in CCl_4. The shortest intermolecular contact in the crystal structure of carbon tetrachloride is a bent contact at 3.52 Å, compared with 3.28 Å in Cl_2. Two additional contacts at 3.54 Å in carbon tetrachloride cause the point of the fingerprint to broaden significantly, whereas in Cl_2 this broadening occurs due to additional contacts at 3.70 Å.

Examples of the chlorinated methanes showed the direct influence of the Cl···Cl interaction on the Hirshfeld surface and the distinct pattern on the two-dimensional fingerprint plots that results from this type of contact. The Hirshfeld surfaces of chlorobenzene, 1,3,5-trichlorobenzene and pentachlorobenzene in Fig. 57 show that, as the chlorine substitution in these molecules increases, the crystal structure changes from one dominated by herringbone packing and C—H···π contacts, similar to benzene (chlorobenzene), to one dominated by planar sheets of molecules in 1,3,5-trichlorobenzene and pentachlorobenzene.

It is clear from both the Hirshfeld surface and the two-dimensional fingerprint plot of chlorobenzene that this molecule packs in a similar manner to the herringbone motif of benzene. The large depression above the ring, which appears as a red circular region on the shape index, is mirrored by the blue region adjacent to the H atom at the top right of the molecule and is due to a C—H···C contact at 2.65 Å (to the closest C atom in the ring). In the fingerprint plot the feature due to this interaction (2 in Fig. 57) blends with a feature due to the shortest H···Cl contact of 2.86 Å. The red fingerprint due to the Cl···Cl contact in chlorobenzene is very sharp and starts on the diagonal from just below 1.8 Å (the shortest Cl···Cl contact is 3.57 Å). A single short H···H contact at 2.21 Å appears on the fingerprint plot as a short spike along the diagonal at 1.1 Å.

The Hirshfeld surface of 1,3,5-trichlorobenzene, and particularly the surface mapped with shape index, shows that this structure packs in offset sheets. Inspection of the colour complementarity of the shape index shows that the top of one molecule packs against the bottom of its neighbour (1). Inspection of the curvedness and d_e surfaces shows that, while

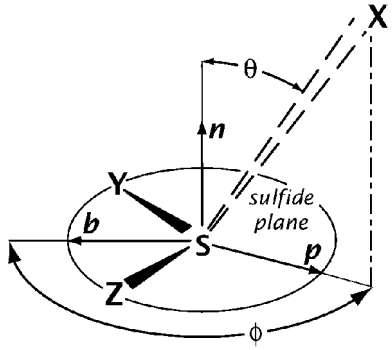

Figure 59
Schematic diagram showing the polar angle θ and azimuthal angle φ describing the S···X interaction.

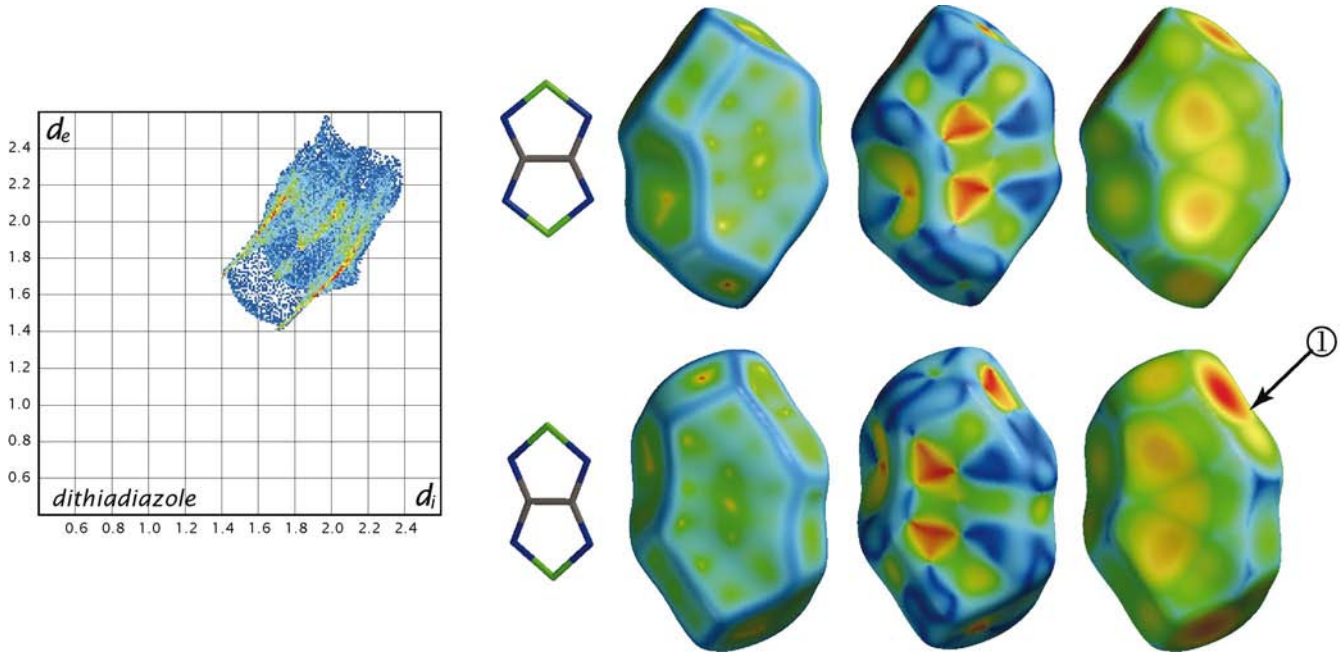

Figure 60
Two-dimensional fingerprint plot and Hirshfeld surface for 1,2,5-thiadiazolo[3,4-*c*][1,2,5]thiadiazole (dithiadiazole; BAWHEM; Kane & Schaeffer, 1981). Although the molecule lies on an inversion centre, front and back views are shown to improve the view of the faces on the sides of the surface.

close H···Cl contacts appear as a red spot on d_e at the Cl atoms, close Cl···Cl contacts are not highlighted by this property, but when the contact is between two Cl atoms, the surface is very flat, producing a red spot on the curvedness surface. The fingerprint plot shows how the structure is different from that of chlorobenzene, with a much broader feature on the diagonal starting from 1.8 Å, caused by an overlap of different Cl···Cl contacts and carbon π–π stacking contacts. The fingerprint labelled 2 is distinctly different from the same region on the fingerprint plot for chlorobenzene; here it is due only to Cl···H contacts. The broad diffuse region of blue points starting from $d_e = d_i \simeq 1.3$ Å is due to two H···H contacts, at 2.64 and 2.88 Å.

The structure of pentachlorobenzene also involves layered packing, although the surface above the molecular plane features broad undulations due to the large Cl atoms pushing into the surface above this planar molecule. The fingerprint plot shows that there are no H···H contacts in the crystal at all, and the structure is dominated by Cl···Cl and Cl···C contacts producing the broad green–red region around the diagonal. The distinctive Cl···H fingerprint (2) is also visible; as with 1,3,5-trichlorobenzene, close contacts from H to Cl atoms appear as a red spot on the d_e surface, while close Cl···Cl contacts appear as a red spot on the curvedness surface.

It is well known that many chlorinated, brominated and iodinated hydrocarbons form isomorphic crystal structures, while fluorinated compounds can sometimes have identical crystal packing to their hydrocarbon analogues (Nangia, 2000). The structures of 1,3,5-trichlorobenzene (Fig. 57) and 1,3,5-tribromobenzene (Fig. 58) are included as examples of isostructural halogenated compounds. The Hirshfeld surfaces of these two compounds are virtually indistinguishable in shape, but close comparison shows a slight difference in the features of the shape index due to layer stacking (adjacent blue and red triangles), reflecting a very slightly different interlayer packing offset. Although these two surfaces are topologically very similar, the surface of 1,3,5-tribromobenzene is significantly larger ($V_H = 191.2$ Å^3 compared with 175.0 Å^3 for 1,3,5-trichlorobenzene), as would be expected. The two-dimensional fingerprint plots for these two crystal structures reflect the structural similarity, with the only differences arising from the different sizes of the Cl and Br

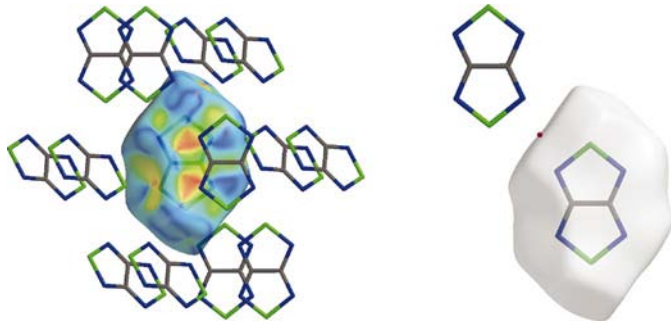

Figure 61
Left: Packing diagram for dithiadiazole, showing the Hirshfeld surface of the central molecule mapped with shape index in semi-transparent mode. Right: Centrosymmetric dimer of dithiadiazole, with one semi-transparent Hirshfeld surface; a red dot has been placed at the inversion centre.

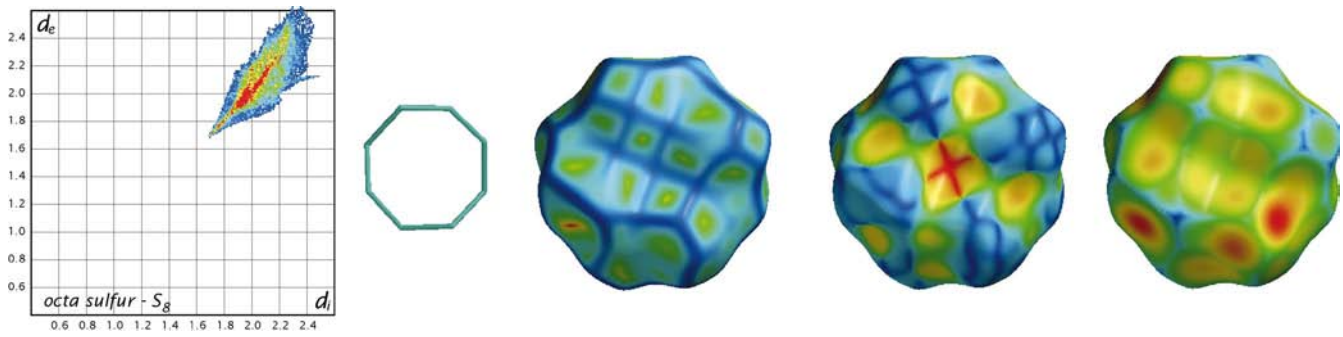

Figure 62
Two-dimensional fingerprint plot and Hirshfeld surface for S_8 (FURHUV; Rettig & Trotter, 1987).

atoms. The spikes due to the $X\cdots$H contact are pushed further apart on the plot for X = Br, with the minimum d_i for the bromine in this contact at 1.89 Å, compared with 1.80 Å for the chlorinated structure, while the closest surface contact to hydrogen is unchanged at 1.14 Å for both structures. The closest halogen–halogen contacts also occur with $d_e^{\min}$ at 1.89 and 1.80 Å for the brominated and chlorinated forms, respectively, slightly greater than the van der Waals radii of 1.85 and 1.75 Å (Bondi, 1964), and these contacts appear on the fingerprint plot as bright-red streaks.

3.6. Molecules containing sulfur

The possible role of sulfur in structure-directing interactions is less well understood than the role of other common heteroatoms (Desiraju, 1989), this uncertainty probably being due to the very low number of simple known crystal structures containing sulfur. The CSD currently contains 981 accurate structures containing only C, H and S atoms,[3] and this relatively low number of structures makes the identification of trends for contacts to sulfur difficult in the absence of stronger structure-directing groups. In an early statistical analysis of 69 crystal structures containing S atoms, Rosenfield *et al.* (1977) demonstrated a distinct angular preference for non-bonded contacts to divalent sulfur. Fig. 59, based on Fig. 1(*a*) from that work, shows the relevant angles describing the S$\cdots X$ interaction. Those authors suggested that S$\cdots X$ interactions fall into two categories: type I interactions have $\theta < 40^\circ$ (that is, X approaches close to perpendicular to the sulfide plane), with atom X usually being an electrophile, and for these contacts φ is not really meaningful; type II interactions have $60^\circ < \theta < 90^\circ$ (that is, X approaches close to the sulfide plane) and usually involve nucleophiles, and the approach is generally approximately along the extension of one of the S atom's bonds, giving $\varphi \simeq 130^\circ$. Guru Row & Parthasarathy (1981) later showed that S$\cdots$S interactions can be rationalized in a similar manner, with most $S_A\cdots S_B$ contacts regarded as an attractive electrophile–nucleophile pairing. That is, a situation exists where S_B approaches S_A parallel to S_A's sulfide plane (type II, S_B is a nucleophile), while S_A approaches perpendicular to the sulfide plane of S_B (type I, S_A is an electrophile).

The Hirshfeld surface for 1,2,5-thiadiazolo[3,4-*c*][1,2,5]thiadiazole (dithiadiazole, Fig. 60) clearly shows that the molecules pack in offset layers of parallel molecular sheets. The complementary blue and red triangles on the shape index surface echo the actual offset, with red triangles showing where two N atoms from an adjacent molecule lie above the centre of the five-membered rings, complementing the corresponding blue triangles above the N atoms; a packing diagram with a semi-transparent Hirshfeld surface mapped with shape index (Fig. 61) shows this more clearly. The two-dimensional fingerprint plot features a pair of sharp spikes due to unusually short N$\cdots$S contacts joined by a region of diffuse blue points that suggest the presence of a ring dimer, as noted in previous examples of hydrogen bonding, although this example is somewhat different because the central diffuse points occur at shorter distance than the N$\cdots$S spike. This N$\cdots$S contact occurs across a centre of symmetry (see the right of Fig. 61) and the offset nature of this dimer means that the N$\cdots$N contact is slightly shorter at 3.05 Å, compared with 3.10 Å for the N$\cdots$S contact, resulting in the unusual appearance on the two-dimensional fingerprint plot. Both the d_e surface around this ring dimer (labelled 1 in Fig. 60) and the shape index surface in the same region feature very similar patterns to those observed in previous examples of ring hydrogen bonds. The charge density around this cyclic motif has been the subject of a recent experimental charge density study on S_4N_4 by Scherer *et al.* (2000), which demonstrated the existence of charge concentrations around the S and N atoms responsible for this characteristic molecular recognition motif.

Octasulfur, S_8, (Fig. 62) shows features on the Hirshfeld surface that are remarkably similar to those observed for carbon tetrachloride, CCl_4 (Fig. 56), another compound where only like-atom–like-atom intermolecular interactions occur between quite large atoms. The curvedness surface emphasizes the fact that the Hirshfeld surface is strongly faceted, with distinct flat regions (green) and highly curved regions (blue). Points on the fingerprint plot are clustered close to the diagonal, because all intermolecular contacts are of course between S atoms, giving similar d_e and d_i for all points on the surface. The small tail on the right of the plot at d_e = 2.1 Å

[3] July 2004 release. Search limited to error-free structures with all atomic positions determined and $R < 0.10$.

and d_i increasing past 2.4 Å is due to a contact to the centre of the ring, corresponding to the distinct red cross above the centre of the ring on the shape index surface, and the adjacent complementary blue cross. This feature occurs because the distance from the surface at the centre of the ring to the nearest atom inside the surface is significantly greater than the distance to the nearest atom outside the surface.

The shape index surface of S_8 features dark-blue crosses on flat regions of the surface near some S···S contacts, patterns that have previously been observed on the Hirshfeld surfaces of the aliphatic hydrocarbons (Fig. 5, H···H contacts) and the chlorinated methanes (Figs. 55 and 56, Cl···Cl contacts). These are more prominent in S_8 than in any of the compounds discussed previously and Fig. 63 shows a detailed view of the shape index surface, highlighting the blue cross and showing the positions of neighbouring atoms in the crystal. This configuration produces a surface that somewhat resembles a smoothed half-cube – that is, a reasonably flat region bounded by four pseudo-edges, with the orientation of these edges determined by the location of the four next-nearest neighbours. The appearance of the shape index on the flat region of the surface confirms that this area is not actually flat, or uniform, but that it has some distinct structure.

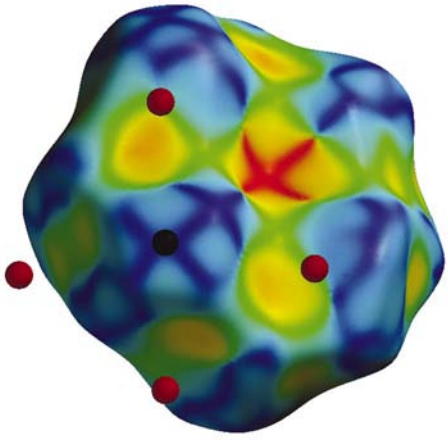

Figure 63
Hirshfeld surface of S_8 mapped with shape index, illustrating the origin of the blue cross on the surface. There are five atoms near the surface in the region of the blue cross, with S···S distances ranging from 3.50 to 3.87 Å; the closest atom, shown in black, lies directly above the surface, and the next four closest atoms are shown in red.

Tetrathiafulvalene (TTF) is polymorphic and exists in a triclinic modification with four half-molecules in the asymmetric unit, as well as a monoclinic form with $Z' = 0.5$; the latter structure was used to create the graphics in Fig. 64. This crystal structure is largely based on the π–π stacking of molecules, as is emphasized by the complementary blue and red diamonds on the shape index surface, marked here by rings over the surface. The two-dimensional fingerprint plot for TTF reflects this π–π stacking, with a series of small red regions along the diagonal corresponding to heavy atom contacts between stacked layers, as well as some S···S contacts within each layer. The shortest S···S contacts in the crystal are at 3.41 Å and appear on the two-dimensional fingerprint plot as the start of a sharp green line at $d_e = d_i \simeq 1.7$ Å. This contact occurs in the area labelled 1 on the d_e surface, although S···S contacts do not feature as red spots on the d_e surface because the contact distances are large. However, the curvedness surface does feature a small red spot of low curvedness characteristic of like-atom–like-atom contacts (not quite visible in this view). The change in colour from pale-blue/green to red on the fingerprint plot starting at $d_e \simeq d_i \simeq 1.8$ Å corresponds to an additional S···S contact at 3.58 Å, as well as the start of the interlayer contacts, the shortest being a C···C contact at 3.62 Å.

The d_e surface of TTF features two bright-red spots at the top of the surface, which are due to the close approach of a pair of H atoms from the end of an adjacent molecule (see the crystal-packing diagram, Fig. 65). This contact is responsible for the 'bifurcated' H···H fingerprint in the figure, because, while this contact involves a pair of H···H contacts at 2.56 and 3.05 Å, the geometry of this contact (shown in the packing diagram) means that it also involves H···C contacts at 3.05 and 3.25 Å. Thus, the fingerprint reflects the partial H···C nature of the contact, and the fingerprint is split across the diagonal. The red spots on the d_e surface labelled 2 and 3 are due to relatively close S···H contacts, at 3.23 and 3.28 Å. Note that in particular the contact labelled 3 produces a small red

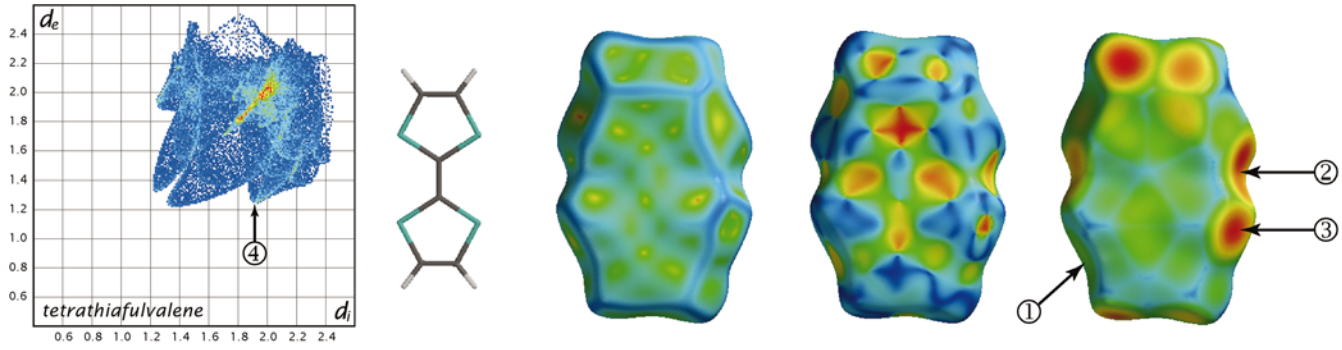

Figure 64
Two-dimensional fingerprint plot and Hirshfeld surface for the monoclinic form of tetrathiafulvalene (TTF; BDTOLE10; Cooper *et al.*, 1974); the range of d_e is 1.22–2.54 Å.

(concave) spot on the shape index surface, reminiscent of other weak hydrogen bonds, such as the C—H···Cl contact in CH_3Cl (Fig. 56). The broad fingerprint labelled 4 results from parts of the surface involved in both the H···C and the H···S contacts discussed above. We believe that the fingerprint plot and the various functions mapped on the Hirshfeld surface for TTF convincingly demonstrate that short contacts *other than* S···S are without doubt important in this structure, and it is relevant to note that the most detailed comparison of intermolecular contacts and interactions between these two polymorphs of TTF (Ellern *et al.*, 1994) ignored the H atoms completely.

4. Concluding remarks

This paper has described the first detailed application of the software tools implemented to exploit the Hirshfeld surface, which was introduced by Spackman & Byrom (1997). This paper also represents the first major investigation of the properties of the Hirshfeld surface, conducted as an integral part of the development of the software tools described. Because the Hirshfeld surface is uniquely defined by the crystal structure, an intrinsic property of the surface such as curvature should contain information that reflects the presence of neighbouring atoms and molecules, and hence close intermolecular contacts. As part of this investigation we have adopted an innovative use of surface curvature and properties derived from it, *curvedness* and *shape index*, which have been shown to convey this information particularly effectively, each providing visual insight into different aspects of the crystal structure.

Curvedness, a measure of 'how much' shape, effectively divides the Hirshfeld surface into a set of patches, where each surface patch has a different nearest-neighbour molecule in the crystal. This attribute of the surface curvedness has been used to identify contacting parts of surfaces by examining the shape of the blue region of high curvedness that outlines each surface patch, conveying essential features of the crystal packing without the need to view and interpret a crystal-packing diagram. Curvedness also has the potential to define a coordination number for a molecule, based on the number of distinct surface patches on its Hirshfeld surface.

Figure 65
Crystal-packing diagram for the monoclinic form of TTF (BDTOLE10; Cooper *et al.*, 1974).

Shape index is a particularly useful property of the Hirshfeld surface because specific types of intermolecular interaction display characteristic patterns on the shape index surface and contacting regions of the surface are naturally mapped in complementary colours. Hydrogen bonds appear with a red concave region on the surface around the acceptor atom and a complementary blue convex region around the hydrogen-bond donor; C—H···π contacts appear with a (usually) broad depression above the π-electron cloud and a corresponding blue region around the C—H donor. For molecules involved in more than one such contact, differences between the patterns on the shape index surface can usually be used to visually assign each donor–acceptor pair (*e.g.* anthracene and phenanthrene). The most visually striking patterns on the shape index surface arise from the packing of parallel sheets of molecules (π–π stacking), where patterns of adjacent red and blue shapes uniquely and rapidly identify the offset of adjacent sheets of molecules (*e.g.* the γ structures of the polycyclic aromatics).

The mapping of contact distances such as d_e on the surface provides a link to more conventional methods of crystal structure analysis that are based on individual contact distances in the crystal. The Hirshfeld surface mapped with d_e highlights close contacts in the crystal as red spots on the surface, but shows these contacts in the context of moderate (green) and more distant (blue) contacts, all of which are important for understanding the overall crystal packing of a molecular crystal. The other distance measure described, d_i, may also provide valuable information about crystal packing if mapped onto the surface in a similar fashion to d_e, but in the present work it has only been used in conjunction with d_e to produce the two-dimensional fingerprint plots.

The two-dimensional fingerprint plots were introduced by Spackman & McKinnon (2002) and have been placed in the fuller context of the original Hirshfeld surfaces in the present work. These plots clearly identify each type of intermolecular contact, such as C—H···π, hydrogen bonding, π–π stacking, H···H contacts and Cl···Cl contacts, but they also enable analysis of very small differences in these patterns and as such represent an entirely new way of summarizing the major intermolecular contacts of an entire crystal structure in a single two-dimensional colour picture.

The size and shape of the Hirshfeld surface are intimately related to the chemical environment surrounding the molecule, making it ideal for use in comparing different crystal structures incorporating the same molecule. Fingerprint plots and surfaces mapped with several functions have been shown to be particularly suited to comparing the crystal structures of closely related molecules, and subsequent papers will explore in detail the application of these plots to polymorphs, different cocrystals and structures with $Z' > 1.0$.

While undertaking the research described in this paper, it became evident to us that more information might be gleaned from the two-dimensional fingerprint plots by generating separate plots for each type of atom–atom contact in the crystal, in order to compare similar crystal structures in even more detail in terms of the relative contribution from each

important intermolecular contact. The capability to link dynamically the information in the two-dimensional fingerprint plots with the Hirshfeld surfaces would also be especially valuable, as the ability to interactively highlight the regions on the surface that contribute to an individual fingerprint would greatly aid the broader understanding and appreciation of the origin of various patterns on the fingerprint plots.

The scalar properties that have been mapped on the Hirshfeld surface in the present paper represent only a fraction of the potential that must exist for mapping properties on the Hirshfeld surface. Because the Hirshfeld surface is smooth, it could potentially be used to display any physical property of the molecule or crystal, and of particular interest would be scalar functions such as the crystalline electron density, the deformation electron density, the Laplacian of the charge density and the electrostatic potential. These functions are already used widely and mapping them onto the Hirshfeld surface would allow these important crystalline properties to be studied at the intermolecular interface in the crystal.

The structures of a large number of molecular crystals have been analysed in preparing this paper, and those selected were chosen to present, in a reasonably systematic fashion, an introduction to the manner in which the Hirshfeld surface reflects the intermolecular interactions and crystal-packing motifs present in different types of molecular crystals. The results firmly establish the Hirshfeld surface as a valuable new tool for visualizing and analysing intermolecular interactions in molecular crystals, and we believe it has the potential to make a unique and even radical contribution to the analysis of molecular crystal structures, particularly when comparing very similar structures or similar motifs in structures of related compounds.

The use of Hirshfeld surfaces for the analysis of molecular crystal structures encourages the adoption of a 'whole of structure' view of intermolecular interactions, rather than concentrating exclusively on assumed 'important' (*i.e.* short) interactions. While discussion of crystal structures in terms of individual atom$\cdots$atom contacts is unavoidable and certainly valuable, a broader picture of intermolecular interactions in the crystal is increasingly desirable; such a picture is available from the Hirshfeld surface. In particular, the Hirshfeld surface mapped with d_e emphasizes contacts between *regions* of neighbouring molecules rather than between individual atoms, and this feature is relevant, for instance, when discussing interactions such as C—H$\cdots\pi$, where the acceptor entity can be a single atom, a C—C bond or a whole ring depending on the individual interaction. Focusing only on atom–atom contact distances and angles in these situations can be misleading and can sometimes miss important features completely (*e.g.* as noted above for the 1,*n*-alkanediamines and for TTF).

A major fraction of the time spent on the research conducted for this paper has been devoted to the development and modification of software for the creation and visualization of the Hirshfeld surfaces. To date, the priority in the development of this software has been for maximum utility by an experienced user and minimal development time: in other words, a research tool. As such it is not particularly user-friendly at present and currently requires some manual manipulation of files, particularly where views of clusters of molecules or several surfaces are desired. While it was not possible to make the development of an integrated software package for generation and interrogation of Hirshfeld surfaces a priority for the present research, software development is ongoing to ensure that the use of the Hirshfeld surface and related tools reaches the potential that has been demonstrated.

As a well defined surface of a molecule in a crystal, the potential applications of the Hirshfeld surface extend much further than those described in this work within the context of crystal structure analysis. Hirshfeld surfaces have already been utilized by others as an alternative molecular surface for large macromolecules (Immel *et al.*, 2001), and Dittrich *et al.* (2002) have investigated the potential of using Hirshfeld surfaces of molecular fragments in investigations of functional-group additivity in oligopeptides. The use of the Hirshfeld surface need not be limited to molecular crystals; comparisons have been conducted between Hirshfeld surfaces of ions in binary ionic crystals (Spackman *et al.*, 2002; Pendas *et al.*, 2002) and interatomic surfaces extracted from Bader's theory of atoms in molecules (Bader, 1990), and we have recently revisited the use of Hirshfeld surfaces for determining molecular electric moments in crystals (Whitten *et al.*, 2004).

Analysis of molecular crystal structures using the tools described in this work is not anticipated to replace the interrogation of crystal structures using conventional methods. Indeed, significant use was made of conventional crystal-packing diagrams to aid the present discussion and analysis. However, it is clear that, when used in conjunction with these conventional methods, the tools we have developed so far, and presented in detail, have the potential to provide researchers in crystallography and related fields with another valuable weapon in the complex battle to understand and rationalize the structure of the molecular solid state.

This work has emerged from a lengthy gestation period, and it is a genuine pleasure to acknowledge the warm encouragement, helpful comments and constructive criticisms provided by numerous friends and colleagues throughout this process. Special thanks to Sally Price, Carolyn Brock, Judith Howard, Gautam Desiraju, Roland Boese, Roger Bishop, Joel Bernstein, Bryan Craven and Dylan Jayatilaka. Robert Bartnik (University of Canberra) provided invaluable assistance with aspects of computational geometry of these surfaces. This research has been funded by small grants from the Australian Research Council and the University of New England; JJM also acknowledges receipt of an Australian Postgraduate Award for the duration of his PhD candidature. The authors express their appreciation for the exceptional efforts made by the editorial staff in Chester, in particular Jillian Bradshaw, to ensure the faithful colour reproduction of the figures in this article.

References

Aakeröy, C. B. (1997). *Acta Cryst.* B**53**, 569–586.
Aakeröy, C. B. & Beatty, A. M. (2001). *Aust. J. Chem.* **54**, 409–421.
Aakeröy, C. B., Evans, T. A., Seddon, K. R. & Pálinkó, I. (1999). *New J. Chem.* **23**, 145–152.
Allen, F. H. (2002). *Acta Cryst.* B**58**, 380–388.
Allen, F. H., Kennard, O., Watson, D. G., Brammer, L., Orpen, A. G. & Taylor, R. (1995). *International Tables for Crystallography*, edited by A. J. C. Wilson, pp. 685–706. Dordrecht: Kluwer Academic.
Allen, F. H., Lommerse, J. P., Hoy, V. J., Howard, J. A. K. & Desiraju, G. R. (1996). *Acta Cryst.* B**52**, 734–745.
André, D., Fourme, R. & Renaud, M. (1971). *Acta Cryst.* B**27**, 2371–2380.
Arteca, G. A. (1990). *Rev. Comput. Chem.* **1**, 191–253.
Bader, R. F. W. (1990). *Atoms in Molecules. A Quantum Theory*. Oxford University Press.
Baumgärtner, A. (1993). *J. Chem. Phys.* **99**, 7496–7501.
Berg, J. A. van den & Seddon, K. R. (2003). *Cryst. Growth Des.* **3**, 643–661.
Berkovitch-Yellin, Z. & Leiserowitz, L. (1980). *J. Am. Chem. Soc.* **102**, 7677–7690.
Berkovitch-Yellin, Z. & Leiserowitz, L. (1982). *J. Am. Chem. Soc.* **104**, 4052–4064.
Bernstein, J., Davis, R. E., Shimoni, L. & Chang, N. L. (1995). *Angew. Chem. Int. Ed. Engl.* **34**, 1555–1573.
Boese, R. & Weiss, H. C. (1998). *Acta Cryst.* C**54**, IUC9800024.
Boese, R., Weiss, H. C. & Bläser, D. (1999). *Angew. Chem. Int. Ed.* **38**, 988–992.
Bolhuis, F. van & Kiers, C. T. (1978). *Acta Cryst.* B**34**, 1015–1016.
Bondi, A. (1964). *J. Phys. Chem.* **68**, 441–447.
Braga, D. (2003). *Chem. Commun.* pp. 2751–2754.
Braga, D., Desiraju, G. R., Miller, J. S., Orpen, A. G. & Price, S. L. (2002). *CrystEngComm*, **4**, 500–509.
Brammer, L., Bruton, E. A. & Sherwood, P. (2001). *Cryst. Growth Des.* **1**, 277–290.
Brock, C. P. & Duncan, L. L. (1994). *Chem. Mater.* **6**, 1307–1312.
Brock, C. P. & Dunitz, J. D. (1982). *Acta Cryst.* B**38**, 2218–2228.
Brock, C. P. & Dunitz, J. D. (1990). *Acta Cryst.* B**46**, 795–806.
Brock, C. P. & Dunitz, J. D. (1994). *Chem. Mater.* **6**, 1118–1127.
Bruno, I. J., Cole, J. C., Edgington, P. R., Kessler, M., Macrae, C. F., McCabe, P., Pearson, J. & Taylor, R. (2002). *Acta Cryst.* B**58**, 389–397.
Burbank, R. D. (1953). *J. Am. Chem. Soc.* **75**, 1211–1214.
Camerman, A. & Trotter, J. (1965). *Acta Cryst.* **18**, 636–643.
Clementi, E. & Roetti, C. (1974). *At. Data Nucl. Data Tables*, **14**, 177–478.
Cooper, W. F., Edmonds, J. W., Wudl, F. & Coppens, P. (1974). *Cryst. Struct. Commun.* **3**, 23–26.
Craven, B. M., McMullan, R. K., Bell, J. D. & Freeman, H. C. (1977). *Acta Cryst.* B**33**, 2585–2589.
Derissen, J. L. & Smit, P. H. (1974). *Acta Cryst.* B**30**, 2240–2242.
Desiraju, G. R. (1987). *Organic Solid State Chemistry*, edited by G. R. Desiraju, pp. 519–546. Amsterdam: Elsevier.
Desiraju, G. R. (1989). *Crystal Engineering: The Design of Organic Solids.* Amsterdam: Elsevier.
Desiraju, G. R. (1995). *Angew. Chem. Int. Ed. Engl.* **34**, 2311–2327.
Desiraju, G. R. (1996). *Acc. Chem. Res.* **29**, 441–449.
Desiraju, G. R. (1997). *Chem. Commun.* pp. 1475–1482.
Desiraju, G. R. (2001). *Curr. Sci.* **81**, 1038–1042.
Desiraju, G. R. (2002). *Acc. Chem. Res.* **35**, 565–573.
Desiraju, G. R. & Gavezzotti, A. (1989). *Acta Cryst.* B**45**, 473–482.
Desiraju, G. R. & Parthasarathy, R. (1989). *J. Am. Chem. Soc.* **111**, 8725–8726.
Desiraju, G. R. & Steiner, T. (1999). *The Weak Hydrogen Bond.* Oxford University Press.
Dittrich, B., McKinnon, J. J., Spackman, M. A. & Luger, P. (2002). *Acta Cryst.* A**58** (Suppl.), C-350.
Do Carmo, M. P. (1976). *Differential Geometry of Curves and Surfaces.* Englewood-Cliffs: Prentice-Hall.
Duncan, B. S. & Olson, A. J. (1993*a*). *Biopolymers*, **33**, 219–229.
Duncan, B. S. & Olson, A. J. (1993*b*). *Biopolymers*, **33**, 231–238.
Dunitz, J. D. & Gavezzotti, A. (1999). *Acc. Chem. Res.* **32**, 677–684.
Ellern, A., Bernstein, J., Becker, J. Y., Zamir, S. & Shahal, L. (1994). *Chem. Mater.* **6**, 1378–1385.
Etter, M. C. (1990). *Acc. Chem. Res.* **23**, 120–126.
Etter, M. C., MacDonald, J. C. & Bernstein, J. (1990). *Acta Cryst.* B**46**, 256–262.
Fabian, L., Argay, G. & Kalman, A. (1999). *Acta Cryst.* B**55**, 788–792.
Fawcett, J. K. & Trotter, J. (1965). *Proc. R. Soc. London Ser. A*, **289**, 366–376.
Feld, R., Lehmann, M. S., Muir, K. W. & Speakman, J. C. (1981). *Z. Kristallogr.* **157**, 215–231.
Ferraris, G., Jones, D. W. & Yerkess, J. (1973). *Z. Kristallogr.* **138**, 113–128.
Fischer, P., Zolliker, P., Meier, B. H., Ernst, R. R., Hewat, A. W., Jorgensen, J. D. & Rotella, F. J. (1986). *J. Solid State Chem.* **61**, 109–125.
Fourme, R. & Renaud, M. (1966). *C. R. Acad. Sci. Paris*, **263**, 69–72.
Gavezzotti, A. (1998). *Crystallogr. Rev.* **7**, 5–121.
Geomview (1992–1996). *Geomview*. Geometry Center, University of Minnesota.http://www.geomview.org/.
Goddard, R., Haenel, M. W., Herndon, W. C., Kruger, C. & Zander, M. (1995). *J. Am. Chem. Soc.* **117**, 30–41.
Goldman, B. B. & Wipke, W. T. (2000*a*). *J. Chem. Inf. Comput. Sci.* **40**, 644–658.
Goldman, B. B. & Wipke, W. T. (2000*b*). *Proteins*, **38**, 79–94.
Guru Row, T. N. & Parthasarathy, R. (1981). *J. Am. Chem. Soc.* **103**, 477–479.
Hazell, A. C., Larsen, F. K. & Lehmann, M. S. (1972). *Acta Cryst.* B**28**, 2977–2984.
Heiden, W., Goetze, T. & Brickmann, J. (1993). *J. Comput. Chem.* **14**, 246–250.
Hirshfeld, F. L. (1977). *Theor. Chim. Acta*, **44**, 129–138.
Huggins, M. L. (1936). *J. Org. Chem.* **1**, 407–456.
Hunter, C. A., Lawson, K. R., Perkins, J. & Urch, C. J. (2001). *J. Chem. Soc. Perkin Trans.* 2, pp. 651–669.
Hunter, C. A. & Sanders, J. K. M. (1990). *J. Am. Chem. Soc.* **112**, 5525–5534.
Hyde, S., Andersson, S., Larsson, K., Blum, Z., Landh, T., Lidin, S. & Ninham, B. W. (1997). Editors. *The Language of Shape.* Amsterdam: Elsevier.
Immel, S., Lichtenthaler, F. W., Lindner, H. J. & Nakagawa, T. (2001). *Tetrahedron Asymmetry*, **12**, 2767–2774.
Izuoka, A., Wakui, K., Fukuda, T., Sato, N. & Sugawara, T. (1992). *Acta Cryst.* C**48**, 900–902.
Jeffrey, G. A., Ruble, J. R., McMullan, R. K. & Pople, J. A. (1987). *Proc. R. Soc. London Ser. A*, **414**, 47–57.
Jönsson, P.-G. (1971). *Acta Cryst.* B**27**, 893–898.
Kane, J. & Schaeffer, R. (1981). *Cryst. Struct. Commun.* **10**, 1403.
Kawaguchi, T., Tanaka, K., Takeuchi, T. & Watanabe, T. (1973). *Bull. Chem. Soc. Jpn*, **46**, 62–66.
Kay, M. I., Okaya, Y. & Cox, D. E. (1971). *Acta Cryst.* B**27**, 26–33.
Kerr, K. A. (1987). *Acta Cryst.* C**43**, 956–958.
Kitaigorodsky, A. I. (1961). *Organic Chemical Crystallography.* New York: Consultants Bureau.
Kitaigorodsky, A. I. (1973). *Molecular Crystals and Molecules.* New York: Academic Press.
Koenderink, J. J. (1990). *Solid Shape.* Cambridge, MA: MIT Press.
Koenderink, J. J. & van Doorn, A. J. (1992). *Image Vision Comput.* **10**, 557–565.
Kuduva, S. S., Sarma, J. A. R. P., Katz, A. K., Carrell, H. L. & Desiraju, G. R. (2000). *J. Phys. Org. Chem.* **13**, 719–728.

Leiserowitz, L. (1976). *Acta Cryst.* B**32**, 775–802.
Leiserowitz, L. (1978). *Acta Cryst.* B**34**, 1230–1247.
Leiserowitz, L. & Nader, F. (1977). *Acta Cryst.* B**33**, 2719–2733.
Lorensen, W. E. & Cline, H. E. (1987). *Comput. Graph.* **21**, 163–169.
McKinnon, J. J. (2003). PhD thesis, University of New England, Australia.
McKinnon, J. J., Mitchell, A. S. & Spackman, M. A. (1998*a*). *Chem. Eur. J.* **4**, 2136–2141.
McKinnon, J. J., Mitchell, A. S. & Spackman, M. A. (1998*b*). *Chem. Commun.* pp. 2071–2072.
McMullan, R. K., Kvick, Å. & Popelier, P. (1992). *Acta Cryst.* B**48**, 726–731.
Marsh, P. & Williams, D. E. (1981). *Acta Cryst.* B**37**, 705–706.
Marsh, R. E. & Herbstein, F. H. (1988). *Acta Cryst.* B**44**, 77–88.
Meyer, A. Y. (1986). *Chem. Soc. Rev.* **15**, 449–474.
Mezey, P. G. (1990). *Rev. Comput. Chem.* **1**, 265–294.
Mezey, P. G. (1993). *Shape in Chemistry: An Introduction to Molecular Shape and Topology*. New York: VCH.
Milledge, H. J. & Pant, L. M. (1960). *Acta Cryst.* **13**, 285–290.
Mitchell, A. S. & Spackman, M. A. (2000). *J. Comput. Chem.* **21**, 933–942.
Müller, A. (1930). *Proc. R. Soc. London Ser. A*, **127**, 417–430.
Müller, A. (1932). *Proc. R. Soc. London Ser. A*, **138**, 514–530.
Nahringbauer, I. (1978). *Acta Cryst.* B**34**, 315–318.
Nangia, A. (2000). *New J. Chem.* **24**, 1049–1055.
Nangia, A. (2002). *CrystEngComm*, **4**, 93–101.
Nangia, A. & Desiraju, G. R. (1998). *Design of Organic Solids*, edited by E. Weber, pp. 57–95. Berlin: Springer-Verlag.
Näther, C., Bock, H., Havlas, Z. & Hauck, T. (1998). *Organometallics*, **17**, 4707–4715.
Nes, G. J. H. van & Vos, A. (1978). *Acta Cryst.* B**34**, 1947–1956.
Nes, G. J. H. van & Vos, A. (1979). *Acta Cryst.* B**35**, 2593–2601.
Ohms, U., Guth, H., Hellner, E., Dannohl, H. & Schweig, A. (1984). *Z. Kristallogr.* **169**, 185–200.
Pendas, A. M., Luana, V., Pueyo, L., Francisco, E. & Mori-Sanchez, P. (2002). *J. Chem. Phys.* **117**, 1017–1023.
Petrícek, V., Císarová, I., Hummel, L., Kroupa, J. & Brezna, B. (1990). *Acta Cryst.* B**46**, 830–832.
Piermarini, G. J. & Braun, A. B. (1973). *J. Chem. Phys.* **58**, 1974–1982.
Price, S. L., Stone, A. J., Lucas, J., Rowland, R. S. & Thornley, A. E. (1994). *J. Am. Chem. Soc.* **116**, 4910–4918.
Ramasubbu, N., Parthasarathy, R. & Murray-Rust, P. (1986). *J. Am. Chem. Soc.* **108**, 4308–4314.
Refson, K. & Pawley, G. S. (1986). *Acta Cryst.* B**42**, 402–410.
Rettig, S. J. & Trotter, J. (1987). *Acta Cryst.* C**43**, 2260–2262.
Robertson, J. M. (1951). *Proc. R. Soc. London Ser. A*, **207**, 101–110.
Rosenfield, R. E., Parthasarathy, R. & Dunitz, J. D. (1977). *J. Am. Chem. Soc.* **99**, 4860–4862.
Rowland, R. S. (1995). *Am. Crystallogr. Assoc. Abstr.* p. 63.
Rudnick, J. & Gaspari, G. (1986). *J. Phys. A Math. Gen. Phys.* **19**, L191–L193.
Sarma, J. A. R. P. & Desiraju, G. R. (1986). *Acc. Chem. Res.* **19**, 222–228.
Scherer, W., Spiegler, M., Pedersen, B., Tafipolsky, M., Hieringer, W., Reinhard, B., Downs, A. J. & McGrady, G. S. (2000). *Chem. Commun.* pp. 635–636.
Schmidt, G. M. J. (1971). *Pure Appl. Chem.* **27**, 647–678.
Sharma, C. V. K. (2002). *Cryst. Growth Des.* **2**, 465–474.
Spackman, M. A. & Byrom, P. G. (1997). *Chem. Phys. Lett.* **267**, 215–220.
Spackman, M. A. & McKinnon, J. J. (2002). *CrystEngComm*, **4**, 378–392.
Spackman, M. A., Meng, X., McKinnon, J. J. & Mitchell, A. S. (2002). *Acta Cryst.* A**58** (Suppl.), C-37.
Steiner, T. (2002). *Angew. Chem. Int. Ed.* **41**, 48–76.
Stevens, E. D. (1979). *Mol. Phys.* **37**, 27–45.
Stewart, R. F. & Jensen, L. H. (1967). *Acta Cryst.* **23**, 1102–1105.
Swaminathan, S., Craven, B. M. & McMullan, R. K. (1984). *Acta Cryst.* B**40**, 300–306.
Takahashi, O., Kohno, Y., Iwasaki, S., Saito, K., Iwaoka, M., Tomoda, S., Umezawa, Y., Tsuboyama, S. & Nishio, M. (2001). *Bull. Chem. Soc. Jpn*, **74**, 2421–2430.
Taylor, R. & Macrae, C. F. (2001). *Acta Cryst.* B**57**, 815–827.
Thalladi, V. R. & Boese, R. (2000). *New J. Chem.* **24**, 579–581.
Thalladi, V. R., Boese, R. & Weiss, H.-C. (2000*a*). *Angew. Chem. Int. Ed.* **39**, 918–922.
Thalladi, V. R., Boese, R. & Weiss, H.-C. (2000*b*). *J. Am. Chem. Soc.* **122**, 1186–1190.
Thalladi, V. R., Nusse, M. & Boese, R. (2000). *J. Am. Chem. Soc.* **122**, 9227–9236.
Thalladi, V. R., Weiss, H.-C., Bläser, D., Boese, R., Nangia, A. & Desiraju, G. R. (1998). *J. Am. Chem. Soc.* **120**, 8702–8710.
Vainshtein, B. K., Fridkin, V. M. & Indenbom, V. L. (1982). *Modern Crystallography*, Vol. II. Berlin: Springer-Verlag.
Vangala, V. R., Bhogala, B. R., Dey, A., Desiraju, G. R., Broder, C. K., Smith, P. S., Mondal, R., Howard, J. A. K. & Wilson, C. C. (2003). *J. Am. Chem. Soc.* **125**, 14495–14509.
Weber, E. (1998). *Design of Organic Solids.* Berlin: Springer-Verlag.
Whitten, A. E., Spackman, M. A., McKinnon, J. J., Meng, X. & Radford, C. J. (2004). In preparation.